INFORMATION TO USERS

This material was produced from a microfilm copy of the original document. While the most advanced technological means to photograph and reproduce this document have been used, the quality is heavily dependent upon the quality of the original submitted.

The following explanation of techniques is provided to help you understand markings or patterns which may appear on this reproduction.

1. The sign or "target" for pages apparently lacking from the document photographed is "Missing Page(s)". If it was possible to obtain the missing page(s) or section, they are spliced into the film along with adjacent pages. This may have necessitated cutting thru an image and duplicating adjacent pages to insure you complete continuity.

2. When an image on the film is obliterated with a large round black mark, it is an indication that the photographer suspected that the copy may have moved during exposure and thus cause a blurred image. You will find a good image of the page in the adjacent frame.

3. When a map, drawing or chart, etc., was part of the material being photographed the photographer followed a definite method in "sectioning" the material. It is customary to begin photoing at the upper left hand corner of a large sheet and to continue photoing from left to right in equal sections with a small overlap. If necessary, sectioning is continued again — beginning below the first row and continuing on until complete.

4. The majority of users indicate that the textual content is of greatest value, however, a somewhat higher quality reproduction could be made from "photographs" if essential to the understanding of the dissertation. Silver prints of "photographs" may be ordered at additional charge by writing the Order Department, giving the catalog number, title, author and specific pages you wish reproduced.

5. PLEASE NOTE: Some pages may have indistinct print. Filmed as received.

University Microfilms International
300 North Zeeb Road
Ann Arbor, Michigan 48106 USA
St. John's Road, Tyler's Green
High Wycombe, Bucks, England HP10 8HR

77-26,296

LUCHINI, John Remo, 1949-
MATHEMATICAL MODEL FOR RUBBER HYSTERESIS.

The University of Michigan, Ph.D., 1977
Applied Mechanics

Xerox University Microfilms, Ann Arbor, Michigan 48106

MATHEMATICAL MODEL FOR RUBBER HYSTERESIS

by
John Remo Luchini

A dissertation submitted in partial fulfillment
of the requirements for the degree of
Doctor of Philosophy
(Applied Mechanics)
in The University of Michigan
1977

Doctoral Committee:

Professor Samuel K. Clark, Chairman
Professor Kenneth C. Ludema
Professor Ivor K. McIvor
Assistant Professor David A. Sonstegard
Associate Professor Alan S. Wineman
Associate Professor Wei-Hsuin Yang

ACKNOWLEDGMENTS

In addition to the aid received from the doctoral committee and the technicians of the Applied Mechanics Department, there are several people who require special thanks.

Professor S. K. Clark, who has served as chairman on this project, has also provided financial support and valuable experience through other research projects over the last five years.

Dr. K. K. Wyckoff served as a constant source of advice and assurance.

Remo Luchini aided in the construction of the load cell and provided other special services.

And last, but not least, is my wife, Tamara. Providing words of encouragement and financial support, she has typed and edited this dissertation and will present me with our first child about the same time Rackham will be presenting me with my degree.

Thus, I dedicate this work to you, Tamara.

TABLE OF CONTENTS

Page

ACKNOWLEDGMENTS i

LIST OF ILLUSTRATIONS v

LIST OF TABLES viii

LIST OF SYMBOLS ix

CHAPTER

1 INTRODUCTION 1

2 PHYSICS OF RUBBER ELASTICITY AND HYSTERESIS 6
- 2.1. Some Macroscopic Properties of Rubber
  - 2.1.1. Quasi-Static Rubber Behavior
  - 2.1.2. Time Dependent Rubber Behavior
  - 2.1.3. Characteristics of Filled Rubber
- 2.2. Some Microscopic Properties of Rubber
  - 2.2.1. Macromolecular Behavior
  - 2.2.2. Basic Models

3 VISCOELASTIC MODELS FOR RUBBER 32
- 3.1. Linear Viscoelasticity
  - 3.1.1. Requirements for Linear Theory
  - 3.1.2. Thermorheological Properties
  - 3.1.3. Sinusoidal Vibrations
- 3.2. Nonlinear Viscoelasticity
  - 3.2.1. Basis of a Theory
  - 3.2.2. Possible General Theories

4 PRESENTATION OF MODEL 49
- 4.1. Distributed Element Model for Hysteresis
  - 4.1.1. Background of Hysteretic Model
  - 4.1.2. Basic Analysis
  - 4.1.3. Jenkins Elements with Stops
- 4.2. Hysteretic Model for Rubber
  - 4.2.1. Deterministic System with Discrete Elements
  - 4.2.2. Stochastic System with Continuous Elements

Page

CHAPTER

5 EXPERIMENTAL VERIFICATION..... 102
5.1. Application of Model
5.1.1. Introduction
5.1.2. Rate Independence Experiment
5.2. Further Development of Model
5.2.1. Characterizing Experiments
5.2.2. Loss Computations

6 LIMITATIONS AND EXTENSIONS..... 150
6.1. Incorporating Other Effects
6.2. Losses from Multiaxial Loadings
6.3. Other Applications

REFERENCES 171

LIST OF ILLUSTRATIONS

Figure		Page
2.1	Typical rubber tension and compression curves	7
2.2	Typical relaxation and creep test data	9
2.3	Typical viscous damped resonance plot	10
2.4	Typical hysteresis loop in dynamic stress-strain cycles	12
2.5	Mullins effect	13
2.6	Change of load deflection curve when cycling	15
2.7	Transmissibility curve for filled natural rubber	19
2.8	Actual dynamic hysteresis loop for filled natural rubber	19
2.9	Relationship of entanglements to creep compliance	22
2.10	Illustration of entanglements and crosslinks	24
2.11	Effect of vulcanization on elastic modulus	25
2.12	Effect of vulcanization on loss modulus	25
2.13	Comparison of various statistical models for rubber elasticity	29
3.1	Construction of temperature-frequency master curve	36
3.2	Master curve of moduli and loss tangent for unvulcanized natural rubber	38
3.3	Comparison of viscoelastic theory and rubber behavior	42
4.1	Simple slip-damper model	51

		Page
4.2	Comparison of Iwan's model with Cooper's data from rubber	53
4.3	A Jenkins element and its behavior	54
4.4	Two Jenkins elements in parallel	56
4.5	Tension response of two Jenkins elements in parallel	56
4.6	Metallic type stress-strain plot	57
4.7	Change of random molecular orientation with stress	62
4.8	Continued tension response of two element system from Figure (4.4)	63
4.9	Hysteresis loop for hypothetical system	65
4.10	Hysteresis loop for hypothetical system	65
4.11	A discrete model with stops and example response curves	66
4.12	Example force-deflection plot for elements starting to slip at δ_1	71
4.13	Linear plot exhibiting loss	75
4.14	Comparison of single and double acting dampers	78
4.15	Example force-deflection plot for elements starting to slip at δ_1	85
4.16	Force-deflection curve generated using arbitrary functions	100
4.17	Comparison of model behavior to rubber behavior	101
5.1	Schematic of the rubber hysteresis experiments	106
5.2	Relation of loss, rate, and cycle size for natural rubber sample	114
5.3	Relation of loss, rate, and cycle size for butyl rubber sample	115

		Page
5.4	Relation of loss, rate, and cycle size for oil extended butyl rubber sample	116
5.5	Losses as a function of cycle size for three carbon-filled, vulcanized rubber samples	118
5.6	Histogram of $[p'(\delta) - q(\delta)]$ for natural rubber sample	129
5.7	Histogram of $[p'(\delta) - q(\delta)]$ for butyl rubber sample	130
5.8	Histogram of $[p'(\delta) - q(\delta)]$ for oil extended butyl rubber sample	131
5.9	Data for natural rubber on probability paper	133
5.10	Data for butyl rubber on probability paper	134
5.11	Data for oil extended butyl rubber on probability paper	135
5.12	Histogram for natural rubber with the approximation function	137
5.13	Histogram for butyl rubber with the approximation function	138
5.14	Histogram for oil extended butyl rubber with the approximation function	139
5.15	Flowchart for program to compute loss	145
5.16	Loss versus cycle size plots for various normal distributions	146
5.17	Loss as a function of cycle size for three rubber samples	148
6.1	Simple loss models with both dry and viscous friction	155
6.2	Typical hysteresis loop for torsion of earthenware clay	163
6.3	Hysteretic loss in cord-rubber composites as a function of maximum bending curvature	168
6.4	Tire drag force as a function of pressure and deflection	169

LIST OF TABLES

Table		Page
5.1	Energy loss from measured areas for natural rubber	111
5.2	Energy loss from measured areas for butyl rubber	112
5.3	Energy loss from measured areas for oil extended butyl rubber	113
5.4	Comparison of average experimental values of energy loss and computed values of energy loss for natural rubber	147
5.5	Comparison of average experimental values of energy loss and computed values of energy loss for butyl rubber	147
5.6	Comparison of average experimental values of energy loss and computed values of energy loss for oil extended butyl rubber	147

LIST OF SYMBOLS

GREEK SYMBOLS:

α	Proportion of areas in normal distribution
α	The "action" of a slip damper
δ	Deflection
δ_i, δ_j	Arbitrary discrete values of deflection
δ_1, δ_2	Specific discrete values of deflection
δ_0	The reference deflection where force on specimen is zero
δ^*	Upper limit of a deflection half-cycle
δ°	Lower limit of a deflection half-cycle
δ_ℓ	The last extremum of a deflection half-cycle, either δ^* or δ°
δ_P	The "equivalent plastic deformation, a notational convenience
Δ	A small amount
$\varepsilon(x)$	Error of an approximation
ζ	The damping factor in a viscous damped system
θ	Phase angle between stress and strain
κ	Spring rate of individual elements in a system
λ	Stretch ratio
μ	Coefficient of dry friction
$\sigma, \sigma_1, \sigma_2$	Standard deviation of a Gaussian normal distribution
Φ	A decreasing function of I_2
ω	Natural frequency of a system
Ω	Excitation frequency of a system

REGULAR SYMBOLS:

a	An arbitrary constant
A	Area of a normal distribution
b	An arbitrary constant
c	An arbitrary constant
C_1, C_2	Mooney material constants
C	Viscous damping coefficient
$d( )$	The differential of ( ), for example: dW, de, ds
D	Amplitude of a deformation or strain cycle
$D(\delta)$	Separation of load and unload curves in a hysteresis loop
e	Strain
$e_i, e_j, \ldots$	Arbitrary discrete values of strain
$e_1, e_2, \ldots$	Specific discrete values of strain
$e(t), e_1(t), e_2(t)$	Arbitrary strain histories
E	Young's elastic modulus
E_0	Dimensionless tangent modulus
E^*	Complex compliance
E'	Viscoelastic storage compliance
E''	Viscoelastic loss compliance
$E\{x\}$	The expected value of the random variable x
$f(e)$	Whiteman's function for the density of yield points
$f(x), f(x,y)$	Arbitrary probability density functions
$F[ ]$	A constitutive functional
$F(\delta)$	Force as a function of deflection

$g(x), g(x,y)$	Arbitrary probability density functions
G	Elastic shear modulus
G*	Complex shear modulus
G'	Viscoelastic shear storage modulus
G"	Viscoelastic shear loss modulus
$h(x), h(x,y)$	Arbitrary probability density functions
i	The imaginary constant $\sqrt{-1}$ or an integer counter, as defined in context
I_1, I_2	First and second strain invariants
j	An integer counter
k	An integer counter
K	Total system spring rate or the initial system spring rate, as defined in context
ℓ	Length
ℓ_0	Original length
M,m	Mass
n	An integer counter
n*	The integer counter for $\delta_i = \delta^*$
n°	The integer counter for $\delta_i = \delta^\circ$
n_ℓ	The integer counter for $\delta_i = \delta_\ell$
N	Number of elements in a discrete system
N_0	Number of elements which started elastically
$N(\sigma)$	Gaussian normal distribution with standard deviation of σ
$p(x), p'(x), p''(x)$	Probability density functions for elements which begin to slip at x
$P(\delta), P'(\delta), P''(\delta)$	Number fraction of elements beginning to slip at the deflection δ

$q(x)$	Probability density function for elements which hit stops at x
$Q(\delta)$	Number fraction of elements which hit stops at the deflection δ
$R(x)$	An integral of the Gaussian normal function
s	Stress
$s(t), s_1(t), s_2(t)$	Arbitrary stress histories
S	Amplitude of a stress or force cycle
t, u, v, w, x, y, z	Arbitrary unknowns which are defined in context
W	A strain energy function

SPECIAL SYMBOLS:

$(\dot{})$	Time derivative of ( )
$\lvert d^n \rvert$	Maximum value of the n^{th} derivative
$[A]$	The matrix of values of A
$\{A\}$	The vector of values of A
$\{a_i\}$	The set of values a_i, where $i=\pm 1, \pm 2, \pm 3, \ldots$
Δt	A small increment of time
$\mid$	"such that" or "given"
Σ	Summation

CHAPTER 1

INTRODUCTION

The purpose of this work is to develop and present a mathematical model for the material behavior of carbon-filled, vulcanized rubber. The use of such a model will simplify the calculation of energy lost during cyclic stress. The model may be applied to loading situations such as that in a pneumatic tire.

Recent interest in the rolling resistance of tires pointed up some difficulties in the use of viscoelastic theory for the prediction of loss. Flügge [1] showed how losses such as rolling resistance can occur with a viscoelastic material. However, his model predicts the loss will be proportional to load squared and dependent on frequency. Experiments on pneumatic tires have shown loss which is linearly related to load and nearly independent of frequency [2]. Experiments on carbon-filled, vulcanized rubber below show similar effects.

The hysteretic character of the model presented in this dissertation is associated with Couloumb dry friction or plasticity only, rather than with the fluid friction of viscoelasticity. Dry friction theory has received limited attention in the past and is thus not as fully developed as theories of viscoelasticity. This dry friction aspect of a general theory of material response has a physical basis in the structure of rubber-like materials. This aspect offers

considerable insight to the behavior of filled rubber. The theory defines hysteretic loss parameters, which can be obtained from a few simple experiments as compared to those required for nonlinear viscoelastic analysis.

This work offers a background in rubber behavior, viscoelastic theory, and dry friction hysteresis theory. A hysteretic theory is developed for application to carbon-filled, vulcanized rubber. Experimental results are then presented and compared to predictions of the hysteretic theory. The limitations, as well as the extensions, of the theory are discussed, and further use of this theory is recommended for other problems involving similar materials.

The special mechanical behavior which characterizes rubber is described in Chapter 2. Rubber can withstand large deformations without failure. The time dependence of rubber behavior is described and compared to linear viscoelastic behavior. While pure-gum rubber follows the predictions of viscoelasticity, carbon-filled, vulcanized rubber has some different characteristics. The Mullins effect, amplitude dependence of material properties, and thixotropic effects are described.

The unique behavior of rubber is due to its molecular construction. Chapter 2 also describes the microscopic behavior of rubber. The effects of entanglements, crosslinks, fillers, and copolymer compounds are mentioned. Models of rubber elasticity based on statistics of the macromolecular structure are presented.

Viscoelastic theory which may be used to model rubber behavior is presented in Chapter 3. Various levels of complexity in the theory are differentiated, and the effect of temperature on material properties is mentioned. Energy loss during cyclic stress and strain of a viscoelastic material is discussed and compared with the behavior of rubber. More general theories are available but, due to their complexity and lack of development for specific cases, another model is investigated.

Chapter 4 develops the specific case of a material which stiffens and exhibits only dry friction hysteresis. Dry friction theory has been historically ignored because of difficulties in the solution of vibration problems of such a system. Carbon-filled, vulcanized rubber exhibits the "soft resonance" behavior of a system in which the stiffness decreases with amplitude [3]. Such behavior is also typical of vibrations of a system with dry friction damping.

A dry friction model can be very useful in a loss problem since rate effects can be ignored. In Chapter 4 an attempt is made to apply an existing model to rubber hysteresis. The stiffening of rubber interferes with the analysis in such a model. The resulting behavior of the model violates the laws of thermodynamics by generating work under cyclic stress.

Improvements are made in the theory to account for the presence of loss in rubber with its stiffening behavior. A model is formulated using discrete elements. These elements do not exist in the rubber, so a stochastic model is also formulated which has parameters that can be estimated statistically. Chapter 4 concludes with a hypothetical force-deformation plot generated by the model. The plot is quite similar to the behavior for a rubber sample.

Chapter 5 presents experimental verification for the model. The rate independent loss character of several different samples of rubber is shown in low deformation rate tests. The model is developed to provide characterizing experiments and loss predictions. Viscous losses are assumed to be negligible compared to dry friction losses in the material. Assumptions are also made regarding the parameters in the model. The parameters are then estimated, and the loss for various force-deflection cycles is predicted and verified.

Chapter 6 discusses limitations and extensions of the model. The model is limited due to a complete lack of viscoelastic properties and thermorheological properties. Some approaches for incorporating such effects are discussed, but specific applications would determine what effects must be added. In addition, the extension of the one-dimensional model to multiaxial loading is not a straightforward procedure. Experimentation in this area is suggested to

test hypotheses which have proved useful for other materials. Some areas where the model should be directly applicable are presented. Studies of the hysteresis of clay or of composite materials may find the current model useful. Rolling loss in pneumatic tires, which generated original interest in this model, is a problem which can be investigated from the framework provided by this model.

CHAPTER 2

PHYSICS OF RUBBER ELASTICITY AND HYSTERESIS

2.1. Some Macroscopic Properties of Rubber

2.1.1. Quasi-Static Rubber Behavior

As commonly used, rubber refers to both a rubber-like material and natural rubber, the product of the tree Hevea Braziliensis. Rubber-like refers to a mechanical behavior and its associated chemical structure and configuration, but not to a chemical compound. The mechanical behavior is characterized by a relatively large deformation before fracture, as compared with other engineering materials such as metals or concrete.

Figure (2.1) presents typical force-deflection curves for rubber. The nonlinear tension curve appears to soften, as with metals, then stiffen; the experiment was carried out over a deflection range impossible for the most ductile of metals. The compression curve is again nonlinear but continually stiffens. In the limit of compression, 100% engineering strain, an infinitely large force would be required as the material is compressed into a thinner and thinner sheet.

2.1.2. Time Dependent Rubber Behavior

This section discusses experimental investigations of rubber. Explanations and models of rubber behavior are discussed later.

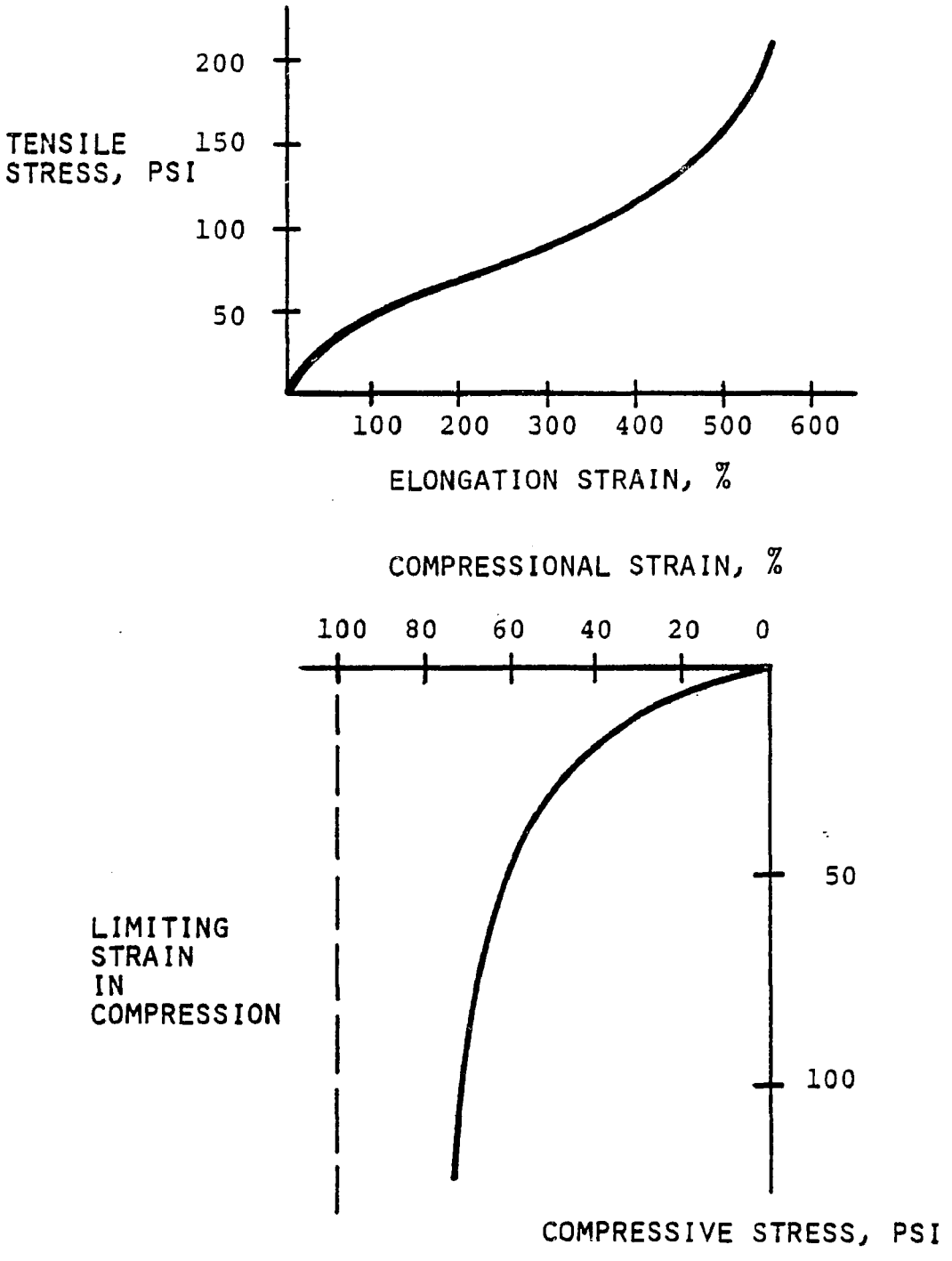


Figure (2.1) Typical rubber tension and compression curves

The time dependence of material properties is of particular importance and is most commonly tested with creep or relaxation tests. Figure (2.2) is a plot of typical relaxation and creep test data. In a relaxation test, a ramp deformation is applied to a rubber block then stopped at a constant deflection, while the force is monitored as a function of time. In a creep test, the force is held constant, usually by a dead weight system, and deflection is monitored as a function of time. The conclusion from these tests is that the strain always lags behind the stress in a dynamic test. This conclusion for rubber corresponds to results of theories of viscoelasticity, in which constitutive equations attribute this time dependent material behavior to a viscous friction internal to the material.

A material with a linear viscoelastic constitutive equation demonstrates behavior in vibration similar to a mechanical system with a dashpot. In particular, a resonance plot for rubber has marked similarity to that of a damped mechanical system. Resonance data for rubber is shown later in Chapter 3. Figure (2.3) simulates a resonance plot for pure-gum rubber, that is, nonvulcanized rubber, which has the same damped resonance apparent in a mechanical system.

In addition, every different strain history leads to a different stress-strain plot, hence a different energy loss. This energy loss is mechanical energy which is converted to heat in the material, and can be determined from the area

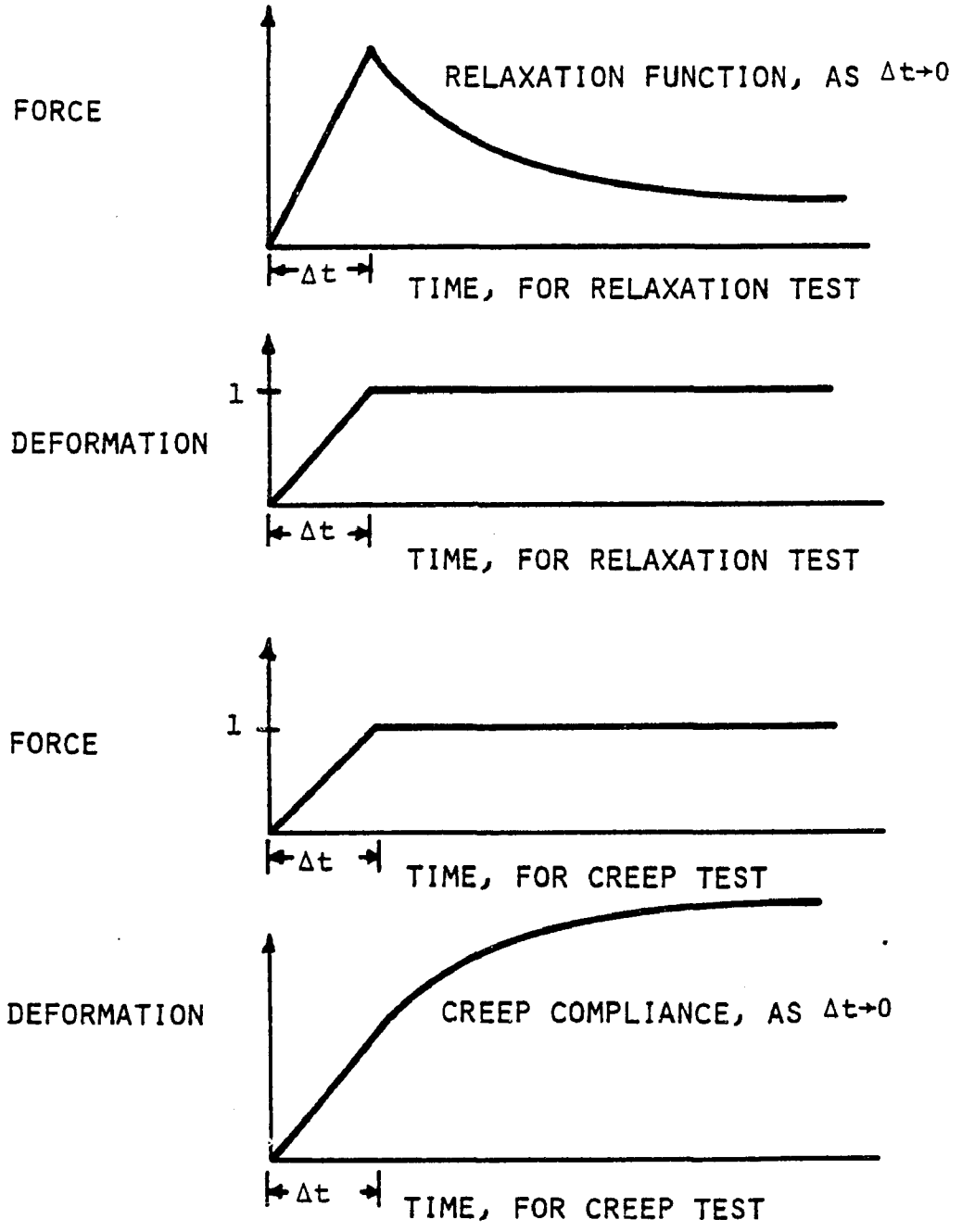
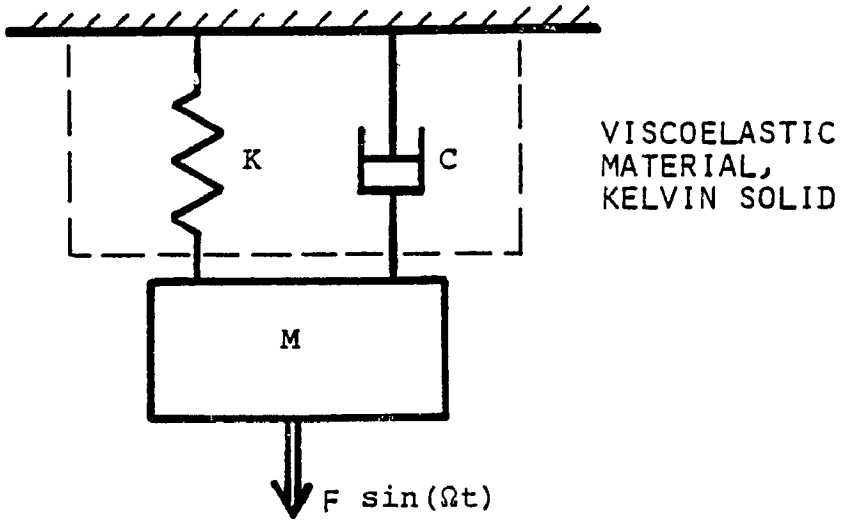


Figure (2.2) Typical relaxation and creep test data



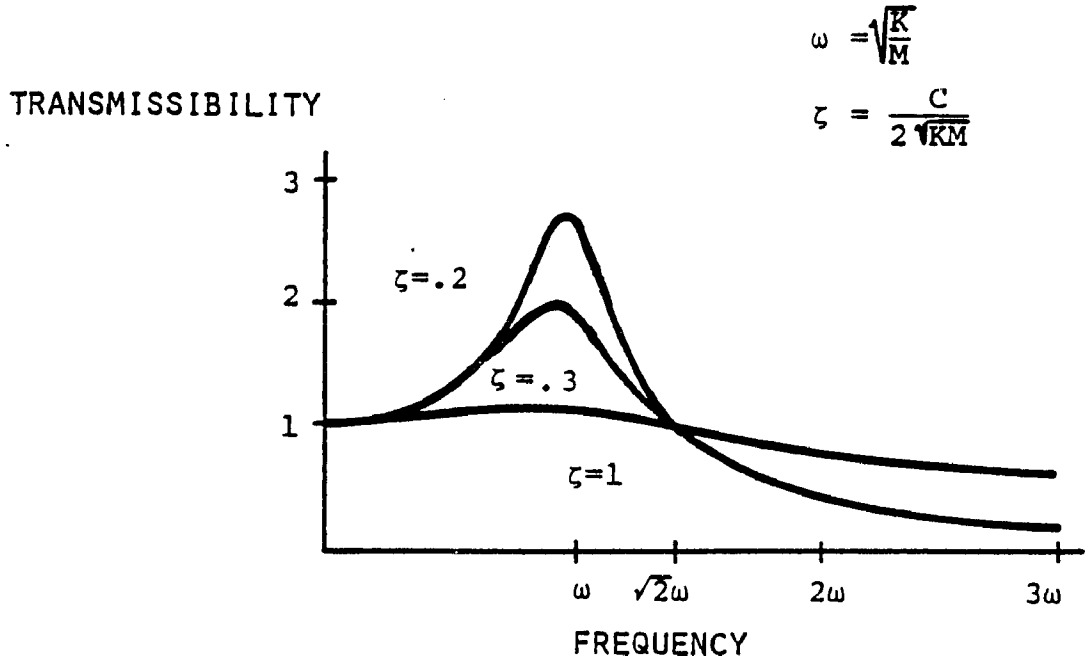


Figure (2.3) Typical viscous damped resonance plot

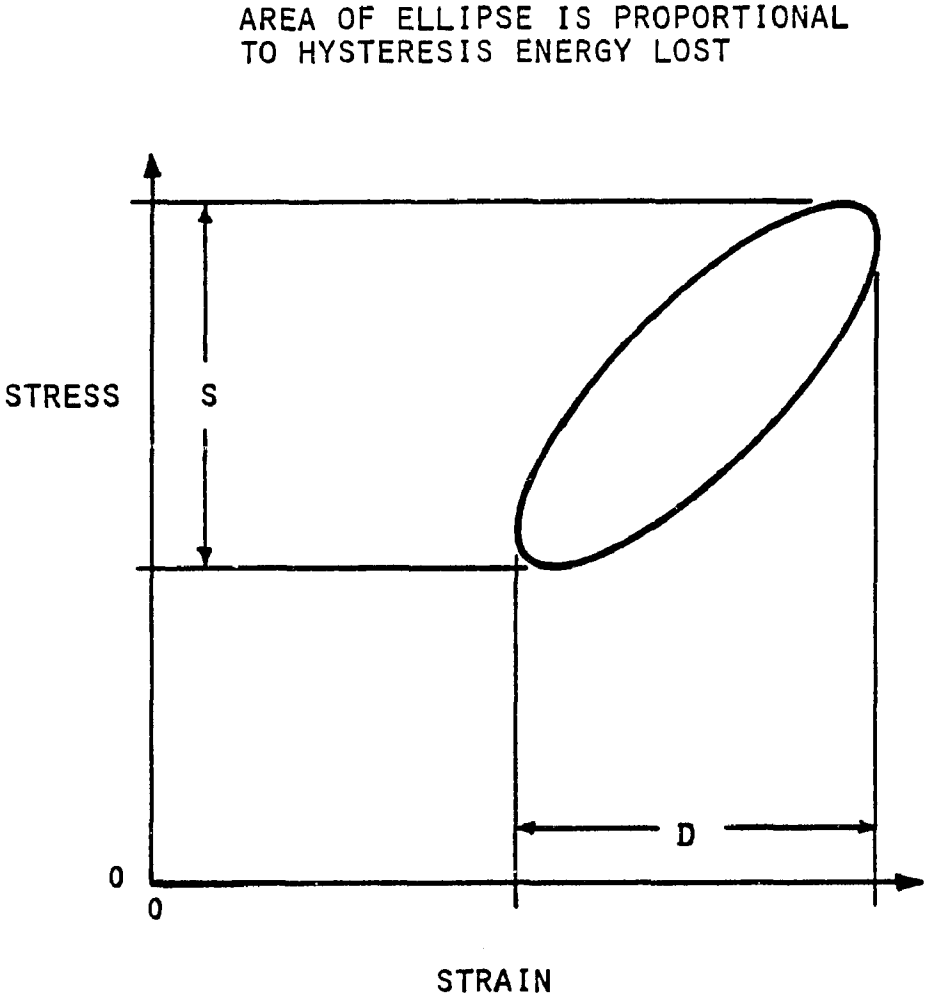
enclosed by the load and return curves on the stress-strain plot. For the Kelvin solid subjected to sinusoidal excitation, the hysteresis loop would have an elliptical shape as illustrated in Figure (2.4).

2.1.3. Characteristics of Filled Rubber

When considering filled rubber, there are clear departures from the behavior of pure-gum rubber. This has been noted in various publications, including Mullins [4,5], Treloar [6], and Cooper [7].

One of the most obvious departures from the linear viscoelastic behavior of pure-gum rubber is the Mullins effect, which is illustrated in Figure (2.5). This figure shows a hysteretic effect for carbon-filled rubber which did not appear in studies of pure-gum rubber. The Mullins effect is the softening of carbon-filled rubber due to initial deformation. After rubber has been loaded with filler, whether it has been vulcanized or not, it will be stiffer than the pure-gum. However, while such rubber always retains some of this increased stiffness, some stiffness is permanently lost with the first application of a given load or deformation.

Bueche [8,9], who originally published Figure (2.5), has explained the Mullins effect based on his model of bonds rupturing between filler particles and rubber molecules. In the figure, a specimen of carbon-filled



D = AMPLITUDE OF STRAIN CYCLE

S = AMPLITUDE OF STRESS CYCLE

Figure (2.4) Typical hysteresis loop in dynamic stress-strain cycles

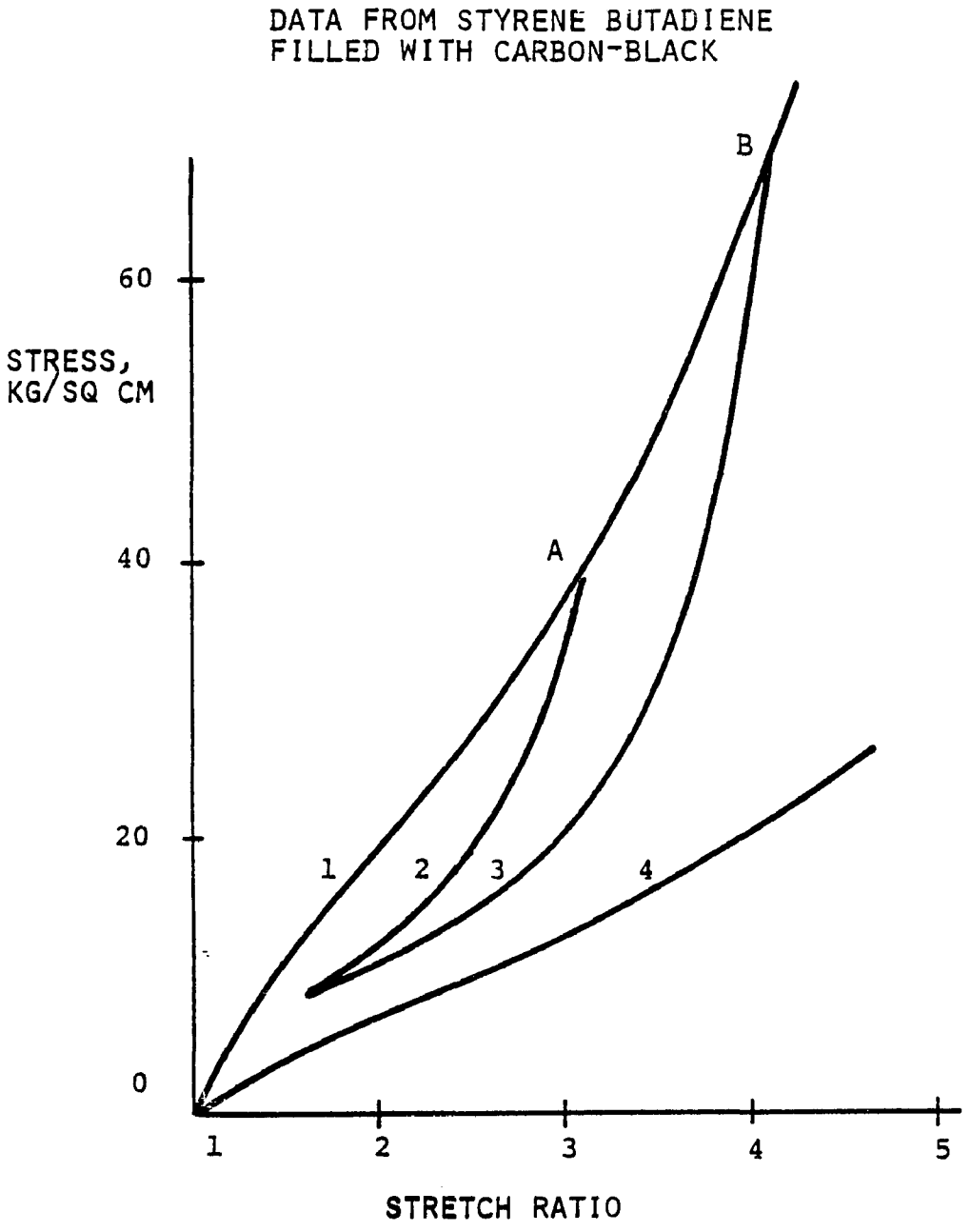


Figure (2.5) Mullins effect from Bueche [8]

butyl rubber was loaded along Curve 1 to Point A. The specimen unloaded along Curve 2. The sample was then reloaded and followed Curve 2 to Point A (approximately), then proceeded to Point B along the curve shown. From Point B the material was unloaded and followed Curve 3. When reloaded, Curve 3 was followed up (approximately) to Point B and beyond, as shown. Bueche then says the load was removed and the specimen was allowed to relax; this is not shown. There is no mention of the maximum deformation applied nor the final relaxed length as compared to the initial length. However, when the specimen was reloaded, Bueche claimed it followed the Curve 4, which is clearly lower than the initial loading curve.

Another feature of the behavior of carbon-filled rubber is the change of the load-deflection curve upon cycling between fixed deflection limits or fixed force limits. Thus, specimens are often "preconditioned" before data is taken from cyclic tests. The initial load-deflection curve may be considered transient, and, after several cycles, a steady-state curve is attained. Such a curve is repeatable and, generally, data reported in the literature comes from preconditioned samples. Figure (2.6) shows an initial curve from zero deflection to 100% elongation, and a loop on the same scale, after 10 cycles at fixed strain limits, for two rubber samples [10]. The shape of the curve changes after the first few cycles so there is less force generated at a

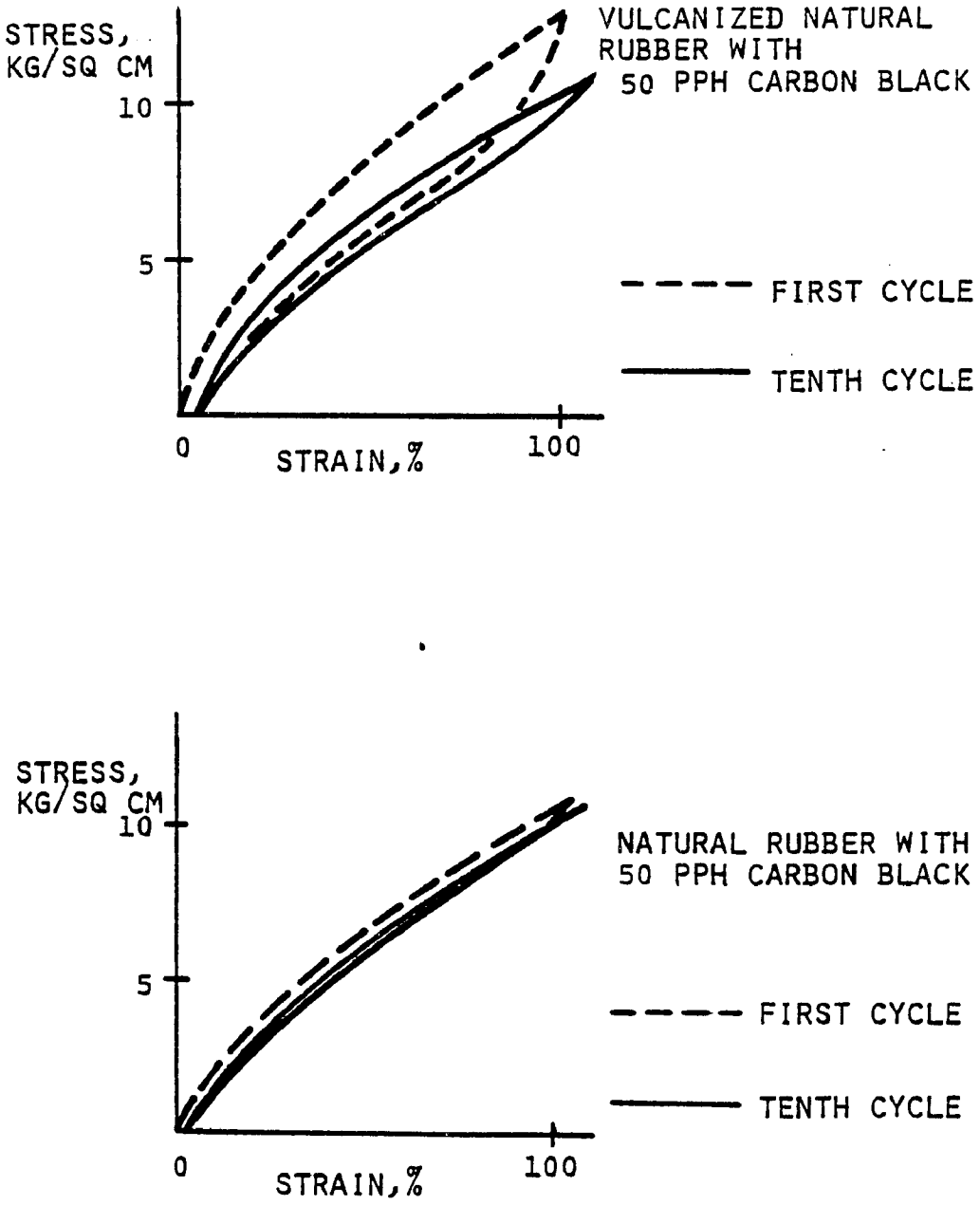


Figure (2.6) Change in load deflection curve when cycling, from [10].

given strain for each curve. In addition to the general shape change and the lowering of the force limits, the enclosed area is smaller. This enclosed area is proportional to the energy lost per cycle per unit of volume. The curves are also very dependent on whether the rubber is vulcanized or not.

In addition to this quasi-static hysteresis due to the filler in the rubber, the dynamic properties of rubber also appear to be altered by the presence of the filler. Recent studies [11] have shown that the low strain oscillatory properties of carbon-black reinforced elastomers are dependent upon the strain amplitude. Since unfilled rubber shows very little change of dynamic properties with amplitude, the behavior of carbon-black filled elastomer has been ascribed to a change in the three-dimensional aggregate structure. This change, which is due to the mechanical work applied to the structure, is called a thixotropic breakdown.

While thixotropic phenomena are a source of mechanical energy loss, this is not the source of loss in a linear viscoelastic medium. A viscoelastic medium is one having rate dependent material properties or some form of strain-history dependent response. Losses occurring in such a media can be attributed to the stress and strain being out-of-phase due to viscosity in the system. A substance

with viscosity would have loss dependent on strain rate or frequency. This will be discussed further in Chapter 3.

If the response of a particular system is assumed to have a particular form, such as linear viscoelastic response, an experiment can give values to parameters in the constitutive relation. The values obtained from experiments can be examined to assess the value of the assumed constitutive relation. For example, in an experiment where viscoelastic tape is applied to a metal beam to dampen vibrations in the beam [12], experiments and viscoelastic computations agree very well.

Most reported experimental results for rubber have used some form of viscoelastic constitutive relation. An experimental program by Gehman, Woodford, and Stambaugh [13] used the Kelvin solid to model the behavior of pure-gum rubber and also filled rubber. The experiments were run at a constant frequency, but the mass of the system was varied. The results for the pure-gum experiments agreed with the theory quite well, but the data for carbon-filled rubber did not match the predictions.

A similar experiment was carried out by Cooper [7]. He used only carbon-filled rubber samples but used several rubber compounds. He maintained the mass of the system constant and ran compressive vibration tests in which he varied the frequency. The experiments were designed to

measure the viscous damping coefficient, spring rate, and frequency response as a function of carbon-black content of the compounds. Cooper assumed the materials could be adequately modeled by a Kelvin solid. Figure (2.7) shows his results for one sample. Comparing the curves in Figures (2.3) and (2.7), the inadequacy of the theory to model the behavior of the physical system can be noted. Also, comparing the loop in Figure (2.8) with the loop in Figure (2.4), further inadequacy of the model can be seen. The transmissibility plot in Figure (2.7) shows the "soft resonance" frequency response which is typical of system in which the stiffness decreases with the amplitude of the deformation. However, it is known that the stiffness of rubber increases with amplitude in compression.

Den Hartog [3] has discussed systems which have amplitude effects. He noted that when stiffness decreases with amplitude, the resonance plot bends towards the amplitude axis, as was seen in Figure (2.7). When the stiffness of the system increases with amplitude, as rubber does in compression, the plot should bend away from the amplitude axis. In a third analysis, for systems with dry friction, Den Hartog showed the transmissibility plot is similar to that of a system which is nonlinearly elastic and has a soft resonance behavior. However, he suggested a method of using an equivalent viscous friction to simplify the solution of dynamics problems where dry friction is

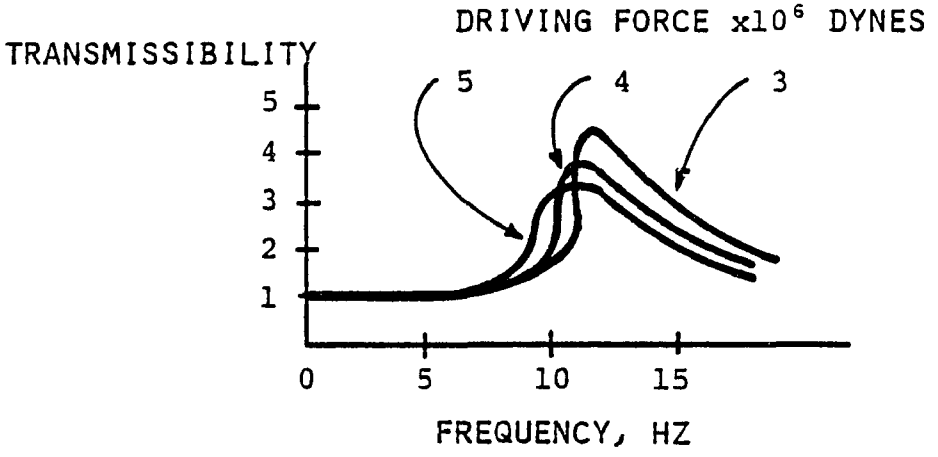


Figure (2.7) Transmissibility curve for filled natural rubber

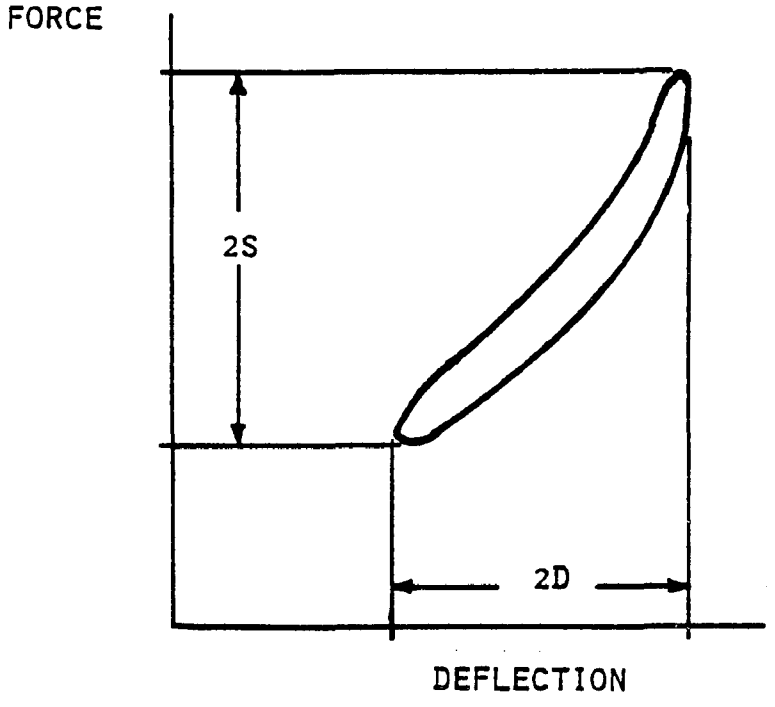


Figure (2.8) Actual dynamic hysteresis loop for filled natural rubber, 52 pph carbon-black, from Cooper [7]

present. Above the resonance peak, it is very difficult to distinguish between dry friction response and viscous friction response.

When Cooper assumed that his samples were linearly viscoelastic, he was able to use the area of the dynamic hysteresis loop to compute an equivalent viscous damping coefficient. Although the loops were not ellipses, the coefficient was computed to give the same damping. The resulting coefficient was not a constant as the viscoelastic analysis would require, but was a function of the frequency. The product of the frequency and the computed coefficient was found to be a constant. Cooper did not notice this is the expected result if the method he used was applied to a system with dry friction damping.

The gross behavior of rubber is obviously affected by the presence of carbon-black filler and by vulcanization. The pure-gum rubber is characterized by a large deformation before fracture and some fluid-like properties. The use of filler and vulcanization enhances the elastic behavior of the material and dimishes its fluid behavior. The next section will show how the microstructure of rubber gives it these material properties.

2.2. Some Microscopic Properties of Rubber

2.2.1. Macromolecular Behavior

Rubber owes most of its peculiar mechanical behavior to its molecular construction. Rubber and plastics consist

of a number of small molecules, called mers, which are chemically linked into huge chains to form a polymer or macromolecule. This molecular structure endows rubber with a mechanical behavior grossly different from that of metals, crystals, or other engineering materials.

Most of the observed viscoelastic properties of pure-gum rubber are due to entanglements, the snarling or intertwining of the macromolecules which hinders their relative motion. Material properties may be adjusted within some limits by use of vulcanization, fillers, or copolymers.

Entanglements prevent pure-gum rubber from behaving as a liquid. These entanglements are what distinguish "rubber" from other polymers or plastics. Such a polymer molecule can travel only a limited distance before being slowed or stopped by a section of another molecule. With additional applied force or after sufficient time, the entanglement may slip, or loosen, allowing the polymer chain to continue its motion.

This is illustrated in Figure (2.9) where sections of a creep compliance curve are labeled with the predominant mechanisms for the observed deformations. The mechanical properties of unvulcanized rubber can be attributed to entanglements holding the molecules together for short times, molecules slipping between entanglements at moderate times, and entanglements slipping at long times. However, over a long period of time the stressed material obtains a new

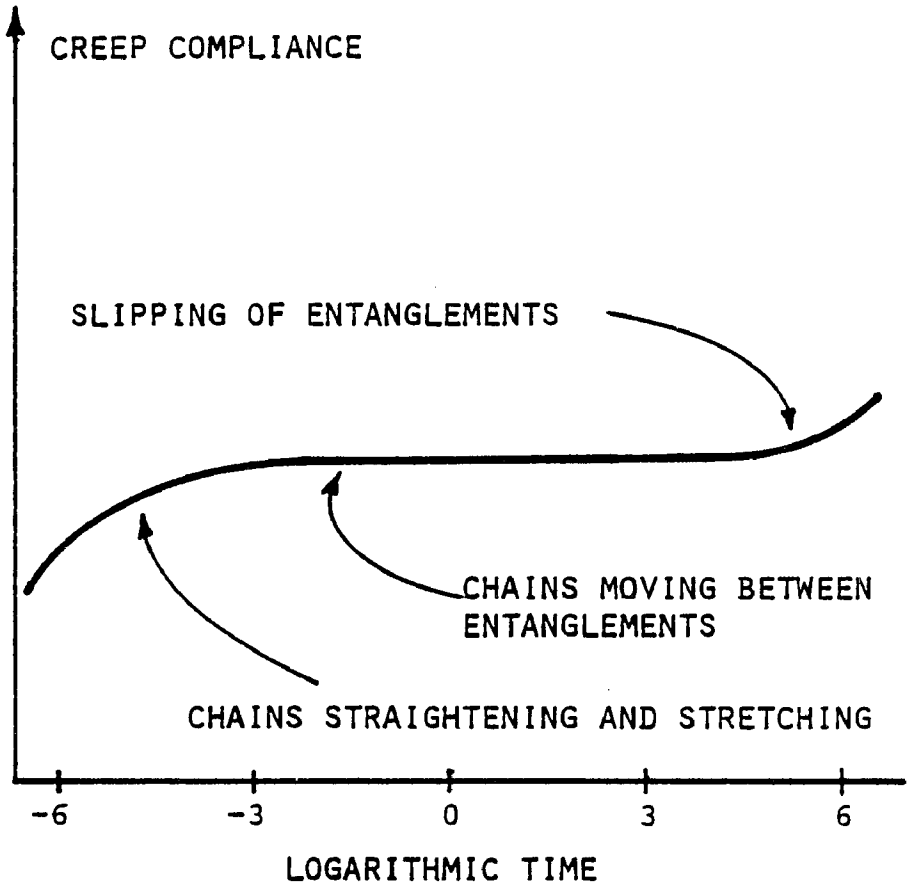


Figure (2.9) Relationship of entanglements to creep compliance

equilibrium configuration and will not return to its original configuration when the stress is removed. There are current investigations of the viscoplastic behavior of such materials, some of which will be discussed later.

The elastic properties of rubber are greatly enhanced by vulcanization, a process for stabilizing rubber structures. In this process, permanent bonds, called cross-links, are formed between chains by a chemical reaction. A vulcanizing agent, such as sulphur, is added to the polymer, and a filler, such as carbon, may be mixed into the compound at the same time. The rubber is then molded and heated. Cross-links are formed when the adjacent chains are chemically joined. Cross-links are responsible for most of the elastic behavior, since pure-gum rubber, which does not have these cross-links, will flow.

Cross-links often form at sites of entanglements in the pure gum. However, not all entanglements are chemically linked; some remain free in the material and some become trapped in the structure as illustrated in Figure (2.10). The amount of cross-linking can be varied by adjusting the length of time the rubber is heated and the amount of vulcanizing material added, while the number of entanglements in the rubber remains fairly constant.

Figure (2.11) shows the qualitative effects on some measure of elastic modulus of rubber due to increasing the number of cross-links. For low levels of cross-linking, most of the elasticity is due to trapped entanglements. With

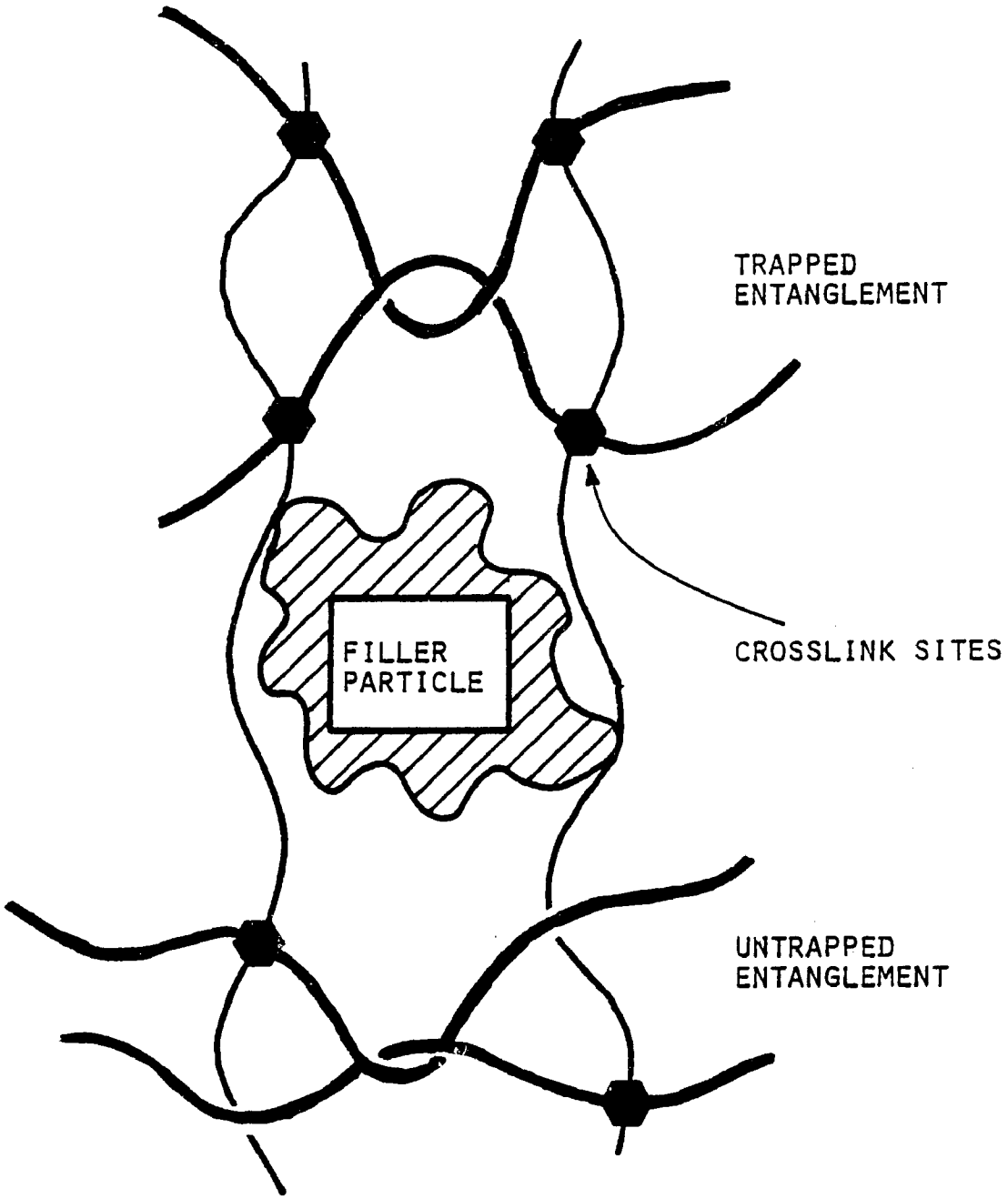


Figure (2.10) Illustration of entanglements and crosslinks

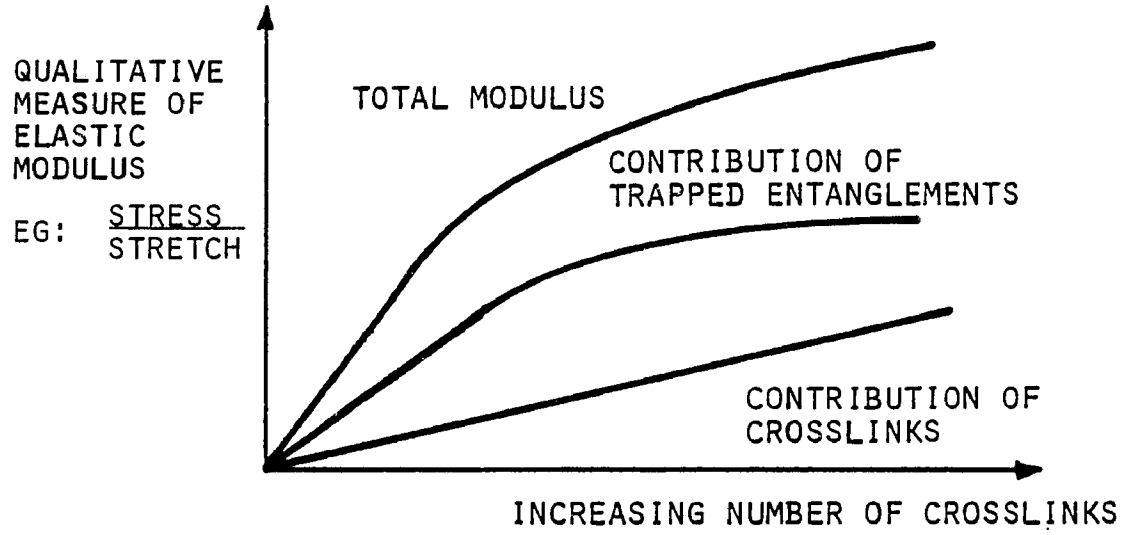


Figure (2.11) Effect of vulcanization on elastic modulus

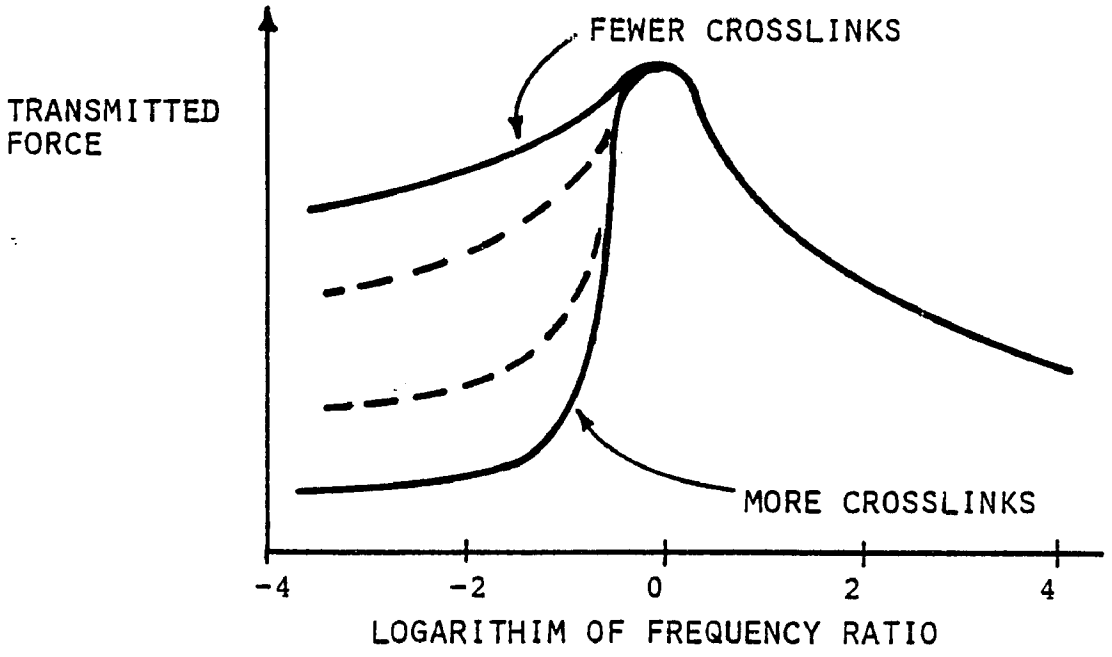


Figure (2.12) Effect of vulcanization on transmitted force

more vulcanization the contribution of entanglements levels off while elasticity due to cross-links continues to increase.

The effect of cross-links and entanglements on the dynamic response of rubber is complicated. Consider the response of a rubber specimen to sinusoidal excitation. Figure (2.12) gives a qualitative display of the decrease in transmitted force at low frequency due to increased vulcanization. As the number of cross-links increases, the plot looks more like the soft resonance observed by Cooper. With relatively more entanglements, the plot is similar to a resonance curve for an ideal viscoelastic material. The frequency axis is normalized to the natural frequency of the sample, but this frequency moves higher, due to a higher modulus, as the number of cross-links increases.

The modulus of rubber can be increased by fillers, as well as by vulcanization. It is well known from theories of composite materials that addition of stiff fibers or filler particles to a softer material will cause the resultant material to be considerably stiffer at a relatively low cost. Thus, carbon-black filler, when added to pure-gum rubber which is then vulcanized, will become mechanically bonded into the material matrix and strengthen the resultant composite. This is shown in Figure (2.10). This carbon-black filler in rubber also affects other properties of the material, such as heat conduction and loss

properties. The Mullins effect referred to above and the amplitude dependence of transmissibility noted by Cooper are primarily due to the presence of carbon-black fillers.

The properties of rubber may be altered by the addition of fillers or by vulcanization. Although the model to be presented in Chapter 4 does not deal with the source of the material properties, there is one more basic parameter which affects the material properties. This is the presence of copolymers, that is, more than one mer in a single macromolecular chain. The specific changes incurred depend on the chemical properties of the component mers and the manner in which they combine in the structure of the macromolecule. In order to provide a more complete background, the basic structures of copolymers will be mentioned.

Copolymers can be random, block, or graft. Random copolymers are formed by mixing different mers before polymerizing them into chains, thus forming macromolecules with two or more mers appearing randomly along the polymer chains. Block copolymers are usually formed by polymerizing a limited amount of a single type of mer, then adding a different type of mer and starting another polymerization reaction. This operation is repeated many times producing a macromolecular material with blocks of two or more polymers connected in a single chain. A graft copolymer is formed by mixing a second type of mer into the solution of an already completed polymer reaction, and then starting a new

reaction such that the new mers graft themselves onto the sides of already existing polymer chains.

2.2.2. Basic Models

A number of models are available for various aspects of rubber elasticity. Some results of these models, but not the detailed developments, are discussed below.

Gaussian statistics produces a model for rubber elasticity which fits data in compression but deviates from rubber behavior in tension. A model derived by James and Guth [14], which uses the inverse Langevin function, accounts for the fact that single chains could not have their ends displaced by more than the chain length; this produces a model which stiffens in tension as rubber really does. The deformation in a macromolecular structure is not homogeneous throughout the material. Treloar [6] further extended the above statistical models to include effects of random chain molecules deforming more or less than the average deformation of the material as a whole, calling this his non-affine deformation model. The results of these models are compared in Figure (2.13).

For these models to be used in solving engineering problems, they should be incorporated into the framework of solid mechanics and the theory of elasticity. Many references could be cited for this framework; one appropriate work is the development of Fung [15]. The use of the strain energy function below follows the discussion of Fung.

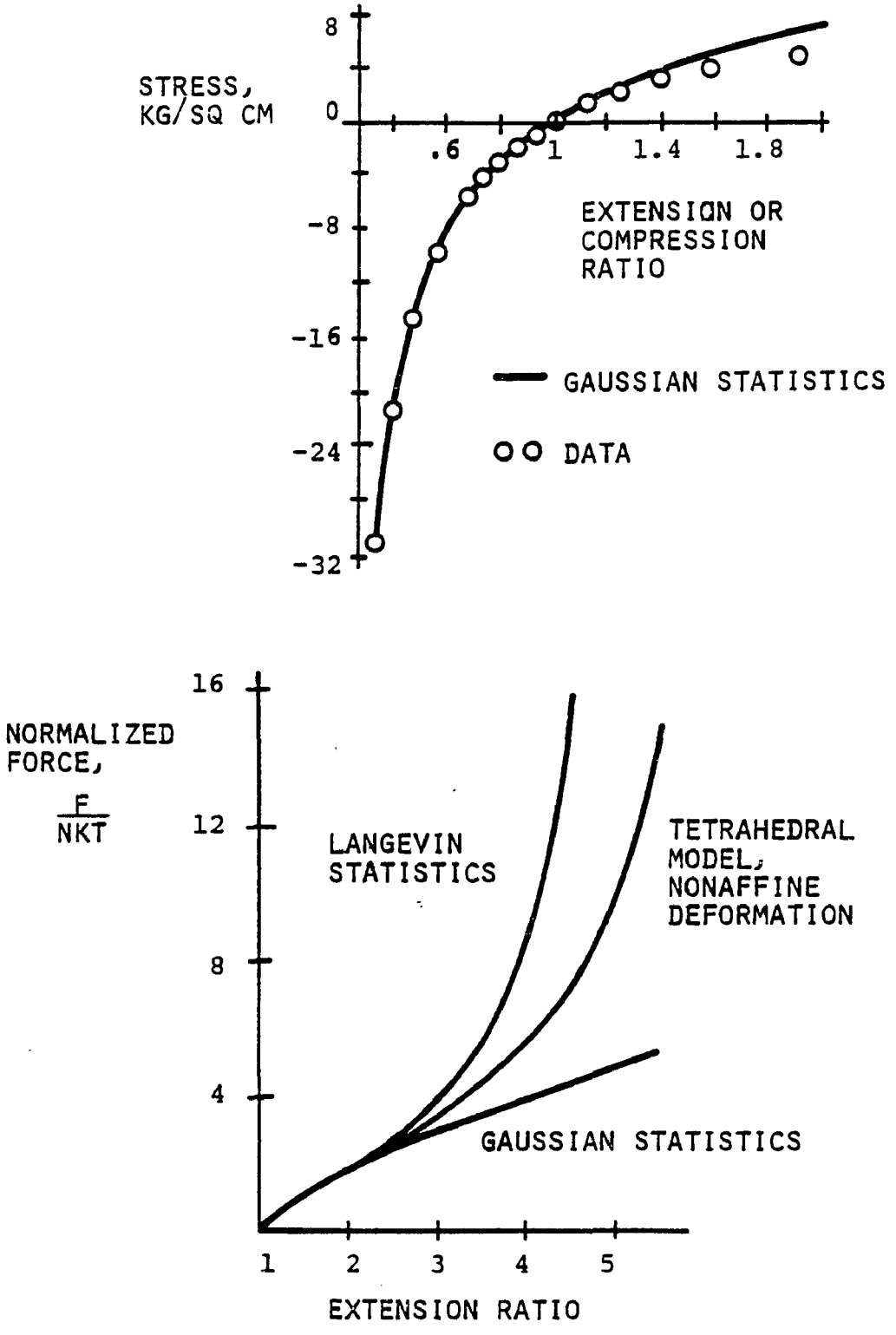


Figure (2.13) Comparison of various statistical models for rubber elasticity

In the theory of elasticity, the existence of a strain-energy function allows the formation of a constitutive equation for calculation of stresses or strains. Mooney [16] proposed such a function for rubber based on the first and second invariants of strain and assuming incompressibility for rubber. This formulation matches the behavior of rubber better than the Gaussian model. The Mooney model has a strain energy function:

$$W = C_1(I_1 - 3) + C_2(I_2 - 3) \tag{2.1}$$

where

W = strain energy

I_1, I_2 = first and second strain invariants

C_1, C_2 = constants

From their experiments, Rivlin and Saunders [17] suggested a form which fit their data better:

$$W = C_1(I_1 - 3) + \Phi(I_2 - 3) \tag{2.2}$$

where

$\Phi(I_2 - 3)$ = a decreasing function of I_2.

However, these are models for rubber elasticity, which implies they ignore any hysteresis effects, as well as time, frequency, or temperature effects. Bychawski [18], who is interested in stresses and dissipated power, has attempted to use a dissipative potential for large deformations of membranes. Bychawski developed a theory where power is derivable from two potentials, one dependent on strain rate and the other on stress state. An incompressible material must be able to generate a hydrostatic stress when there

is no strain and, hence, no work. However, with Bychawski's theory, cyclic hydrostatic pressure can do work and, thus, dissipate power in the material, even if the material is assumed to be incompressible. However, the specific form of his functions must be determined from the known properties of the materials. Thus, the problem of characterizing the material in terms of specific functions remains.

The theories presented above characterize some properties of the system of interest but are insufficient to handle hysteretic loss. While viscoelastic theory can handle this type of loss problem, most problems solved in the literature assume simple stress states and linear viscoelasticity. Problems involving nonlinear materials have experimental and mathematical complications which increase the difficulty in obtaining analytical solutions.

CHAPTER 3

VISCOELASTIC MODELS FOR RUBBER

3.1. Linear Viscoelasticity

3.1.1. Requirements for Linear Theory

Viscoelasticity of rubber, mentioned above, will be more formally presented in this section. A viscoelastic material is sometimes considered to be a solid which has the properties of a spring-dashpot system. However, in this paper any time dependent material behavior will indicate a viscoelastic material.

At least three definitions for viscoelastic materials are commonly used in the literature of mechanics. First, linear viscoelastic materials are those which exhibit strain and strain-rate dependent material behavior and satisfy the scaling and superposition relations defined below. Such conditions imply dependence on strain history. Second, viscoelastic materials may exhibit strain and strain-rate dependent behavior but need not fulfill scaling and superposition. If the material specifically does not fulfill the requirements, then it is nonlinearly viscoelastic. Third, hysteretic materials, which need not be viscoelastic, require only that the material dissipate mechanical energy but do not require strain-rate dependent material properties. This last term encompasses all materials of the previous classes as well.

Consider first a linear viscoelastic material. Such a material will have a response to some stimulus. If the stimulus were increased or decreased by some factor, the response would similarly be increased or decreased by the same factor. This property is called scaling, which requires that, given:

$$s(t) = F[e(t)] \tag{3.1}$$

where

$s(t)$ = a stress history

$e(t)$ = a strain history

$F[\ ]$ = a constitutive functional

c = a constant

then

$$cs(t) = F[ce(t)] \tag{3.2}$$

The second requirement for linearity is superposition. For this to hold, the response to any combination of stimuli must be the sum of the responses to the individual stimuli. Superposition requires that, if given:

$$s_1(t) = F[e_1(t)] \tag{3.3}$$

$$s_2(t) = F[e_2(t)] \tag{3.4}$$

where

$s_1(t), s_2(t)$ = two stress histories

$e_1(t), e_2(t)$ = two strain histories

$F[\ ]$ = a constitutive functional

then

$$s_1(t) + s_2(t) = F[e_1(t) + e_2(t)] \tag{3.5}$$

These conditions for linearity, scaling, and superposition are often not too restrictive to make some valid predictions. Creep compliance and relaxation modulus rely on scaling for their definition. In addition, these assumptions do not restrict the temperature dependence of the material properties.

3.1.2. Thermorheological Properties

Some viscoelastic properties of materials can be related to the thermal motions of the molecular structure. The actual motion of sections of the polymer can be related to the probability that the energy of the section exceeds some value. This probability is affected by the strain energy of the material but also by its thermal energy. As the ambient temperature is reduced, thermal motions become slower and the response to stress changes becomes more sluggish so the rubber appears stiffer, that is, its modulus increases. At sufficiently low temperatures little molecular motion occurs, and the behavior resembles that of a stiff, brittle glass in which the deformation is due largely to straining of interatomic bonds.

The relative magnitude of the strain induced molecular velocities and thermal velocities is important in determining the stiffness of the system. Williams, Landel, and Ferry [19] offered a temperature/strain-rate equivalence relation. This is the well known W-L-F relation which shows

quantitatively how the temperature affects the time dependence of material properties in a polymeric material. Use of the W-L-F relation allows the construction of a stiffness versus frequency plot for sinusoidal oscillations in a short amount of real time by running tests at different temperatures. This construction is illustrated in Figure (3.1). A material which behaves in this way is said to be thermorheologically simple.

3.1.3. Sinusoidal Vibrations

Next consider application of a sinusoidally varying stress to a linear viscoelastic material. The strain will vary sinusoidally also but, due to the viscosity of the system, it will lag behind the applied stress. The stress can be considered to be the sum of an elastic stress which is in-phase with the strain and a viscous stress which is out-of-phase with the strain. The elastic and viscous stress components can be considered as corresponding to two separate moduli, so that the effective elastic compliance can be thought of as a complex compliance:

$$E^* = E' + iE'' \; ; \; i = \sqrt{-1} \tag{3.6}$$

made up of an elastic, in-phase component E' and a viscous, out-of-phase component E". The phase angle between stress and strain is related to the magnitude of these two components by the relation:

$$\tan \theta = \frac{E''}{E'} \tag{3.7}$$

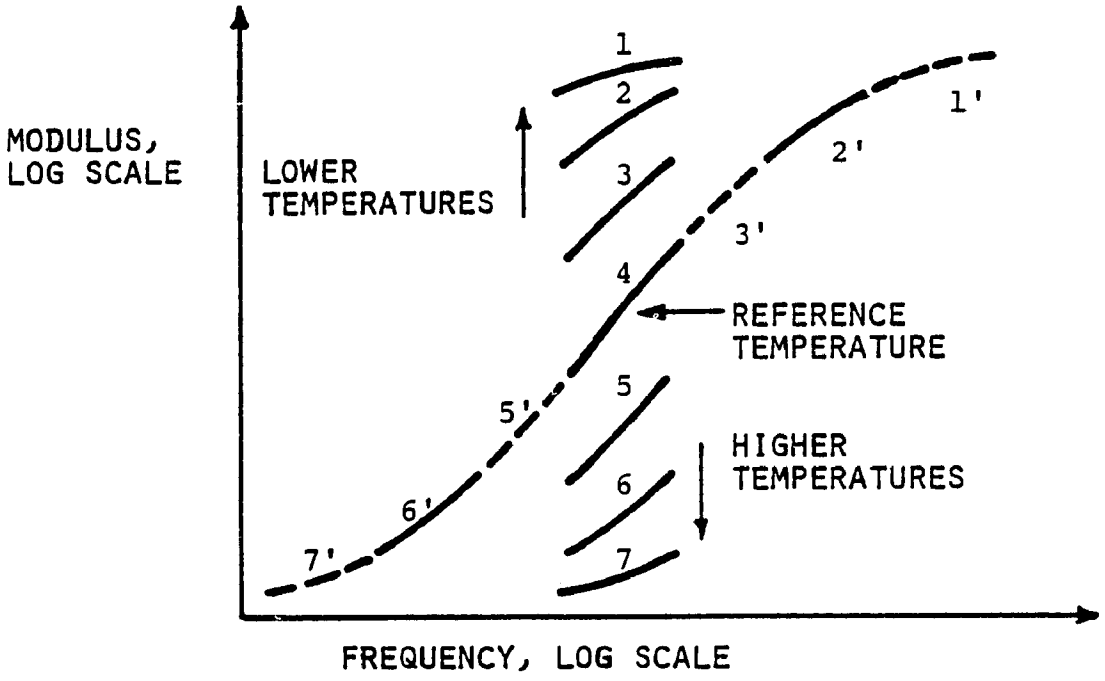


Figure (3.1) Construction of temperature-frequency master curve

Corresponding to the complex compliance E* is also a complex shear modulus:

$$G^* = G' + iG'' \; ; \; i = \sqrt{-1} \tag{3.8}$$

The stress-strain plot for such a material for sinusoidal vibrations is an ellipse as illustrated earlier in Figure (2.4). The area of this loop corresponds to the amount of energy lost per cycle:

$$\text{Energy loss per cycle} = \text{area of ellipse} = \pi \sin\theta \; S \; D \tag{3.9}$$

where

S = amplitude of the total stress cycle

D = amplitude of the total strain cycle

This equation allows θ to be calculated from the stress-strain plot of an experiment. The next graph, Figure (3.2), shows the way that the elastic modulus, loss modulus, and $\tan\theta$ vary with frequency. These data were taken over a wide temperature range, then reduced by a temperature/strain-rate transformation to show frequency effects at constant temperature. Regions where various mechanisms are prevalent are labeled.

Consider a system with an oscillating stress which gives rise to an oscillating strain. The work which must be supplied by an outside source of energy is:

$$W = \int dw = \int s\dot{e} \, dt \tag{3.10}$$

Some of this work is recoverable and some is dissipated as heat in the material. Upon one complete cycle or over one

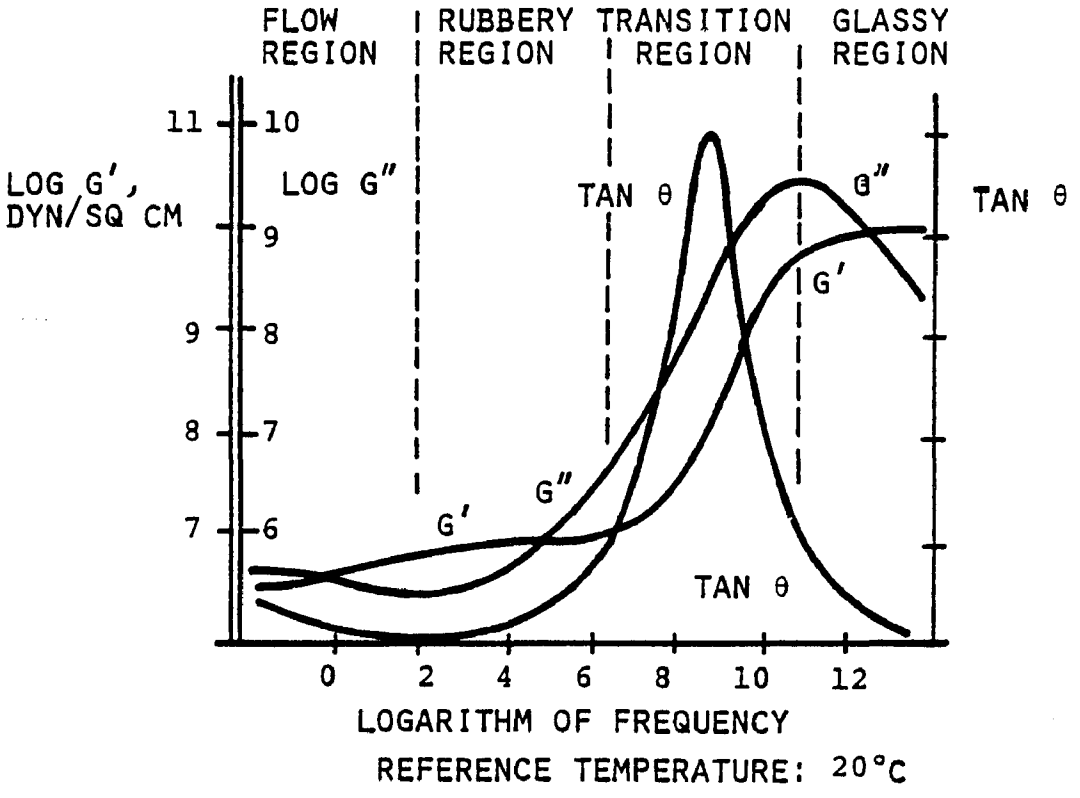


Figure (3.2) Master curve of moduli and loss tangent for unvulcanized natural rubber

period of oscillation, the result of the integral will be the energy loss. Let:

$$s(t) = s_0 \cos \Omega t \tag{3.11}$$

$$e(t) = s_0 [E'(\Omega) \cos \Omega t - E''(\Omega) \sin \Omega t] \tag{3.12}$$

Then:

$$W = - s_0^2 \Omega \int \cos \Omega t \, [E' \sin \Omega t + E'' \cos \Omega t] \, dt \tag{3.13}$$

Over one period of time this becomes:

$$\text{Loss/Cycle} = - s_0^2 \Omega \, E'' \frac{\pi}{\Omega} = -\pi s_0^2 E'' \tag{3.14}$$

Thus, the amount of work per cycle is the same function of frequency as $E''(\Omega)$. Also, for the dissipated energy to be non-negative as required by the second law of thermodynamics, E" must be negative or zero for all frequencies.

Linear viscoelasticity offers some insights to the forms of E". For the Kelvin solid which was shown in Figure (2.3), the functional form of $E''(\Omega)$ is:

$$E''(\Omega) = - \frac{a\Omega}{b + c\Omega^2} \tag{3.15}$$

where a, b, and c are coefficients which can be found from standard viscoelastic analysis such as that by Flügge [1]. Thus, for the Kelvin solid, as Ω approaches 0 or as Ω approaches ∞, the loss per cycle goes to zero.

A Maxwell fluid is a model in which a spring and a dashpot are combined in series. Such a material would have a loss modulus:

$$E''(\Omega) = - \frac{a}{\Omega} \tag{3.16}$$

where a is another coefficient to be found from a viscoelastic analysis. Thus, as Ω approaches ∞, the loss per cycle goes to zero. However, the material behaves as a viscous fluid at slow rates and dissipates most of the input energy. When Ω approaches 0, the loss approaches ∞.

A three-parameter solid has a loss modulus of the form:

$$E''(\Omega) = - \frac{a}{b + c\Omega^2} \tag{3.17}$$

Although the coefficients may be numerically different, this has the same limiting behavior as the Kelvin solid. A three-parameter fluid has a loss modulus of the form:

$$E''(\Omega) = - \frac{a + \Omega^2}{b\Omega} \tag{3.18}$$

This gives the same limiting behavior as the Maxwell fluid.

Linear viscoelastic theory can be developed on the basis of combinations of the above models. For any combination resulting in a linear viscoelastic fluid, the limiting behavior will be the same as for the Maxwell fluid. For any combination resulting in a viscoelastic solid, the limiting behavior will be the same as for the Kelvin solid. For either case the loss goes to zero as the frequency goes to infinity. For the fluid the loss goes to infinity as the frequency goes to zero, while for the solid the loss goes to zero as the frequency goes to zero.

A number of papers [12, 20-24] have presented solutions to viscoelastic vibration problems. Some have included effects of thermomechanical coupling, since the dissipation of mechanical energy in the material appears as heat. This heating of the material can change the properties of the material considerably, permitting an equilibrium solution for some systems but material failure in others. The problems deal with purely sinusoidal excitation, at a constant frequency, of a meterial which is known to be linearly viscoelastic. The properties used in calculations were obtained from manufacturers' data or approximated data from the literature, and the materials were assumed to be thermorheologically simple.

There are two main problems with these solutions. First, they require complete information on the material properties' dependence on stress, strain, temperature, time, and frequency. Second, the resultant equations are highly nonlinear due to the coupling by the W-L-F relation of the wave equations and heat equations. These equations will then require efficient numerical computation techniques for solution. However, there are a number of cases where the material properties are known and techniques are available for solution. For example, properties for viscoelastic damping tapes are available from manufacturers, and the literature contains properties for many polymers.

It is generally accepted that unfilled rubber behaves in a linear viscoelastic fashion. Figure (3.3) shows two

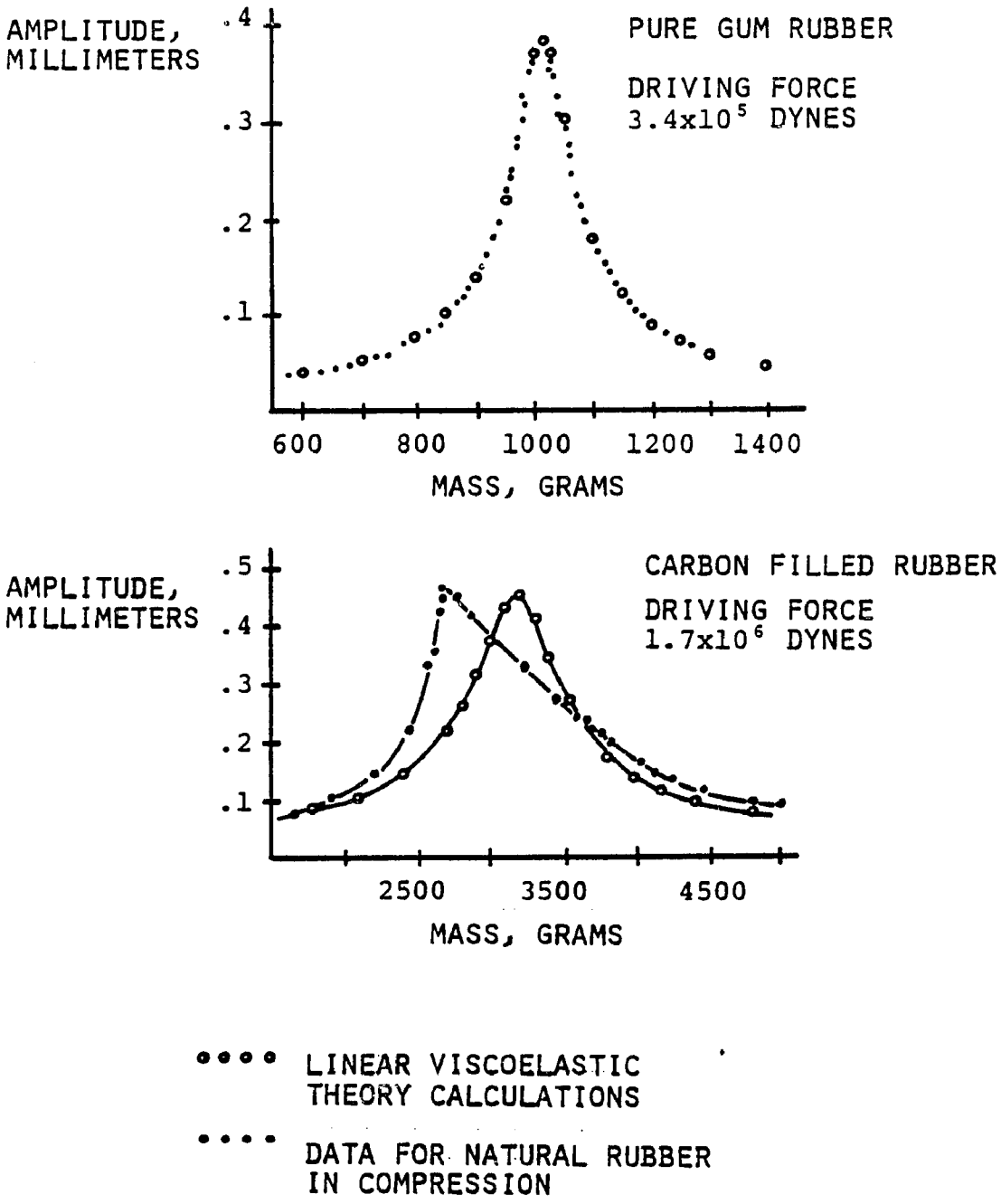


Figure (3.3) Comparison of viscoelastic theory and rubber behavior

figures from Gehman, Woodford, and Stambaugh [13]. Each graph compares the experimental behavior of a sample of rubber with the prediction of viscoelastic theory for a Kelvin solid. The experimental program compensated for mass effects by using a system mass much larger than the material mass. By varying the mass attached to the rubber sample, the material frequency of the system was changed, producing an effect equivalent to changing the frequency of oscillation. The first curve is for pure-gum rubber tested in compression. The fit with the points predicted by viscoelastic theory for the Kelvin solid is good. The second curve shows the data for carbon-filled rubber in compression varies from the prediction by the authors. The data shows the soft resonance discussed earlier but, above the resonance peak, viscoelastic theory can match the curve adequately. There is a strain-amplitude dependence in loss and modulus at larger strains, which has been noted by many authors. The analysis of vibration of filled rubber does not follow that of unfilled rubber due to this amplitude dependent behavior.

Carbon-black filled rubber appears to deviate from linear viscoelastic theory. Recalling the Mullins effect in filled rubber, it can be seen that superposition does not hold. Thus, if the appropriate properties of filled rubber could be cataloged, a vibration problem for filled rubber still could not be handled as a linear viscoelastic vibration problem.

3.2. Nonlinear Viscoelasticity

3.2.1. Basis of a Theory

Nonlinear viscoelasticity encompasses a great number of possible material behaviors. Some examples would be that stress-strain behavior is dependent on the maximum strain previously applied, the relaxation function is dependent on strain level, or the time-temperature-frequency relationship with stress is strain-amplitude dependent. Concepts from the linear theory may be applicable, but the relative simplicity of obtaining material properties no longer exists. If G*, E*, or relaxation functions are allowed to vary with strain amplitude, frequency, or temperature in an unrestricted fashion, they must be specified as tabulated numerical functions of the appropriate variables. These data may then be fitted to a curve or used directly in a numerical scheme. In addition, nonlinear viscoelasticity may include materials which are not thermorheologically simple. To check the applicability of the W-L-F relation, data must be taken at many frequencies and temperatures.

There is evidence that filled rubber is, in fact, such a nonlinear viscoelastic material. Payne [25] has noted that due to the amplitude dependent behavior of filled rubber, the analysis of vibration does not follow that of unfilled vulcanized rubber. Treloar [6] notes that if a dynamic modulus and a dynamic viscosity are assumed for

rubber, the modulus appears constant with frequency but the viscosity appears to decrease with frequency. This can be explained in terms of a distribution of relaxation times in the bulk material. However, both this modulus and viscosity depend on the amplitude of the vibration, the cause of which has not adequately been explained. There may exist transformations for amplitude dependence similar to the W-L-F equivalence relation. Such a relation would provide a method to handle the data. However, since it requires a large amount of data for transformation and is basically an empirical fit, it is still inadequate for the problem solution.

Other materials show nonlinear behavior, including asphaltic concrete, solid propellants, and some strain hardening metals. Nonlinear viscoelasticity is one theory which is being developed to explain such material behavior. Any new theory should be able to specify the measurements to be taken and to predict structural behavior from these material properties. Several new theories will be mentioned and the pros and cons of each briefly discussed.

3.2.2. Possible General Theories

Perhaps the simplest form of nonlinear material is one which possesses the scaling property but not the superposition property. Such a material will have a relaxation modulus independent of strain amplitude but may exhibit the Mullins effect.

This theory has been developed by Farris, Fitzgerald, and others [26-28] for mechanically degradable polymers, which are also called permanent memory materials. Materials to which this theory is applicable are asphaltic concrete and highly filled polymers, such as solid propellants and carbon-black filled rubber. Viscoelastic theories rely on material memory. Most integral viscoelastic theories used to date are based on the fading memory concept. Thus, recent events affect behavior more than distant past events.

Farris [28] feels there is sufficient evidence that all hysteresis effects and most of the viscoelastic behavior in permanent memory materials can be caused by the time dependent failure of the polymer on a molecular basis. A material with permanent memory will undergo a change in microstructure due to previous deformation history, this will affect the material properties for all subsequent deformations. His permanent memory theory assumes polymer chains are elastic and, once they fail, they permanently leave the distribution. Thus, the hysteretic behavior depends on the highest deflection experienced by the material.

This theory is a special case of a general cumulative damage theory applied to filled polymers which exhibit behavior not present in fading memory materials. Using a measure of maximum strain, Farris uses his theory to assess

damage in the filled polymers he models. This theory has the effect that a new material results each time a new strain maximum is reached, although the material properties are constant between changes. However, the developed theory is directed toward structural response to a few successively larger stress cycles. It provides little insight for a problem of vibrations at various levels of stress. Since material properties remain constant until a new maximum strain is obtained, repeated cycling at a single level requires only one set of properties.

Work by Derman, Bodner, and Partom [29] has dealt with similar materials and effects as have been discussed in this section. They call the materials anelastic and hold that there is an anelastic portion of the total applied stress that is responsible for energy loss, rate dependence of the moduli, and delayed elastic effects such as creep and recovery. This theory is also capable of handling plastic and viscoplastic deformations.

The technique of Derman, Bodner, and Partom requires numerical integration of governing differential equations over finite time steps. The computations use the equations of force balance and geometry, as well as the constitutive equations. Thus, nonlinear geometric effects are included with nonlinear material effects and the effects of deformation history. This model is directed toward low frequency or structural type problems. Since computations must be

performed over finite time steps, a great number of computations are necessary in order to accurately model high frequency vibrations. In their paper, computations are carried out at frequencies of less than 0.1 Hz.

These two theories above fit into a general frame free theory of simple materials proposed by Noll [30]. There are a number of other workers, using headings such as viscoplastic or dissipative materials, who are also looking at this concept as a general supporting theory for solid mechanics [31]. Using set theory the material element is described by a state variable which defines its position in space, its current condition, and the net effect of its history. The element also has a set of possible conditions in space with the associated processes which will carry the element to these new states. Topological rules provide that, as certain states are entered, other states become accessible only after a period of time. Thus, rate or time dependence can be included. Attainment of some states makes other states totally inaccessible; thus, permanent memory or damage effects can be incorporated.

The theoretical framework exists for general nonlinear viscoelasticity-viscoplasticity. The main problem with the theory is that it is developed to the point where an engineering problem solution is available only for simple cases or a few specific cases such as those mentioned above.

CHAPTER 4

PRESENTATION OF MODEL

4.1. Distributed Element Model for Hysteresis

4.1.1. Background of Hysteretic Model

Thus far, some available models for hysteresis in rubber have been discussed. Most are based on the fluid character of rubber and the statistical mechanics of the time and temperature behavior of the material. However, in filled, vulcanized rubber other mechanisms are present and may be dominant in certain types of loadings. The remainder of this dissertation will consider a hysteretic model for loss in rubber. This model simulates loss mechanisms, such as the breaking and reforming of cross-links under stress and the motion of long chain molecules around filler particles [32].

The model proposed is similar to one used in metal fatigue and structural damping but has been modified so as to be applicable to rubber hysteresis problems. Several of the nonlinear viscoelastic effects apparent in rubber can be explained by this model and, in addition, the model is directly applicable to nonsinusoidal vibrations. The amplitude dependent frequency response and the soft resonance behavior of rubber are direct consequences of this model.

The model is useful for problems where the above properties are observed in the physical system. This formulation, which has a physical basis, is generally simpler

to use for both data observation and problem solution than comparable viscoelastic models. However, while it is efficient in specific problems, no generality is implied for this model and some of its limitations are discussed in Chapter 6.

As early as 1940, Timoshenko [33] proposed that a nonlinear stress-strain curve might be modeled by a combination of elastic and plastic elements. Such a material model is equivalent to a mechanical system involving Couloumb friction. Den Hartog [3] has discussed vibrations of systems with nonlinear damping. Models using bilinear hysteresis have been used by Caughey [34-36] and others [37-39] to simulate damping in buildings and machinery on vibrating foundations. A study by Iwan [40] used such a model to study material dynamics and damping capabilities. Another application of this idea was Whiteman's study of the cumulative effects of fatigue in hysteretic materials [41].

In order to clarify some of the concepts, consider first the simple slip damper model in Figure (4.1). If we consider the power loss at the mass as its frictional force times its velocity, $\dot{y}(t)$, then for sufficiently slow rates of ths system, $(\dot{x}(t))$, and small displacements $(x(t))$, the mass never moves and there is no power loss.

For some range of velocities, the mass will undergo a stick-slip motion where the power loss is almost independent of $\dot{x}(t)$ since the velocity of the mass will be determined by μ, m, and K. For a higher speed range, the mass will slip

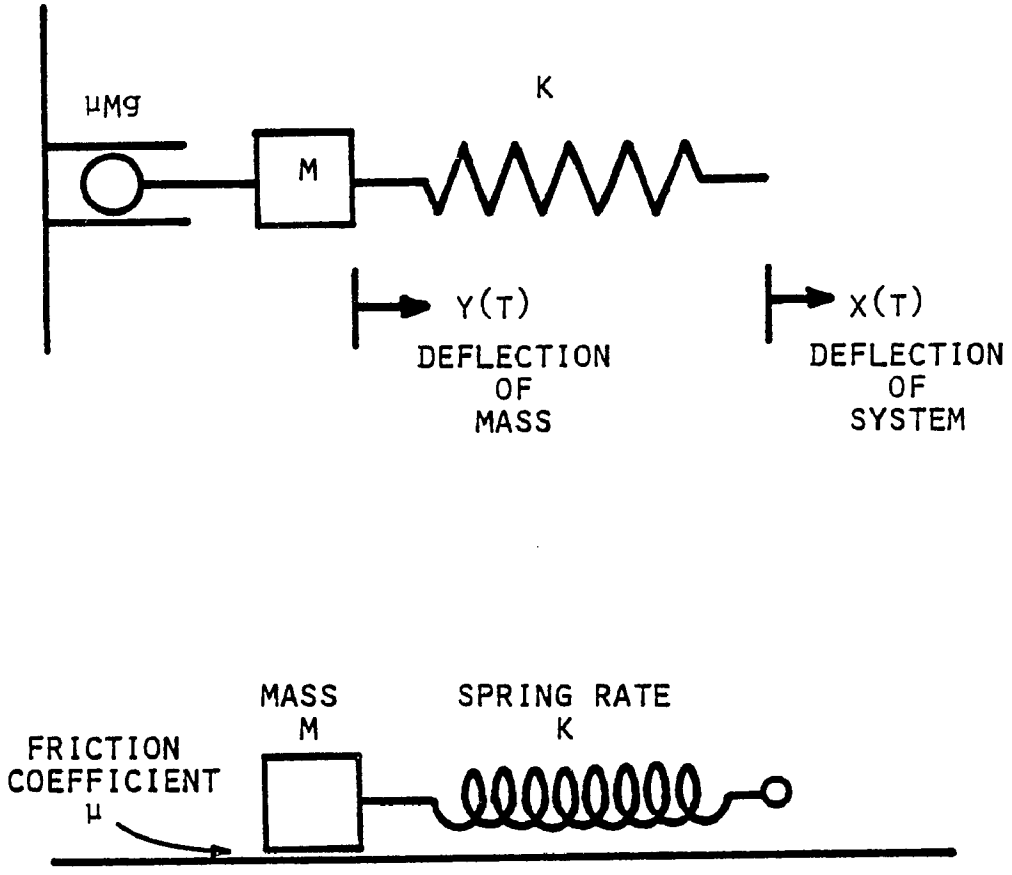


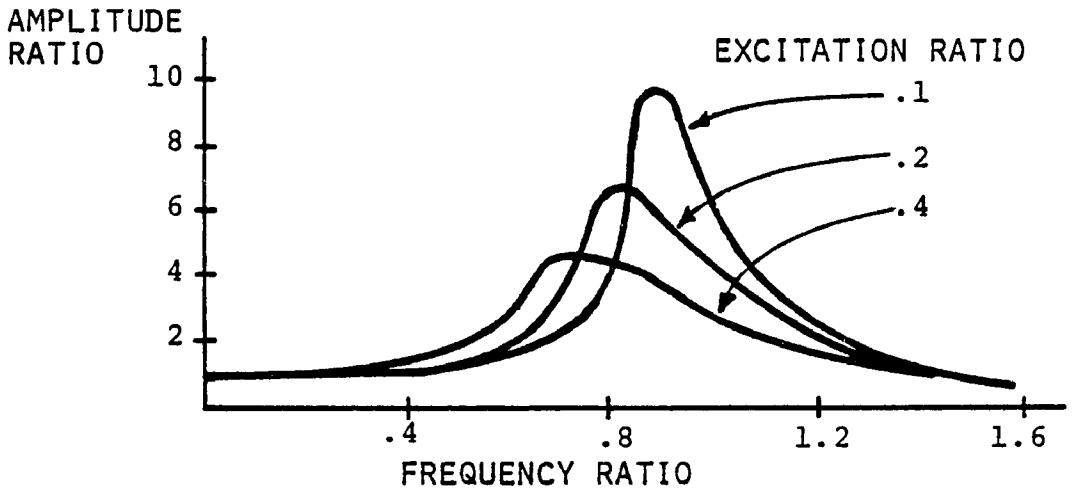
Figure (4.1) Simple slip-damper model

constantly and will have a power loss highly dependent on $\dot{x}$. In the context of a vibration problem discussed by Den Hartog, for frequencies below some critical value the motion is indeterminant due to the stick-slip type motion, but above this frequency a resonant behavior is observed.

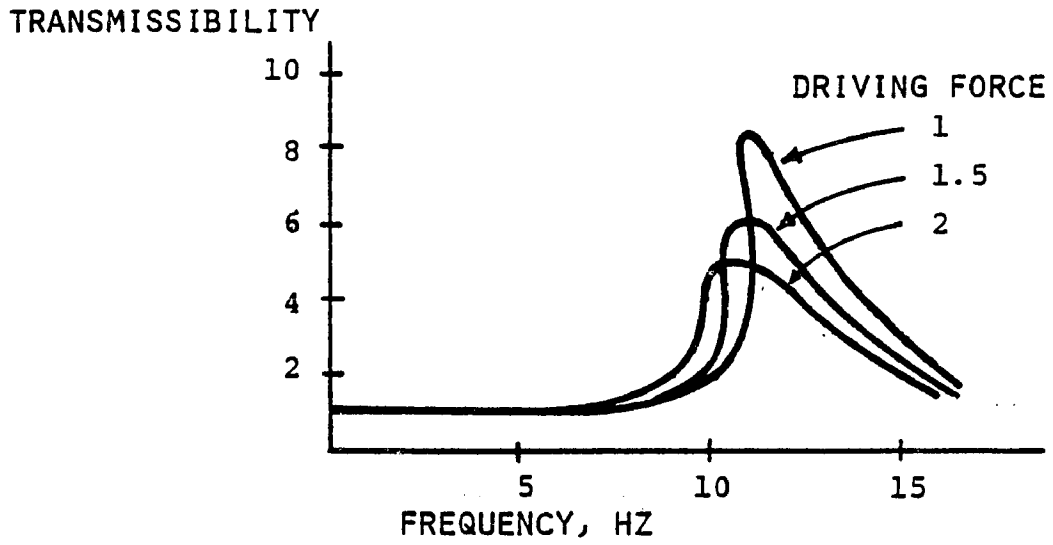
The studies by Caughey and Iwan dealt with the vibratory behavior of such mechanical systems. One model used by Iwan is of particular interest. The system was a hypothetical distribution of elastic-plastic elements for which resonance plots were obtained by the method of slowly varying parameters. The data from Iwan is plotted in Figure (4.2) below. It is to be compared with the data taken by Cooper for rubber, which was shown earlier but is shown again in Figure (4.2). Thus, most experiments cannot separate material, time dependent behavior from mass effects. With appropriate experimental design, one effect can often be made negligible with respect to the other. However, test results can be interpreted in terms of viscoelastic theory even when mass effects are not negligible. Similarly, some of the observed properties of vulcanized, carbon-filled rubber may be modeled by the dynamics of a hysteretic system.

4.1.2. Basic Analysis

A Jenkins element is a linear spring attached to a Couloumb friction damper. The behavior of a Jenkins element is shown in Figure (4.3). A parallel combination of Jenkins elements would give an initial linear stress-strain plot



Response of Iwan Model [40]



Data from Cooper [7] for a rubber block in compression

Figure (4.2) Comparison of Iwan's model with Cooper's data from rubber

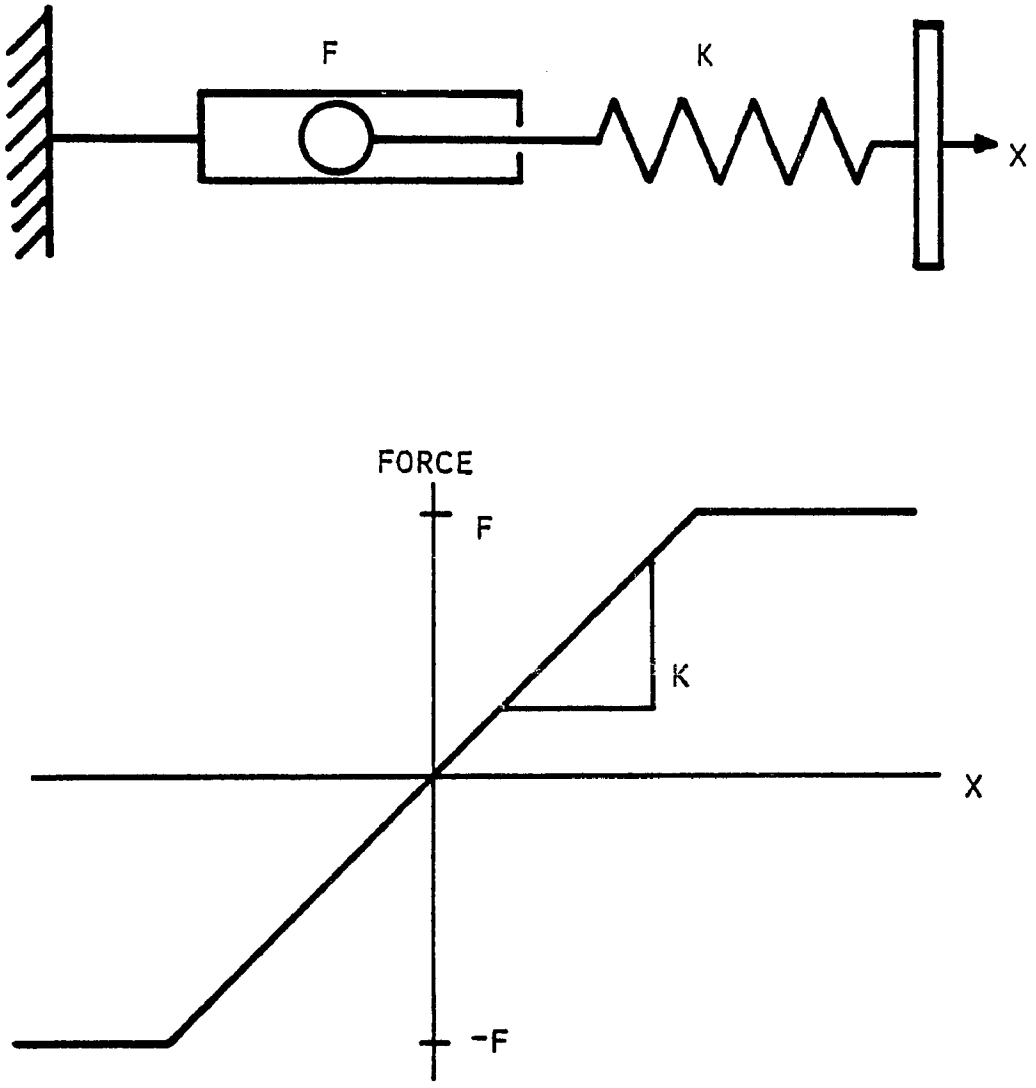


Figure (4.3) A Jenkins element and its behavior

followed by a region with negative curvature as strain increases. Such a model could be used directly to get qualitative information as was done by Caughey and Iwan. This model could also be matched to a material stress-strain plot, as was done by Whiteman to get quantitative information.

The model proposed by Whiteman uses a number of elasto-plastic, or Jenkins, elements. For such a model the return curve from a stress-strain state is different from the loading curve, thus producing a hysteretic loss. When two of these elements are put in parallel, as shown in Figure (4.4), and the frictional force of each of the elements is quite different, a plot such as Figure (4.5) would be produced. Whiteman suggested that, with enough of these elements, a stress-strain plot could be produced exhibiting a smooth curve from the proportional limit to the yield point, as is shown in Figure (4.6).

Following Whiteman's analysis, consider that the specimen is a bundle of parallel Jenkins elements all of which have some extension at which they yield, which is to say, each has a yield load. We assume Hooke's law is valid up to the yield strain and, after this point, the strain exerts a constant force for greater extensions. Consider a single element, i, which has a stress, s, strain, e, and elastic modulus, E, until it fails at e_i. For elastic range, where $e < e_i$:

$$s = Se \tag{4.1}$$

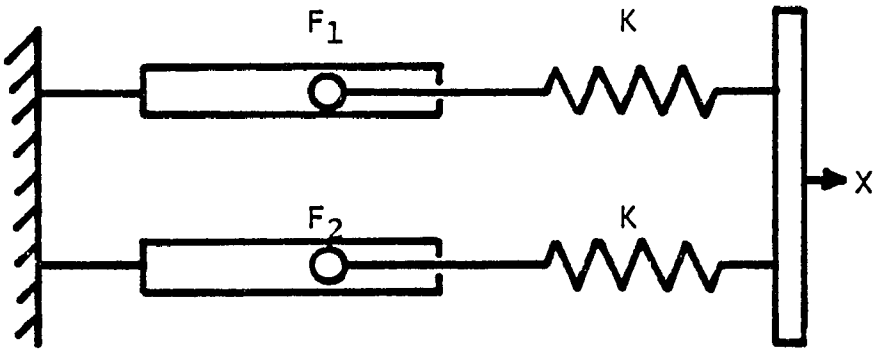


Figure (4.4) Two Jenkins elements in parallel

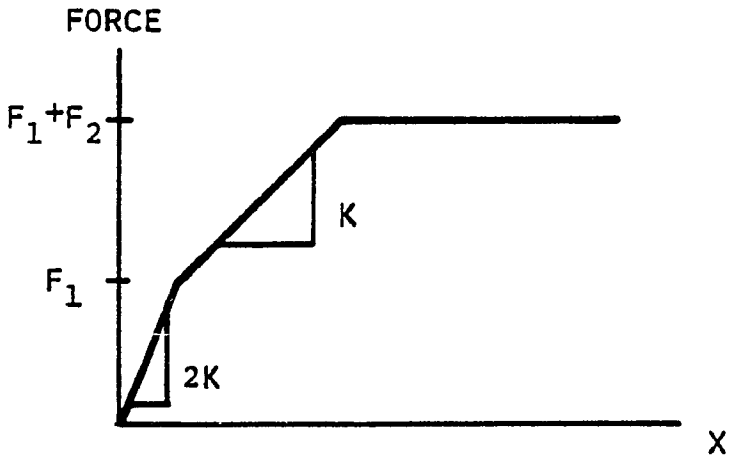


Figure (4.5) Tension response of two Jenkins elements in parallel

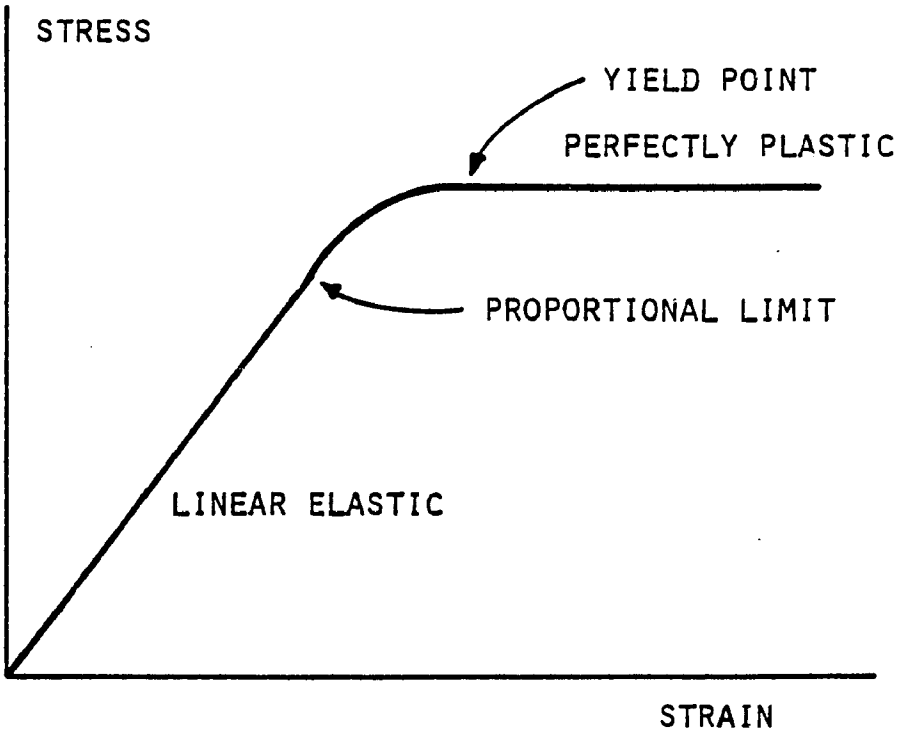


Figure (4.6) Metallic type stress-strain plot

If the specimen is taken to have unit area and is made up of N elements of equal area, there will be N such elastic-plastic transitions at various values of deflection or strain. The number of elements beginning to slip within some limits of extension can be referred to as a number of elements slipping at the same value of strain if the region were sufficiently small. Allowing the number of regions to grow but the region size to approach zero, Whiteman assumes that in the limit there is some density of yield points as a function of strain. Taking the ratio of this density to the original number of elements, N, a frequency of yield points, f(e), is obtained.

If one assumes that all the elements will have failed at some value of strain, say e_j, then:

$$\int_0^{e_j} f(x)dx = 1 \qquad (4.2)$$

where

$$f(x) = \frac{\text{density of yield points at x}}{\text{original number of elements}}$$

For any value of strain, $e < e_j$, the integral will have some value from 0 to 1 depending on how many (what fraction of) elements have failed to that point.

At any given strain the fraction of elements in the plastic region is given by:

$$\int_0^{e} f(x)dx = \text{fraction of elements behaving plastically} \qquad (4.3)$$

The fraction which are still behaving elastically will be the remainder:

$$\int_0^{e_j} f(x)dx = 1 - \int_0^{e} f(x)dx \tag{4.4}$$

From the individual element's loading characteristics, the expression for the total load or stress, s, can be found as a function of the strain. It will be a sum of the contributions of the elements behaving elastically and the elements behaving plastically. The contribution of the elastic elements is:

$$Ee \left(1 - \int_0^{e} f(x)dx\right) \tag{4.5}$$

From Whiteman's analysis, and as will be seen later, the contribution of the plastic elements is:

$$E \int_0^{e} xf(x)dx \tag{4.6}$$

Giving the total stress as:

$$s = E \left\{e \left(1 - \int_0^{e} f(x)dx\right) + \int_0^{e} xf(x)dx\right\} \tag{4.7}$$

To obtain the values of the cumulative frequency distribution, $\int_0^{e} f(x)dx$, Whiteman investigated the slope of the stress-strain curve. Assuming $f(0) = 0$ and calling E_0 the dimensionless tangent modulus, he obtains:

$$E_0 \equiv \frac{1}{E}\frac{ds}{de} = 1 - \int_0^{e} f(x)dx \tag{4.8}$$

which shows that the dimensionless tangent modulus represents the cumulative frequency distribution of those elements in the elastic region.

In a material such as aluminum, which was used by Whiteman, there is an initial linear elastic response. Thus, the dimensionless tangent modulus will be unity initially, and f(n) will be zero up to the proportional limit. At the perfectly plastic limit, E_0 will be zero, showing that all elements are slipping and the integral of the frequency distribution is unity.

It is interesting to apply this model to rubber. However, some of the assumptions in Whiteman's model do not apply to rubber. First, rubber has no limiting perfectly-plastic behavior. Second, there is no initially linear force deformation relation.

The third, and most significant, departure of rubber behavior from Whiteman's assumptions is the stiffening of the rubber in compression. This would cause the function f(e) to become negative for compression. The use of such a form for f(e) in computing dissipation would predict a negative energy loss. This would require the material to generate energy under cyclic stress.

A negative number of elements behaving plastically implies that some elements are becoming elastic in compression which were either not active at $\lambda = 1$ or were plastic and have become elastic again. The physics of the macromolecules must be examined further for potential sources of these effects.

4.1.3. Jenkins Elements with Stops

It is known that the initially random orientation of the long chain molecules in rubber is altered by the effect of applied stress. This is illustrated in Figure (4.7). Under tension the chains tend to align along the applied stress as the loose helix of the molecule straightens. The material shortens in the transverse direction and entanglements (trapped and untrapped) bind the molecules. These effects combine to cause increasing stiffness with strain. However, at the same time as the matrix is getting stiffer, some slippage occurs. Cross-links can break and reform as polymer molecules slip between themselves and filler particles. Thus, the material undergoes some irreversible deformation at the same time as its modulus is increasing.

In the macroscopic model using Jenkins elements, this may be visualized as the slip dampers coming to the end of their travel in one direction and hitting a stop. The model should also allow for the possibility of a slip damper with no friction in the collection of elements. This will account for a molecular chain which is initially unentangled in the matrix but becomes caught after some amount of displacement.

Figure (4.4) showed two Jenkins elements in parallel. The springs have the same modulus but the dampers slip at different forces (f_1 and f_2). This model will behave in tension as was shown in Figure (4.5). If this system were loaded to a greater deflection the dampers would stop sliding. Then a plot such as Figure (4.8) would result.

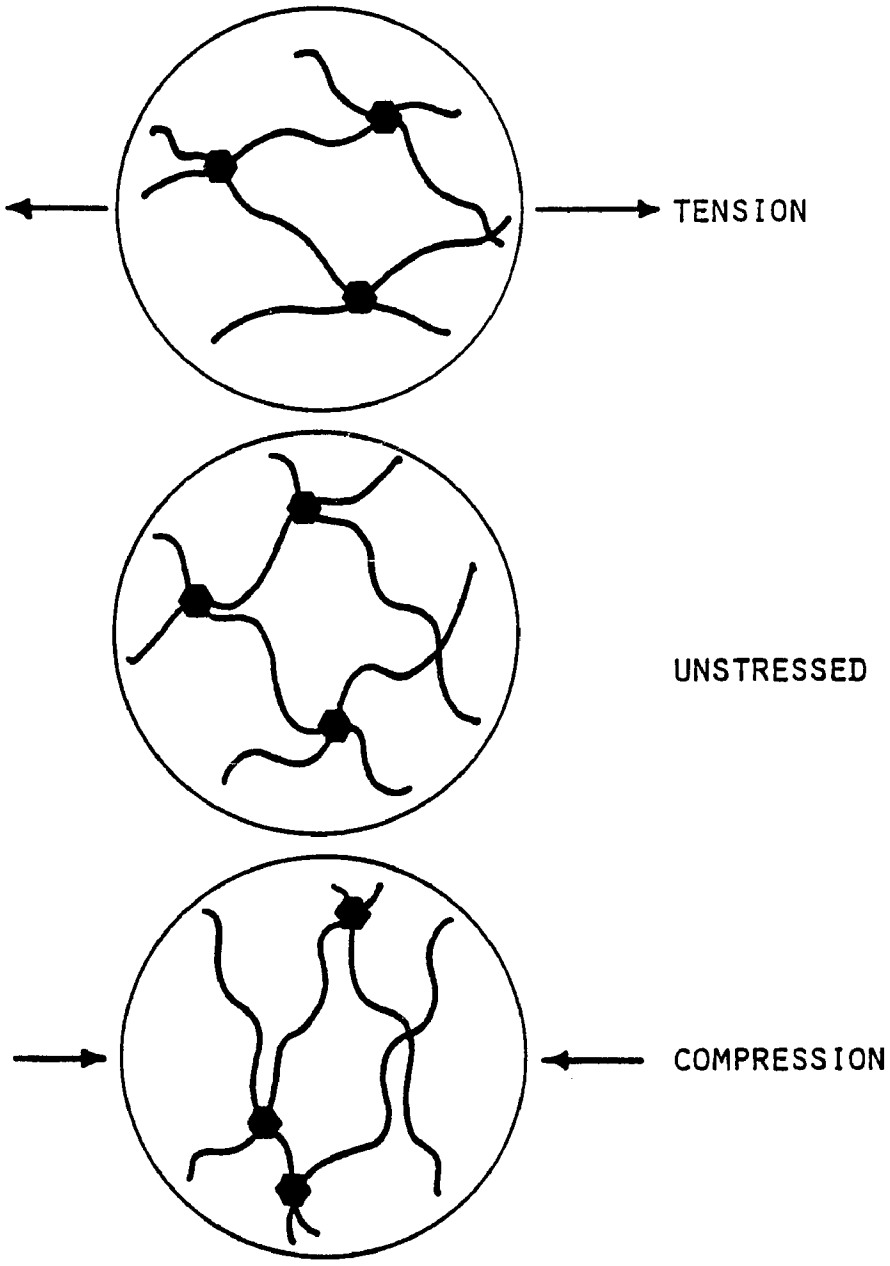


Figure (4.7) Change of random molecular orientation with stress

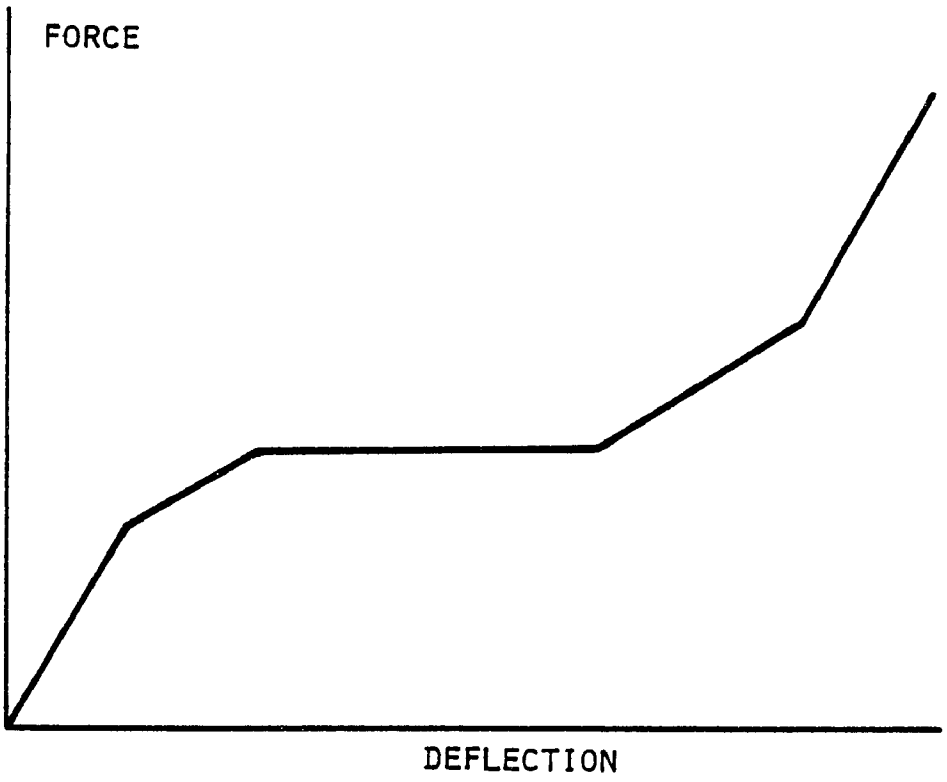


Figure (4.8) Continued tension response of two element system from Figure (4.4)

Consider a hypothetical system of Jenkins elements with stops. Let the system travel ten units of deflection. During this deformation let eleven Jenkins elements become active. Note that additional elements may exist in the system without changing this response if these elements slip at zero force and do not hit stops within the ten units of deflection. The distribution of where the elements begin to slip or hit stops will affect the shape of the loading and unloading curves. The example in Figure (4.9) uses eleven elements which are active in the range of deflection. Some of these elements slip at zero force and thus contribute no loss but will cause the stiffening when they hit their stops.

Another choice for the distribution of the eleven elements can generate the same loading curve as shown in Figure (4.9) but a different return curve. This loop shown in Figure (4.10) has less hysteretic loss and does close upon itself at zero deflection. This distribution concentrates the loss elements at lower deflections with more dampers hitting stops at the lower deflections so as to match the loading curve of Figure (4.9). Note that both figures show stiffening and loss.

In order to illustrate the behavior of such systems for several limits of deflection, consider the hypothetical system of thirteen Jenkins elements with the same spring rate, as shown in Figure (4.11). In this particular system, nine slip dampers begin to slide at zero force.

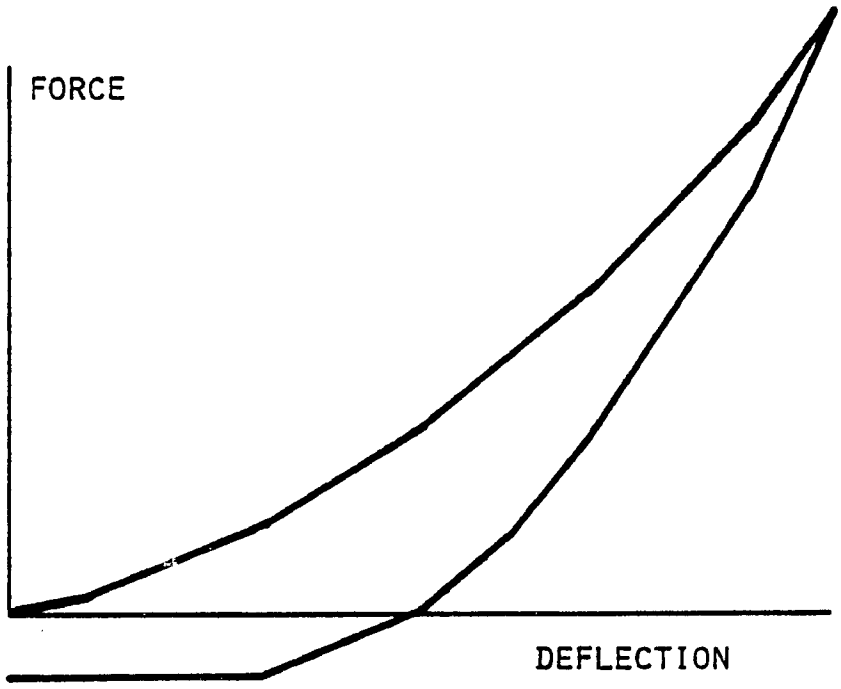


Figure (4.9) Hysteresis loop for hypothetical system

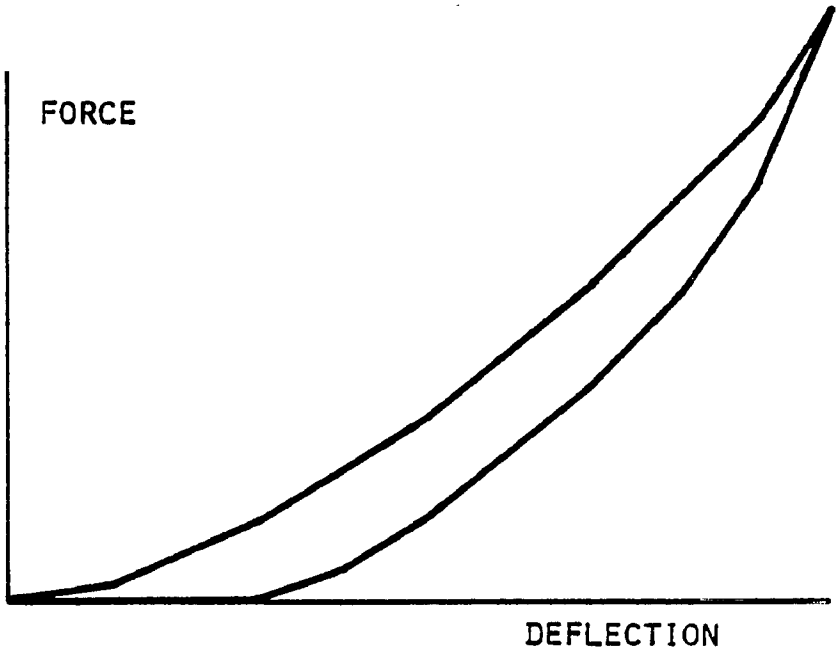
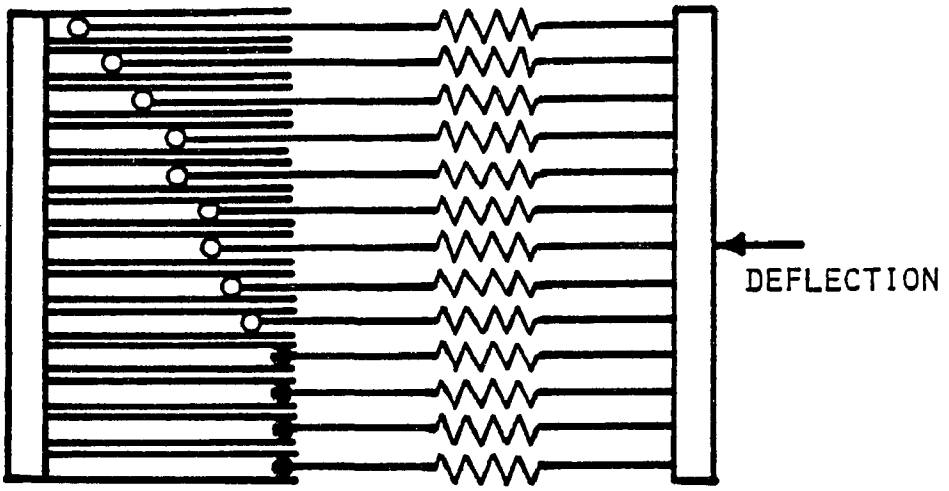


Figure (4.10) Hysteresis loop for hypothetical system



Model of system

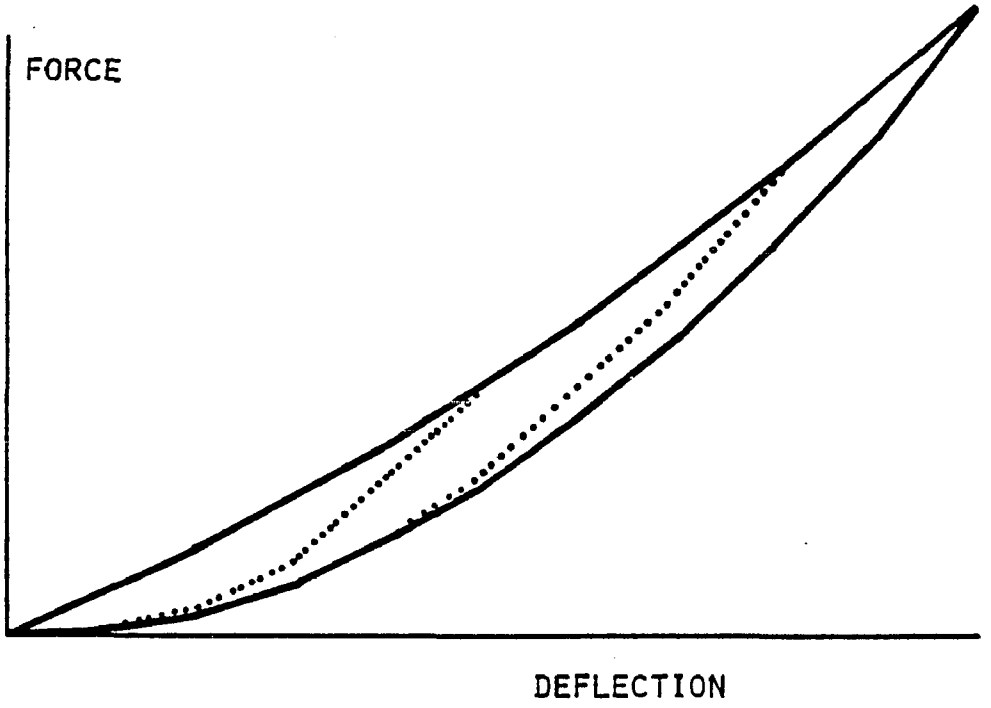


Figure (4.11) A discrete model with stops and example response curves

These slip dampers, represented by open circles in the figure, only contribute to the stiffening effect as they hit their stops. Four other dampers, represented by filled circles, slip at various non-zero forces and contribute to the loss effect. These four dampers have been chosen for simplicity, in such a way that they will not contribute to the stiffening effect within the range of deflection.

The resultant force-deflection curve for compression of this system is shown in Figure (4.11). The solid line illustrates the loop for a deflection large enough that all the stiffening and slipping elements are active at the level where loading is reversed. The dashed lines show the resulting curves if loading were reversed at two intermediate levels.

In order to generate these force-deflection loops, it was necessary to keep track of which dampers were sliding, how far they could slide, and what force was generated by elastic and slipping elements. By describing such a system in a fashion similar to Whiteman's model for aluminum, a functional form for the loop could be obtained. By considering the rubber matrix as a continuous distribution of Jenkins elements, any fluid properties of the material will be ignored. Since the interest in this model is in describing the hysteresis of the material, if the loss properties match well between the model and a specimen of rubber, the model serves a useful function.

4.2. Hysteretic Model for Rubber

4.2.1. Deterministic System with Discrete Elements

Incorporating the idea of "stops" with the basic Jenkins element model of Whiteman should provide a model for rubber hysteresis. Thus, a distributed element model can be developed with somewhat different assumptions. At any given deflection, or strain, there will be some number of elements which fail plastically or begin to slide. There will also be some number of elements which become elastic by hitting their stops at this deflection. In addition, there is a number of elements which start off elastically which we may call N_0. As with the Whiteman analysis, let the elements all have the same spring rate, κ, but allow them to fail at various force or deflection levels.

At a reference deflection where $F = 0$ and $\delta = \delta_0$, the initial number of elastic elements generates the initial spring rate of the system:

$$K = \kappa N_0 \tag{4.9}$$

The use of the reference deflection, δ_0, allows the formulation to apply to a material after it has been exercised and is no longer in the virgin state. The initially elastic elements are those which do not slide free at the reference deflection. If the total number of elements in the system is N, then there are $(N - N_0)$ elements which are initially inactive, that is, sliding freely at the reference deflection.

Define:

$N_0P(\delta)$ = number of elements beginning to slip at δ.

$N_0Q(\delta)$ = number of elements hitting stops at δ.

Thus, $P(\delta)$ and $Q(\delta)$ are proportions based on the initial number of elastically active elements. This will prove to be more convenient than a fraction of the total number of elements in the system, N, since the number of inactive elements is an indeterminant quantity. In the limiting cases of linear elasticity and perfect plasticity, N may be found, but then the Whiteman analysis may prove adequate.

Now, consider a discrete system where the functions $P(\delta)$ and $Q(\delta)$ will be zero everywhere except at a finite number of points where they take on rational values. For simplicity, consider all deflections where either function has non-zero values to be included in the set:

$$\{\delta_i\} = \{\, \delta_i \mid \delta_i < \delta_{i+1}, \quad i = 0, \pm1, \pm2, \pm3, \cdots \} \tag{4.10}$$

and $\delta = \delta_0$ is the reference deflection as before.

Now the load from δ_0 to δ_1 may be expressed simply as:

$$F(\delta) = K(\delta - \delta_0); \quad \delta_0 \leq \delta \leq \delta_1 \tag{4.11}$$

At $\delta = \delta_1$, however, the slope may increase due to elements hitting stops:

$$\text{Increase in slope} = KQ(\delta_1) \tag{4.12}$$

However, these newly elastic elements will not slide as far as those starting at $\delta = \delta_0$. Thus:

Force generated by elastic deformation =

$$K(\delta - \delta_0) + KQ(\delta_1)\ (\delta - \delta_1);$$

$$\delta_1 \leq \delta \leq \delta_2 \qquad (4.13)$$

At the general discrete point, δ_n:

Force generated by elastic deformation =

$$K(\delta_n - \delta_0) + K \sum_{i=1}^{n} Q(\delta_i)(\delta_n - \delta_i)\ ;$$

$$\delta = \delta_n \qquad (4.14)$$

The slope of the force deflection curve will be reduced by elements beginning to slip. Such elements must be removed from the elastic response and an additional force, generated by sliding friction, can be included in the total response:

Elastic response lost when slipping occurs at δ_1=

$$K\ \delta_n\ P(\delta_1);\ \delta_n > \delta_1 \qquad (4.15)$$

Sliding friction force =

$$K\ \delta_1\ P(\delta_1);\ \delta_n > \delta_1 \qquad (4.16)$$

These two effects can be noted in Figure (4.12). In this figure, the behavior for elements starting to slip at δ_1 is shown:

Net response lost =

$$P(\delta_1)\ K\ (\delta_n - \delta_1);\ \delta = \delta_n \qquad (4.17)$$

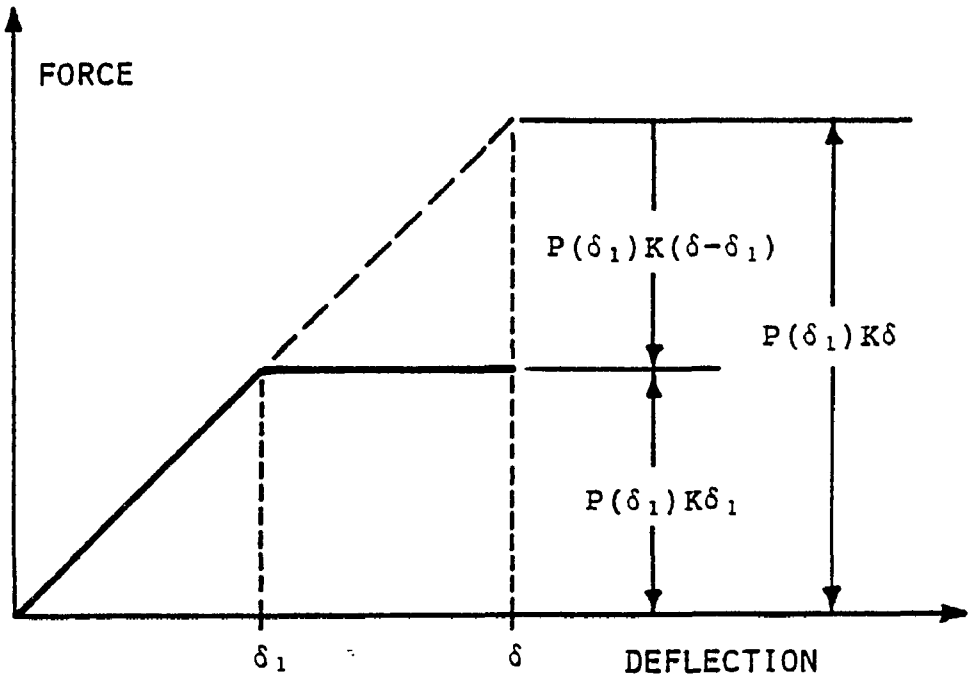


Figure (4.12) Example force-deflection plot for elements starting to slip at δ_1

Combining this with line (4.13) gives:

$$F(\delta) = K(\delta - \delta_0) + KQ(\delta_1)(\delta - \delta_1)$$

$$- KP(\delta_1)\delta + KP(\delta_1)\delta_1;$$

$$\delta_1 \leq \delta \leq \delta_2 \qquad (4.18)$$

or:

$$F(\delta) = K(\delta - \delta_0)$$

$$+ K\left\{Q(\delta_1) - P(\delta_1)\right\}(\delta - \delta_1);$$

$$\delta_1 \leq \delta \leq \delta_2 \qquad (4.19)$$

And at the general, discrete, point, δ_n, this becomes:

$$F(\delta_n) = K(\delta_n - \delta_0)$$

$$+ K\sum_{i=1}^{n}(\delta_n - \delta_i)\left\{Q(\delta_i) - P(\delta_i)\right\} \qquad (4.20)$$

At any general deflection, δ, Equation (4.20) becomes:

$$F(\delta) = K(\delta - \delta_0)$$

$$+ K\sum_{i=1}^{n}(\delta - \delta_i)\left\{Q(\delta_i) - P(\delta_i)\right\}; \qquad (4.21)$$

$$\delta_n < \delta < \delta_{n+1}$$

The first terms represent the force due to elements remaining elastic throughout. The summation terms involving $Q(\delta_i)$ represent the additional force generated by elements originally sliding freely but hitting a stop at δ_i. The summation terms involving $P(\delta_i)$ represent the elastic response which is not present due to elements having slipped and the forces generated by sliding friction.

This expression is similar to an expression in Whiteman's analysis before converting a summation into the integral in Equation (4.7). Define:

ℓ_0 = initial length

$E = \frac{K}{\ell_0}$ = initial modulus

$\frac{\delta_n - \delta_0}{\ell_0} = e_n$ = strain at δ_n

$\frac{E\ F(\delta_n)}{K\ \ell_0} = s(e_n)$ = stress at δ_n

Then Equation (4.21) can be written as:

$$s(e_n) = Ee_n$$

$$E \sum_{i=1}^{n} (e_n - e_i)\left(Q(e_i) - P(e_i)\right) \qquad (4.22)$$

where P and Q are now functions of the strain. This compares to Whiteman's expression in Equation (4.7):

$$s(e_n) = Ee_n \left(1 - \sum_{i=1}^{n} f(e_i)\right) + E \sum_{i=1}^{n} e_i f(e_i) \qquad (4.23)$$

The equations are the same if:

$$f(e_i) = Q(e_i) - P(e_i) \qquad (4.24)$$

The new formulation can overcome some of the difficulties which prevented using the Gaussian model of rubber to find $f(e_i)$. In the Whiteman analysis, elements could only become plastic and not become elastic again until the load was reversed. This requires that if an element fails it must appear in the cumulative distribution for plastic elements. This new analysis allows that

if an element begins to slide at nearly the same deflection as another element hits a stop, this will not be apparent in the cumulative distributions.

Thus, the total number of elements in each distribution (elastic and plastic) may remain constant if both P(x) and Q(x) change simultaneously. In the example shown in Figure (4.13) one element hits a stop exactly when another element begins to slide. Thus, although the plot appears linear it is not elastic as can be seen by the loss incurred.

Whiteman assumes a constant number of elements, all of which begin elastically and all of which have failed by some finite value of strain. While this new model also has a constant number of elements, that fact does not provide useful information since any number of elements may begin sliding at zero deflection without affecting the results.

In order to generate a return curve, assumptions regarding the nature of the slip dampers and their distribution must be made. Due to the symmetry in tension and compression for metals, the models used by Whiteman [41] and Iwan [40] assumed that the elemental behavior and the form of the distribution were perfectly symmetric. The Bauschinger effect in metals implied the existence of double-acting dampers. The Bauschinger effect is the change in the proportional limit of the load-deflection

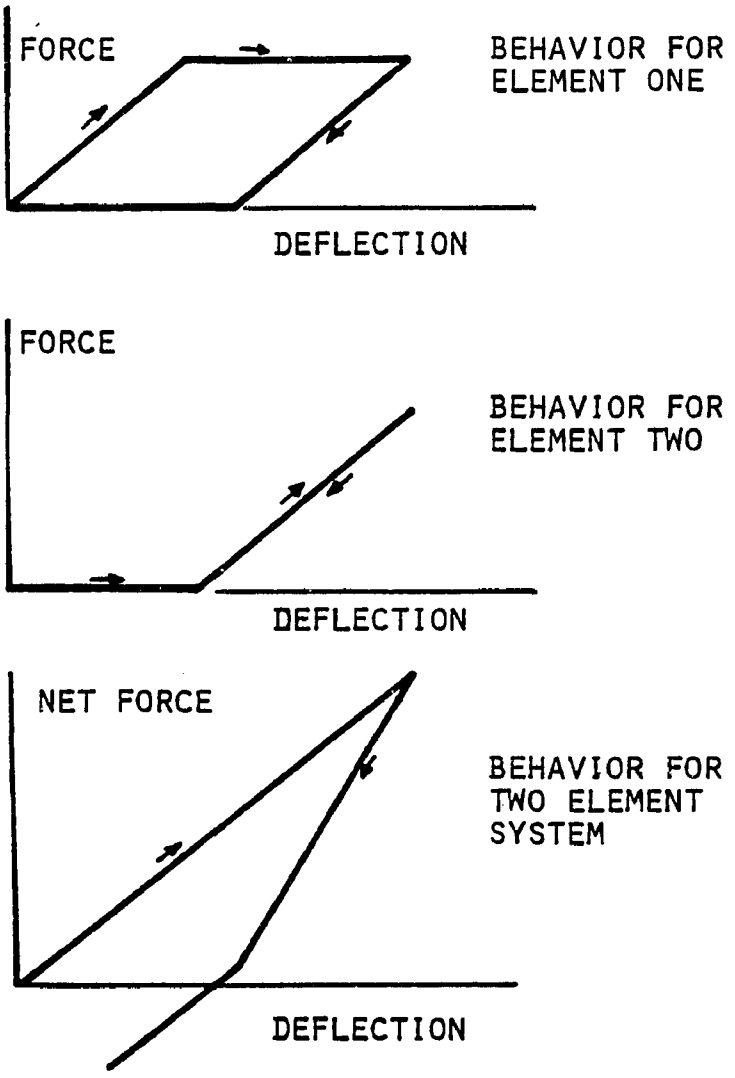


Figure (4.13) Linear plot exhibiting loss

curve upon return from a stress state where plastic deformation has occurred. A double-action dry friction damper is one in which the friction force generated in opposing forward motion is equal in magnitude to the friction force generated in opposing reverse motion. A single-action damper would generate force in only one direction and would slide freely in the reverse direction. The use of double-action dampers resulted in a change in the function representing the slip of the elements, due to the amount of plastic strain. However, the assumption of double-action dampers may not be appropriate for rubber. There is no pronounced Bauschinger type effect in rubber, and there are several possible mechanisms for loss.

It can be visualized that a long chain molecule which responded elastically in tension will buckle in compression, and another chain which is elastic in compression will slide freely in tension. A bond between a polymer molecule and a filler particle which would break in tension may not break in compression; another bond which breaks in compression may not break in tension. This illustrates how some slip dampers in the model may be single-acting, either in compression or for tension.

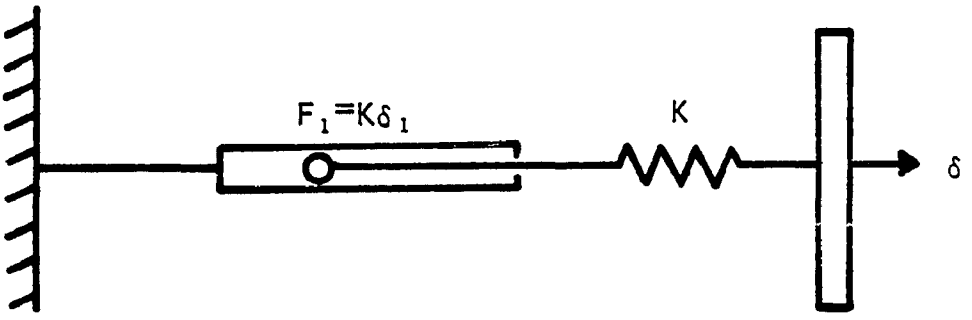
On the other hand, mechanisms for loss in vulcanized, carbon-filled rubber may be double-acting. The breaking and reforming of a cross-link is a loss mechanism which has similar characteristics in tension or compression. An amount of strain energy, or thermal energy, is required to break a specific cross-link and generally it does not

matter whether the energy comes from compression or tension. Some kind of friction may exist when a molecule slides over a filler particle; if so, this is another source of double-action damping.

The choice between single-acting or double-acting damping is not clear. Fortunately, the theoretical framework below does not require a specific assumption, and it will consider "α" action dampers. For single-acting dampers, $\alpha = 1$; for double-acting dampers, $\alpha = 2$. A comparison of single-acting and double-acting dampers is illustrated in Figure (4.14). In the single-acting damper system the distribution is essentially unchanged after a single cycle, whereas in the double-acting damper system the distribution remains dependent on the elemental and system strains.

Consider loading the system to the force $F(\delta^*)$, where δ^* is one of the discrete points in $\{\delta_i\}$, with $i = n^*$, and then unloading. Because the effects are elastic, the portions of Equation (4.22) not involving $P(\delta)$ will unload exactly as they loaded. However, the portion of the unloading expression involving $P(\delta)$ will be different.

The physical effects of unloading are: all elements which were at stops or were sliding with friction begin to recover the elastic deformation of their springs; only elements which were sliding with zero friction force slide in the reverse direction immediately. Elements which were



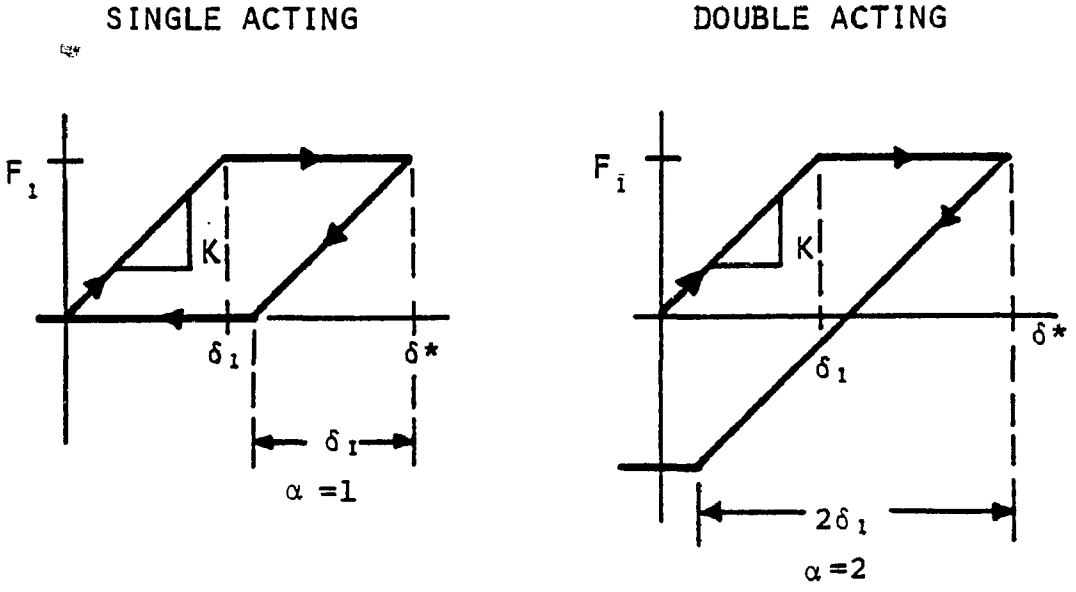


Figure (4.14) Comparison of single and double acting dampers

initially elastic and then began to slip as determined by $P(\delta)$ will unload elastically. Those elements which had been sliding with friction will begin to slide in the reverse direction according to a new distribution function.

The distribution of elements failing plastically or beginning to slip on the return from δ^* will be a new function $P'(\delta)$ which depends on δ^* and "α", the action of the slip dampers. An element which began to slip at δ_i on the way to δ^* will slip on its return from δ^* at $(\delta^* - \alpha\delta_i)$. The cases $\alpha = 1$ and $\alpha = 2$ were illustrated in Figure (4.14). However, there were $N_0 P(\delta_i)$ elements beginning to slip at δ_i; therefore, the same number of elements should slip at $(\delta^* - \alpha\delta_i)$ on the return. Thus:

$$P'(\delta^* - \alpha\delta_i) = P(\delta_i) \tag{4.25}$$

or:

$$P'(\delta_n) = P\left(\frac{\delta^* - \delta_n}{\alpha}\right) \tag{4.26}$$

It is now assumed that any deflection of interest was in the set of deflections $\{\delta_i\}$. Therefore, $\frac{\delta^* - \delta_n}{\alpha}$ is an element of $\{\delta_i\}$.

With the above assumptions on the nature of the return curve of such a system, an expression for the return curve can be generated. Let the material start at a reference deflection, δ_0. The material at δ_0 would be unloaded with a stretch ratio of 1; therefore, the stress and strain are both zero. This material is loaded to a deflection of δ^*, which is one of the discrete points $\{\delta_i\}$ with $i = n^*$. At this point, the force will be:

$$F(\delta^*) = K(\delta^* - \delta_0) + K \sum_{i=1}^{n^*} (\delta_{n^*} - \delta_i) \left\{ Q(\delta_i) - P(\delta_i) \right\} \quad (4.27)$$

from the previous development. If unloading now begins, all of the elements will begin to unload elastically. The elastic portion of the expression should remain unchanged.

The initially elastic elements were those which were either at stops at δ_0 or those which would eventually begin to slip at some deflection. Such elements will begin to unload elastically when the direction is reversed. For such elements unloading from δ_n to δ^*:

Force recovered from initially elastic elements =

$$K(\delta_n - \delta^*) \quad (4.28)$$

At δ_{n^*-1}, the force recovered from an element which hit a stop at δ_{n^*-1} is $\kappa(\delta_{n^*-1} - \delta^*)$. At this deflection, the force in the element is reduced to zero; the element will then slide freely until a stop is hit in the reverse direction. Similarly, the force recovered from an element which hit a stop at δ_{n^*-2} is $\kappa(\delta_{n^*-2} - \delta^*)$. The force recovered from all elements that hit a stop at δ_{n^*-2} is $K(\delta_{n^*-2} - \delta^*)Q(\delta_{n^*-2})$. Therefore, the force recovered from elements which hit stops between δ_n and δ^* is:

$$K \sum_{i=n}^{n^*} (\delta_i - \delta^*)\, Q(\delta_i) \quad (4.29)$$

However, elements which hit stops between δ_0 and δ_n will all unload elastically. These are elements which are active from δ^* to δ_n and never come off of their stops.

Force recovered from elements which hit stops between δ_0 and δ_n =

$$K(\delta_n - \delta^*) \sum_{i=1}^{n} Q(\delta_i) \tag{4.30}$$

Combined with the elastic terms of Equation (4.27), these expressions yield an expression for the elastic portion of the unloading curve.

This elastic unloading response actually shows more recovery than there should be. Some force is not recovered due to elements starting to slip. An element which begins to slip at δ_i on the return from δ^* to δ_n does not recover an amount of force equal to:

Correction for force not recovered =

$$\kappa(\delta_n - \delta_i) \tag{4.31}$$

The correction for all such elements which begin to slip at δ_i is thus:

Force not recovered due to elements which begin to slip at δ_i on the return from δ^* =

$$K(\delta_n - \delta_i)\ P\left(\frac{\delta^* - \delta_i}{\alpha}\right) \tag{4.32}$$

In this expression the number fraction of elements slipping at δ_i on the return from δ^* uses the original function P but at a transformed argument as shown in Equation (4.26).

Therefore, the total response lost due to elements starting to slip at any δ_i from δ^* to δ_n is:

$$K \sum_{i=n^*}^{n} (\delta_n - \delta_i)\ P\left(\frac{\delta^* - \delta_i}{\alpha}\right) \ ; \ \delta_n < \delta^* \tag{4.33}$$

This must be combined with the previous expressions for elastic response and the actual force at δ^* from Equation (4.27):

$$F(\delta_n) = F(\delta^*) + K(\delta_n - \delta^*)$$

$$+ K \sum_{i=1}^{n} (\delta_n - \delta^*)\, Q(\delta_i)$$

$$+ K \sum_{i=n}^{n^*} (\delta_i - \delta^*)\, Q(\delta_i)$$

$$+ K \sum_{i=n^*}^{n} (\delta_n - \delta_i)\, P\left(\frac{\delta^* - \delta_i}{\alpha}\right) \qquad (4.34)$$

Reducing this expression gives:

$$F(\delta_n) = K(\delta_n - \delta_0) + K \sum_{i=1}^{n} (\delta_n - \delta_i)\, Q(\delta_i)$$

$$+ K \sum_{i=n^*}^{n} (\delta_n - \delta_i)\, P\left(\frac{\delta^* - \delta_i}{\alpha}\right)$$

$$- K \sum_{i=1}^{n^*} (\delta^* - \delta_i)\, P(\delta_i) \qquad (4.35)$$

The final summation in Equation (4.35) is equivalent to a force lost to plasticity. For convenience, "equivalent plastic deformation" will be defined as:

$$\delta_p(\delta_0, \delta^*) = \sum_{n=1}^{n^*} (\delta^* - \delta_i)\, P(\delta_i) \qquad (4.36)$$

It is important to realize this is not a net plastic deformation that could be observed when all load is removed. The net plastic deformation is that value of δ_n which makes $F(\delta_n) = 0$ in Equation (4.35). This "equivalent plastic deformation", δ_p, is a notational convenience as will be seen below. Thus:

$$F(\delta_n) = K(\delta_n - \delta_0) + K \sum_{i=1}^{n} (\delta_n - \delta_i)\, Q(\delta_i)$$

$$+ K \sum_{i=n^*}^{n} (\delta_n - \delta_i)\, P\left(\frac{\delta^* - \delta_i}{\alpha}\right)$$

$$- K\delta_p(\delta_0, \delta^*) \qquad (4.37)$$

Let us next consider continued unloading of the system to some deflection, $\delta°$, and then reloading. The lower limit of a cycle is $\delta°$, which is one of the discrete points $\{\delta_i\}$ with $i = n°$. Note that $\delta°$ is not necessarily the same as δ_0. No generality will be lost if $\delta^* > \delta_0$ and $\delta^* > \delta°$, but allow $\delta° > \delta_0$ or $\delta° < \delta_0$ or $\delta° = \delta_0$. At $\delta°$, Equation (4.40) becomes:

$$F(\delta°) = K(\delta° - \delta_0) + K \sum_{i=1}^{n°} (\delta° - \delta_i)\, Q(\delta_i)$$

$$+ K \sum_{i=n^*}^{n°} (\delta° - \delta_i)\, P\left(\frac{\delta^* - \delta_i}{\alpha}\right)$$

$$- K\delta_p(\delta_0, \delta^*) \qquad (4.38)$$

To this, terms representing the response of elements behaving elastically or plastically can be added for reverse loading. For reloading from $\delta°$ to δ_n, all sliding elements begin to react elastically again when the load is reversed.

Force from initially elastic elements =

$$K(\delta_n - \delta°) \qquad (4.39)$$

Some elements which hit stops will not come off of the stops before reaching δ_n. These elements are always active from $\delta°$ to δ_n:

Force from elements which hit stops between δ_0 and δ_n =

$$K(\delta_n - \delta^\circ) \sum_{i=1}^{n} Q(\delta_i) \tag{4.40}$$

Some elements which hit stops will come off of their stops on the way to δ_n. These elements will respond:

Force from elements which hit stops between δ_n and δ° =

$$K \sum_{i=n}^{n^\circ} (\delta_i - \delta^\circ)\, Q(\delta_i) \tag{4.41}$$

The change in the distribution of elements beginning to slip after an excursion to δ° must also be considered. The elements which began to slip at δ_i on the way to δ^*, and then began slipping at $(\delta^* - \alpha\delta_i)$ on the way to δ°, will also begin to slip on the way to δ^* again at $(\delta^\circ + \alpha\delta_i)$. This is illustrated in Figure (4.15). Since there are $N_0 P(\delta_i)$ elements which began to slip at (δ_i), this must be the same number of elements which begin to slip at $(\delta^\circ + \alpha\delta_i)$.

Similar to the definition of $P'(\delta)$ from Equations (4.25) and (4.26), define a new function $P''(\delta)$. The distribution of elements beginning to slip on the way from δ° after an excursion to δ^* will be a new function $P''(\delta)$ which depends on δ° and α. This new function is related to the original function P:

$$P(\delta_i) = P''(\delta^\circ + \alpha\delta_i) \tag{4.42}$$

then:

$$P''(\delta_i) = P\left(\frac{\delta_i - \delta^\circ}{\alpha}\right) \tag{4.43}$$

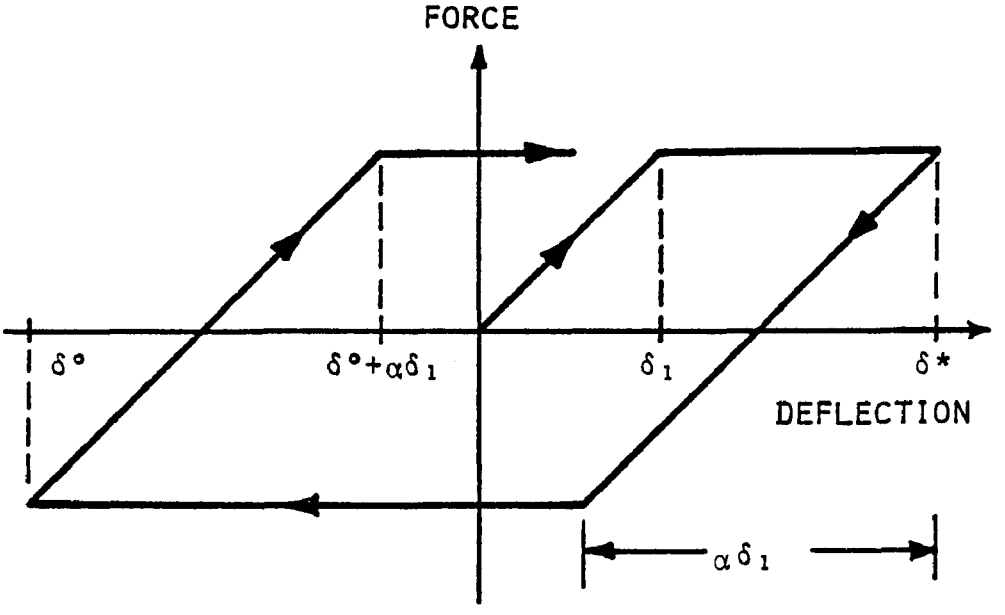


Figure (4.15) Example force-deflection plot for elements starting to slip at δ_1 after excursion to δ° and δ^*

Analogous to the response of the system after excursion to δ^*, the combined response of all elements beginning to slip between δ° and δ_n is:

Force from elements which slip =

$$K \sum_{i=n^\circ+1}^{n} (\delta_i - \delta_n)\, P\left(\frac{\delta_i - \delta^\circ}{\alpha}\right) \; ; \; \delta_n > \delta^\circ \qquad (4.44)$$

Combining the expressions for elastic response and plastic response from δ° to δ_n with the force at δ° from Equation (4.38) yields the force at δ_n after excursions to δ^* and δ°:

$$\begin{aligned} F(\delta_n) = {} & K(\delta_n - \delta_0) + K \sum_{i=1}^{n} (\delta_n - \delta_i)\, Q(\delta_i) \\ & + K \sum_{i=n^\circ+1}^{n} (\delta_i - \delta_n)\, P\left(\frac{\delta_i - \delta^\circ}{\alpha}\right) \\ & + K \sum_{i=n^*}^{n^\circ} (\delta^\circ - \delta_i)\, P\left(\frac{\delta^* - \delta_i}{\alpha}\right) \\ & + K\delta_p(\delta_0, \delta^*) \end{aligned} \qquad (4.45)$$

Now the definition of equivalent plastic deformation may be extended to:

$$\begin{aligned} \delta_p(\delta_0, \delta^*, \delta^\circ) = {} & \sum_{i=n^*}^{n^\circ} (\delta_i - \delta^\circ)\, P\left(\frac{\delta^* - \delta_i}{\alpha}\right) \\ & + \delta_p(\delta_0, \delta^*) \end{aligned} \qquad (4.46)$$

Giving:

$$F(\delta_n) = K(\delta_n - \delta_0) + K\sum_{i=1}^{n}(\delta_n - \delta_i)\,Q(\delta_i) + K\sum_{i=n^\circ+1}^{n}(\delta_i - \delta_n)\,P\left(\frac{\delta_i - \delta^\circ}{\alpha}\right) - K\delta_p(\delta_0, \delta^*, \delta^\circ) \qquad (4.47)$$

In this form, the similarity among Equations (4.27), (4.37), and (4.47) is quite clear. The general form will thus be:

$$F(\delta_n) = K(\delta_n - \delta_0) + K\sum_{i=1}^{n}(\delta_n - \delta_i)\,Q(\delta_i) + K\sum_{n_\ell}^{n}(\delta_i - \delta_n)\,P\left(\frac{\delta_i - \delta_\ell}{\alpha}\right) - K\delta_p(\delta_0 \cdots \delta_{\ell-1}) \qquad (4.48)$$

where:

δ_ℓ was the last extremum reached by the material.

δ_p is the equivalent plastic deformation to δ_ℓ defined incrementally, as above.

4.2.2. Stochastic System with Continuous Elements

These ideas must now be applied to a real material rather than the hypothetical, discrete system of the previous section. The discrete deflections and discrete functions will be replaced with continuous deflections and functions. Thus, it will be considered that a large number of very weak elements exist in the material. In the limit, these elements will produce the same initial spring rate, K.

It is known [42] that the elastic modulus of rubber can be statistically related to the number of molecules per unit of volume. The elastic system is stochastic as opposed to the deterministic system of the previous section. It seems reasonable to associate a Jenkins element with each molecule. To use such a scheme, the treatment must be statistical.

The loss system is also stochastic as opposed to deterministic. A cross-link may break when it receives sufficient energy. However, the source of energy may be deformation or temperature. Each of these energy sources is not distributed uniformly in the material. A molecular chain may slip over a filler particle at some value of tension. However, the tension may not always have the same relation to the net material deformation. It is known that the deformation of rubber is not homogeneous, which is also called nonaffine deformation.

Thus, the treatment will be restricted by the randomness of the continuous distributions involved. A specific value obtained in one experiment may not be the same value obtained in the next experiment. However, such values should be reasonably close to each other and to some average value.

At the approximate deflection, δ, the experiment should produce $P(\delta)$ on the average. In this problem there is scatter due to experimental error and the stochastic

processes in the material. To handle these effects, the random variable concept from statistics will prove useful.

In its most intuitive form, a random variable is the outcome of an experiment. In this sense, the value is neither variable nor random. In some experiments the observed value may be assumed constant with error producing some scatter. In other cases the observed value will have stochastic variations in addition to experimental error.

To illustrate the use of a random variable, consider measuring the acceleration due to gravity, g, in a pendulum experiment. It is generally agreed that g is a constant which can be obtained from the length and period of a pendulum. Consider two experimental designs. The first experiment uses cotton twine, wooden weights, an electric timer, and a meter stick marked in centimeters. The second experiment uses piano wire, lead weights, a stopwatch, and a micrometer.

The first experiment will have considerable scatter due to experimental error. However, the uncontrolled variations due to the size of the weights, the extensibility of the string, and the different levels of accuracy in the measurements will cause additional scatter. If a large number of experiments were performed, the average value should be close to g. This value would be close enough to predict the outcome of similar experiments.

The second experiment will have less scatter. In addition to fewer sources of error, stochastic variations

are minimized by controlling parameters which are not measured. The fairly uniform level of accuracy in measurement should allow rounding off to this level and obtaining a constant value of g for most experiments.

The second experiment could thus be considered deterministic, since all relevant parameters can be controlled or measured. The first experiment, although claiming to measure a constant of nature, is stochastic. In either instance, the observations may be considered random variables but will prove a convenience only in the first design.

As the term is used in statistics, a random variable does not require a specific form or distribution, nor does it require a specific source or nature of the variations. Without going into the notational formalities of statistics, a random variable, X, can be defined as a function whose value is determined by each possible outcome of a given experiment, x. The random variable is associated with a probability function, f(x). This probability density has the properties:

$$f(x) \geq 0 \tag{4.49}$$

$$\int_{-\infty}^{\infty} f(x)dx = 1 \tag{4.50}$$

$$\text{Probability } (a<X<b) = \int_{a}^{b} f(x)dx \tag{4.51}$$

Intuitively, the more likely the outcome of an experiment the higher the value of probability density for

that event. The most probable event is not where f(x) is maximum. By Equation (4.51), the probability that any specific event will occur is zero. However, an "expected value" can be defined as:

$$E\{X\} = \int_{-\infty}^{\infty} x\, f(x)dx \tag{4.52}$$

From statistics the expected value is the "average" value of all possible outcomes weighted by the probability of the outcome.

The probability density for the random variable, X, may also be dependent on another variable. Then, the probability density will have the properties:

$$f(x,y) \geq 0, \text{ for all } x,y \tag{4.53}$$

$$\int_{-\infty}^{\infty} f(x,y)dx = h(y) \tag{4.54}$$

$$\text{Probability } (a<X<b \mid y) = \int_{a}^{b} f(x,y)dx \tag{4.55}$$

The expected value of X is now a function of y:

$$E\{X\} = \int_{-\infty}^{\infty} x\, f(x,y)dx = g(y) \tag{4.56}$$

Using these concepts in the context of a system of Jenkins elements, the functions P and Q may be considered to be random variables. This idea of random variables may be used with either discrete or continuous systems. If the number of elements hitting stops at δ is obtained by a statistical process, Q will have variations due to this effect. If the experiment cannot resolve the difference between an element hitting a stop at δ from an element hitting

a stop between $\delta-\Delta$ and $\delta+\Delta$, there is another source of variation. A deterministic approach will produce results which are in error relative to the accuracy of measurement in a stochastic system.

In a discrete, stochastic system, there will be a probability distribution for P and another for Q at each of the discrete deflections. In a continuous, stochastic system, the probability distributions will also be continuous functions of deflection. The previous part of this chapter considered a discrete, deterministic system. The next portion discusses a continuous, stochastic system.

The probability is zero that a specific proportion of elements begin to slip at a specific deflection. However, if a range of proportions and deflections is specified, the probability will be nonzero in general. In the continuous, stochastic system the expected value of the proportion is a density function of the deflection. Equation (4.56) indicated such a condition.

Let $f(x,y)$ be the probability density per unit length for the proportion of elements, x, beginning to slip at some deflection, y. Similarly, $g(x,y)$ is the probability density per unit length for elements hitting stops. Thus, the expected values of $P(\delta)$ and $Q(\delta)$ in the range $a<\delta<b$ are:

$$E\left\{P(\delta);a<\delta<b\right\} = \int_a^b p(y)dy \qquad (4.57)$$

and

$$E\left\{Q(\delta);a<\delta<b\right\} = \int_a^b q(y)dy \qquad (4.58)$$

where:

$$p(y) = \int_{-\infty}^{\infty} x\, f(x,y)dx \tag{4.59}$$

$$q(y) = \int_{-\infty}^{\infty} x\, g(x,y)dx \tag{4.60}$$

It becomes necessary to use the expected values in the analysis. This has the effect of converting the summations in the previous development to integrals. The following is a simple illustration. $P(\delta_i)$ becomes:

$$E\{P(\delta) \mid \delta_{i-1}<\delta<\delta_i\} = \int_{\delta_{i-1}}^{\delta_i} p(y)dy \tag{4.61}$$

$\sum_{1}^{n} P(\delta_i)$ becomes:

$$\sum_{1}^{n} \int_{\delta_{i-1}}^{\delta_i} p(y)dy = \int_{\delta_0}^{\delta_n} p(y)dy \tag{4.62}$$

Thus, Equation (4.26) becomes:

$$F(\delta) = K\left\{\delta - \delta_0 + \int_{\delta_0}^{\delta} (\delta - y)q(y)dy - \int_{\delta_0}^{\delta} (\delta - y)p(y)dy\right\} \tag{4.63}$$

The restriction on deflection being in discrete units no longer applies.

Assuming "α" acting dampers as before, the return from an excursion to δ^* may be expressed:

$$F(\delta) = K \left\{ (\delta - \delta_0) + \int_{\delta_0}^{\delta} (\delta - y) q(y) dy \right.$$

$$\left. - \int_{\delta^*}^{\delta} (\delta - y)\ p\left(\frac{\delta^* - y}{\alpha}\right) dy - \delta_p \right\} \qquad (4.64)$$

where:

$$\delta_p = \int_{\delta_0}^{\delta^*} (\delta^* - y) p(y) dy \qquad (4.65)$$

It should be noted that Equations (4.63) and (4.64) predict the same force at δ^*.

Similar to Equation (4.45), the expression for the load after excursion to δ^* and δ° is:

$$F(\delta) = K \left\{ (\delta - \delta_0) + \int_{\delta_0}^{\delta} (\delta - y) q(y) dy \right.$$

$$\left. - \int_{\delta_0}^{\delta} (\delta - y)\ p\left(\frac{y - \delta^\circ}{\alpha}\right) dy - \delta_p \right\} \qquad (4.66)$$

where:

$$\delta_p = \int_{\delta^\circ}^{\delta^*} (\delta^\circ - y)\ p\left(\frac{\delta^* - y}{\alpha}\right) dy$$

$$+ \int_{\delta_0}^{\delta^*} (\delta^* - y)\ p(y) dy \qquad (4.67)$$

It should be noted that Equations (4.66) and (4.64) predict the same force at δ°.

Subsequent cycles between δ^* and δ° will have the same form as Equation (4.64) on the way to δ°, and the form of

Equation (4.66) on the way to δ^*. However, the δ_p will be redefined at each extremum. Thus, it may be seen that after another cycle to δ^* the equation for loading will be the same as in Equation (4.69) but a new δ_p will be:

$$\delta_p = \int_{\delta^\circ}^{\delta^*} (\delta^* - y)\ p\left(\frac{y - \delta^\circ}{\alpha}\right) dy + \int_{\delta^\circ}^{\delta^*} (\delta^\circ - y)\ p\left(\frac{\delta^* - y}{\alpha}\right) dy + \int_{\delta_0}^{\delta^*} (\delta^* - y)\ p(y)dy \qquad (4.68)$$

Additional cycles will multiply the first two integrals by the number of cycles to δ^*. A similar situation exists for δ_p at δ°.

Next, compare the force at δ^* from Equation (4.64) and the force at δ^* from Equation (4.66). Call the difference in forces from the two equations $D(\delta)$. Thus:

$$D(\delta) = F(\delta)\{\text{from (4.66)}\} - F(\delta)\{\text{from (4.64)}\} \qquad (4.69)$$

Evaluating $D(\delta^*)$ and substituting for δ_p from Equations (4.65) and (4.67) as appropriate:

$$D(\delta^*) = K\left\{\int_{\delta^\circ}^{\delta^*} (\delta^* - y)\ p\left(\frac{y - \delta^\circ}{\alpha}\right)dy + \int_{\delta^\circ}^{\delta^*} (\delta^\circ - y)\ p\left(\frac{\delta^* - y}{\alpha}\right) dy\right\} \qquad (4.70)$$

Now make two changes of variables:

$$w(y) = \left(\frac{y - \delta^\circ}{\alpha}\right) \; ; \; dw = \frac{dy}{\alpha} \; ; \; w^* = w(\delta^*) \qquad (4.71)$$

$$x(y) = \left(\frac{\delta^* - y}{\alpha}\right) \; ; \; dx = \frac{-dy}{\alpha} \; ; \; x^\circ = x(\delta^\circ) \qquad (4.72)$$

This gives:

$$D(\delta^*) = K \left\{ \int_0^{w^*} (\delta^* - \delta^\circ - \alpha w) p(w) \; \alpha dw \right.$$

$$\left. - \int_{x^\circ}^{0} (\delta^\circ - \delta^* + \alpha x) p(x) \; \alpha dx \right\} \qquad (4.73)$$

which becomes:

$$D(\delta^*) = K\alpha^2 \left\{ \int_0^{w^*} \left(\frac{\delta^* - \delta^\circ}{\alpha} - w\right) p(w) dw \right.$$

$$\left. - \int_0^{x^\circ} \left(\frac{\delta^* - \delta^\circ}{\alpha} - x\right) p(x) dx \right\} \qquad (4.74)$$

Since w and x are dummy variables in this equation, and $w^* = x^\circ$:

$$D(\delta^*) = 0 \qquad (4.75)$$

This means the force at δ^* is the same after each cycle. However, it must be recalled that the equations deal with "expected values" and not exact values. Thus, after loading to δ^* and δ°, the subsequent cycles between these deflection limits will give approximately the same force at δ^* after each cycle. A similar situation exists for loading to δ°; the force at δ° will be approximately the same each time the material reaches that limit.

Note also that the same two integrals appearing in Equation (4.70) appear in the expression for δ_p in Equation (4.68). Thus, δ_p is approximately a constant from δ^* to δ° for all cycles. On the return from δ° toward δ^*, δ_p takes on another value which is approximately constant for all cycles.

The energy loss can be computed from the force-deflection equations. Integration of Equations (4.64) and (4.67) for $\delta^\circ < \delta < \delta^*$ will give the expected value of the area enclosed by the load-deflection curves. However, the elastic parts of the curves will cause no loss and will cancel in the integration.

Another method to obtain the enclosed area of the force-deflection curve is to integrate the difference in forces at each deflection. Evaluating $D(\delta)$ from Equation (4.69):

$$D(\delta) = K \left\{ - \int_{\delta^\circ}^{\delta} (\delta - y)\, p\left(\frac{y - \delta^\circ}{\alpha}\right) dy + \int_{\delta}^{\delta^*} (\delta - y)\, p\left(\frac{\delta^* - y}{\alpha}\right) dy - \int_{\delta^\circ}^{\delta^*} (\delta^\circ - y)\, p\left(\frac{\delta^* - y}{\alpha}\right) dy \right\} \qquad (4.76)$$

Use the changes of variable $p\left(\frac{\delta^* - y}{\alpha}\right) dy \Big\}$ (4.71) and (4.72):

$$\frac{D(\delta)}{K\,\alpha^2} = -\int_0^{w(\delta)} \left(\frac{\delta - \delta^\circ}{\alpha} - w\right) p(w)\,dw$$

$$+\int_0^{x(\delta)} \left(\frac{\delta - \delta^*}{\alpha} + x\right) p(x)\,dx$$

$$-\int_0^{w(\delta)} \left(\frac{\delta^\circ - \delta^*}{\alpha} + x\right) p(x)\,dx \qquad (4.77)$$

The integral of $D(\delta)$ from δ° to δ^* will give the loss for that particular loop:

Loss from δ° to δ^* =

$$L(\delta^\circ,\delta^*,\alpha) =$$

$$\int_{\delta^\circ}^{\delta^*} D(\delta;\delta^\circ,\delta^*,\alpha)\,d\delta \qquad (4.78)$$

In order to better visualize the results of this formulation, consider its use for the generation of a force-deflection curve. Knowledge of the physical system to be modeled suggests several characteristics of the unknown functions. Without attempting to match any specific material or system, the following functions were selected for a trial run with single-action dampers:

$$p(\delta) = 0.01\ \exp-[\delta/0.5]^2 \qquad (4.79)$$

$$q(\delta) = 0.025\ \exp-[(10-\delta)/1000]^2 + 0.025\ \exp-[(10+\delta)/1000]^2 \qquad (4.80)$$

This choice of the functions provides some of the behavior of rubber. The curve stiffens in both tension and compression. The curve also shows hysteretic loss. The

loss function, $p(\delta)$, will give symmetric loss characteristics about the origin. The loss will increase rapidly near zero deformation but increase linearly with deformation at larger deformations. The stiffening function, $q(\delta)$, will cause the force-deformation curve to increase in slope symmetrically in tension and in compression. The resultant curve is shown in Figure (4.16) for a deflection of five units in tension and compression.

Rubber does not stiffen symmetrically and its loss is spread out more than that of Figure (4.16). Another choice of the two functions will produce the curve shown on the right in Figure (4.17). This choice of the functions provides a fairly good visual match to the data shown on the left in Figure (4.17). The data in this figure is from a sample of carbon-filled, vulcanized butyl rubber. Experiments producing this type of data are described in Chapter 5.

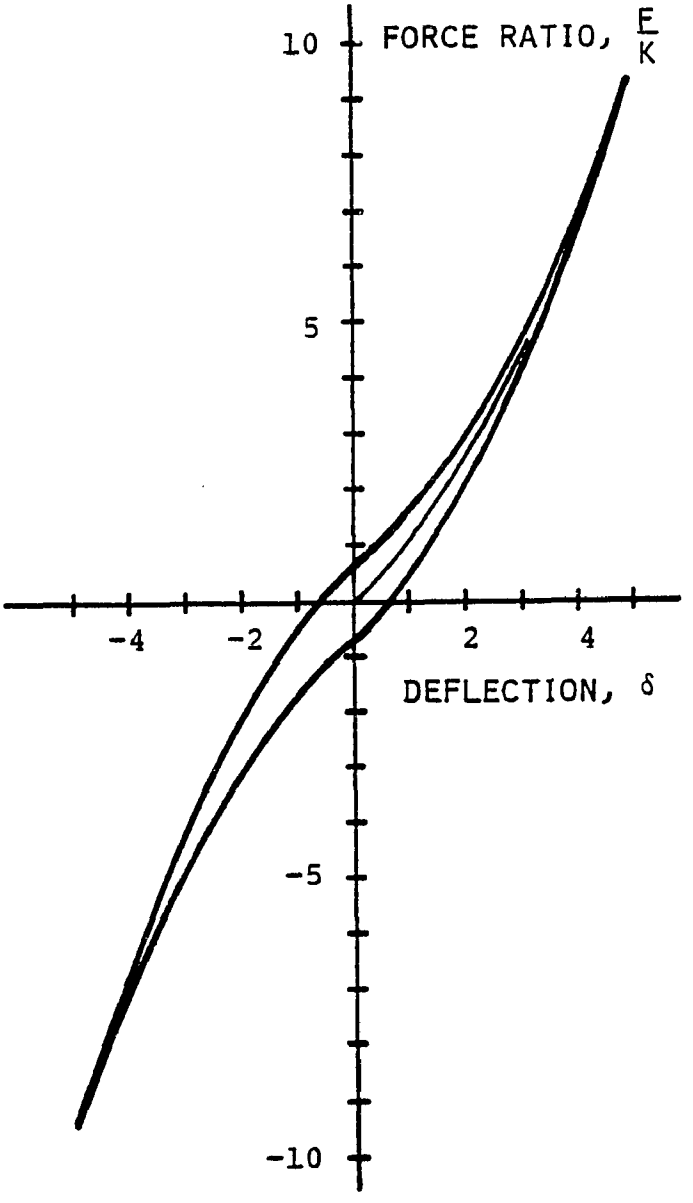


Figure (4.16) Force-deflection curve generated using the arbitrary functions in Equations (4.84) and (4.85)

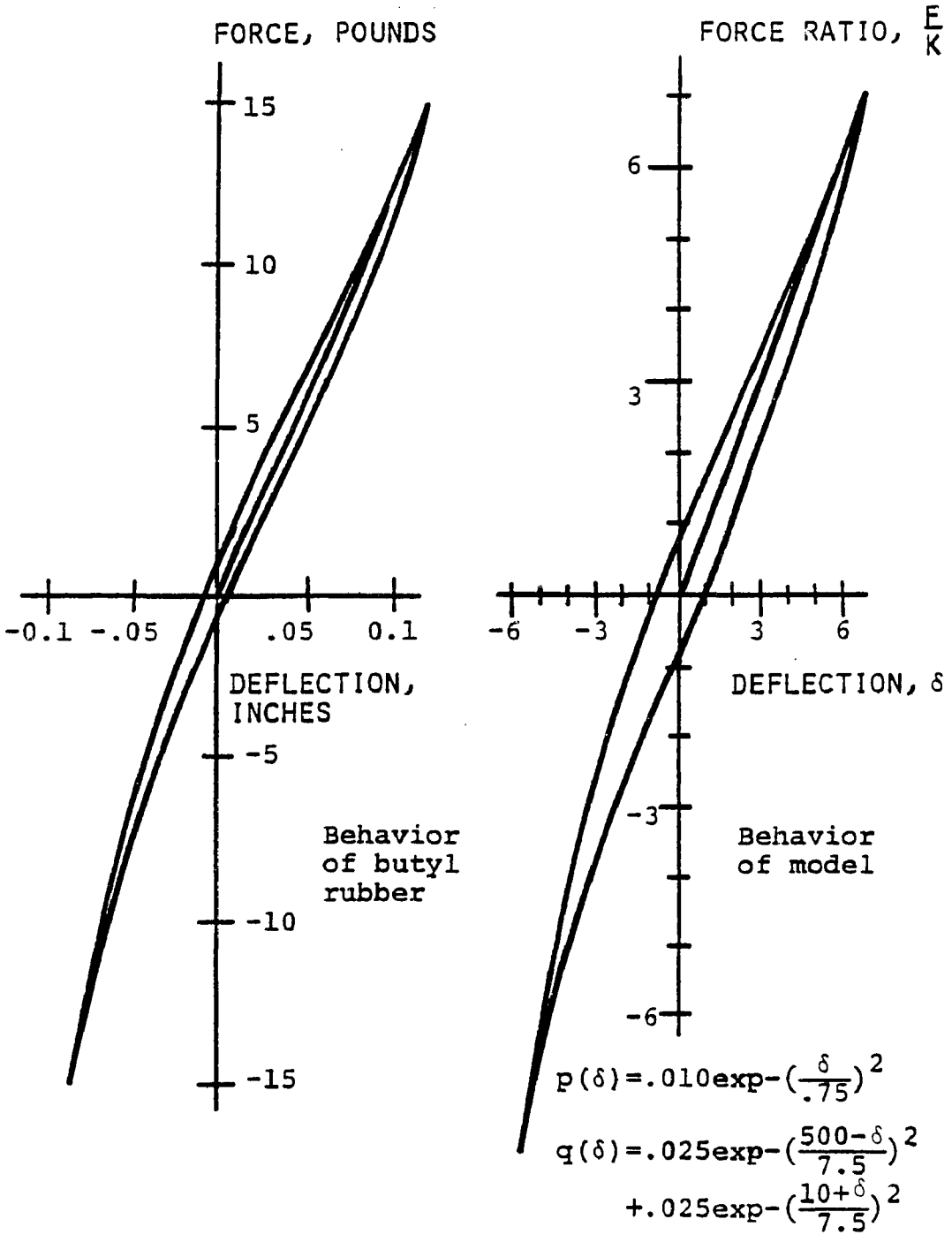


Figure (4.17) Comparison of model behavior to rubber behavior

CHAPTER 5

EXPERIMENTAL VERIFICATION

5.1. Application of Model

5.1.1. Introduction

Chapter 4 presented a mathematical model suitable for use in computing hysteretic loss of a material or system. This chapter will consider the conditions under which the model may be appropriate and how the model may be applied. In particular, the application will be to three samples of carbon-filled, vulcanized rubber.

The model can provide both stress-strain and hysteretic behavior of a material. However, the primary interest of this study is the model's ability to accurately and easily predict qualitative and quantitative hysteretic behavior. Other techniques have adequately modeled elastic or visco-elastic behavior but not loss behavior.

In order to apply the model to rubber, assumptions must be made regarding the loss processes in the material. The model specifies that the sole source of loss in the system is dry friction or plasticity. Previous chapters have shown how such processes may exist in rubber. There have also been examples of viscous processes which may exist in samples of rubber. For the model to be valid, these viscous processes must produce negligible loss compared to dry friction losses.

Note that the material need not be totally free of any time dependent processes. The materials in this experimental program did show some relaxation behavior, but the requirements for linearity were not met. The scaling property appeared valid but the superposition property did not hold for the full range of deflections in the experiment (approximately ±4% strain). Thus, the materials were, at best, nonlinear viscoelastic.

The independence of loss with frequency of cycling is a property of the dry friction model. Recall that for a viscoelastic solid, the loss is a function of the rate of loading. Thus, for the materials in the study, the variation of loss with frequency must be checked. In the experimental program it was noticed that the shape of the hysteresis loop varied somewhat with the rate of loading, but the loss remained quite constant. For the purposes of this study, the dynamic effects were made insignificant by keeping the material mass low, keeping the rates slow, specifying displacements, and measuring resultant forces. Such experiments are quasi-static, and the viscous loss properties of the material are negligible.

The most useful application of the model is to enable an experimenter to draw some conclusions about the one-dimensional loss problem and design a characterizing experiment accordingly. A viscoelastic model predicts complicated effects based on strain level as well as strain

rate or sinusoidal frequency. The current model predicts only a strain level effect. With due regard to the development of Chapter 4, an experimental program may be set up to characterize the loss of the material based on the level of deformation. Thus, a fairly simple interpolation of data could give the loss at any desired level of deformation.

5.1.2. Rate Independence Experiment

From Chapter 4 it should be noted that an experimental program using this model must first verify the rate independence of loss for the range of cycle size and rate of interest. Data can then be obtained which would allow inference of loss for any cycle based on interpolation of data. However, it should be noted that the development of the model has been one-dimensional, quasi-static loading. Thus, to avoid dynamic effects, the rates should be small and both force and deflection should be measured.

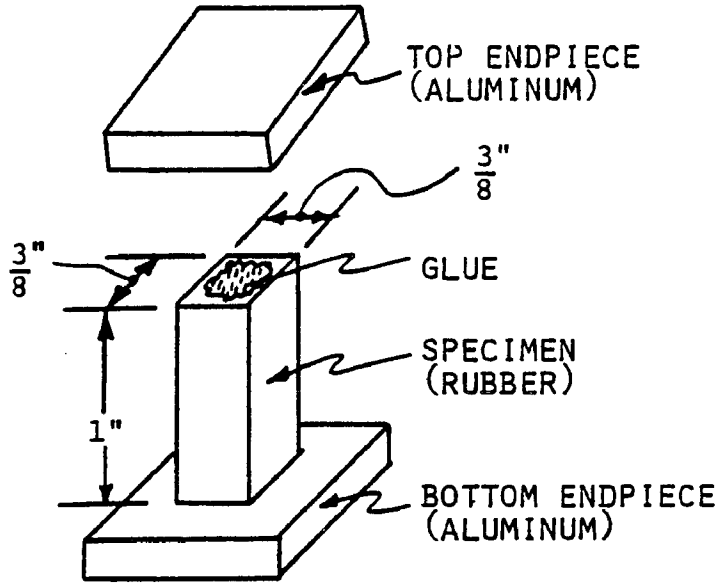
An Instron machine is suitable for testing rubber specimens at slow rates and over known deflection limits [43]. A load cell was built to measure the force resulting from tension or compression of the rubber specimens. This load cell was calibrated and balanced into the force measurement channel of the Instron machine. Special clamps were built to hold the rubber specimens. The Instron machine was calibrated in inches and pounds so these common engineering units were used rather than S.I. units.

The experiment is shown schematically in Figure (5.1). The rubber specimens were all carbon-filled and vulcanized. They were produced in sheets of nominal 3/8 inch thickness. From these sheets test coupons were cut. The coupons were 3/8 inch by 3/8 inch in section, and 1 inch long (approximately 1 cm x 1 cm x 2.5 cm). The coupons were then bonded to aluminum end-pieces with a cyanoacrylate glue to form the test specimens. The specimen could be gripped by the end pieces. The rubber materials for testing were a natural rubber, a butyl rubber, and an oil extended butyl rubber.

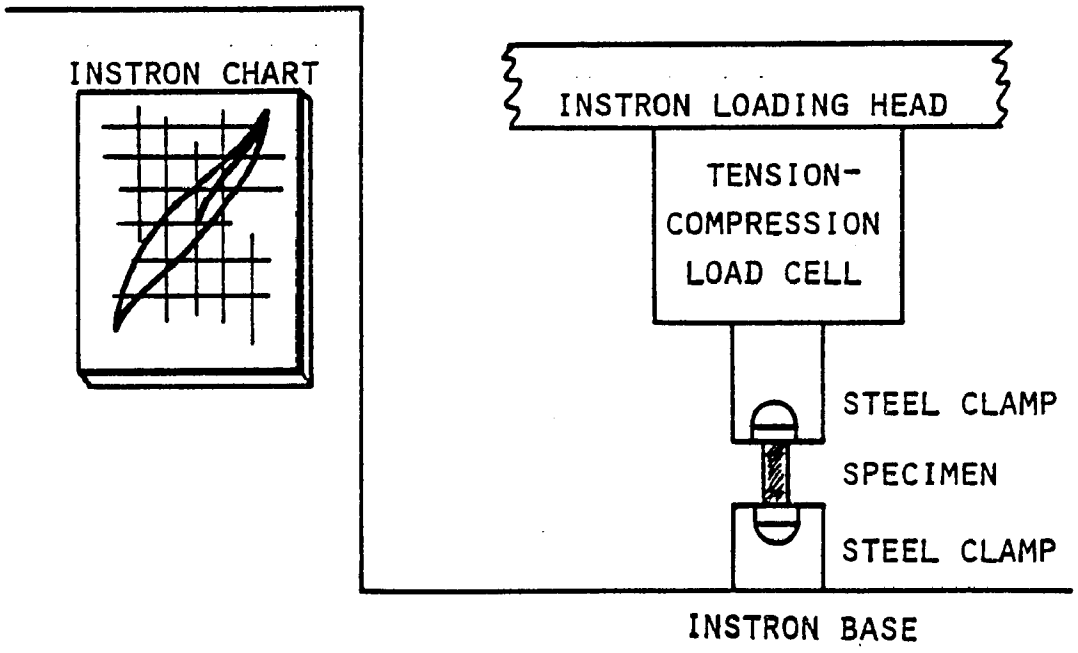
The experimental procedure was similar for each of the three materials, although some differences may be noted later such as variation in the Instron gear combinations. The basic procedure is as follows:

A. Before actual testing began:
    1. Calibrate load cell.
    2. Mount specimen.
    3. Cycle at least 100 times at maximum test deflection.
    4. Dismount specimen.
    5. Let material rest several days.

B. Experimental test:
    1. Calibrate load cell.
    2. Mount specimen.
    3. Set zero force and deflection.



Rubber test specimen



Experimental set-up

Figure (5.1) Schematic of the rubber hysteresis experiments

4. Select gearing and cycle size.
5. Cycle to obtain a stable loop.
6. Reset to zero deflection.
7. Reset cycle size/reset gearing/repeat.
8. Dismount specimen.
9. Check load cell calibration.

Several points of the procedure need elaboration. Before testing any of the materials, each was cycled to remove the complication of the Mullins effect. The model does not require virgin material and, in fact, the transient Mullins effect creates additional complications. The initial loops would have different energy losses than later loops due to this effect. Thus, the order of testing would have a larger effect than the rate of the tests.

This fact was noted with the first few tests where, even at the same rate, the energy loss varied with the number of cycles for about the first 10 to 20 cycles. It was noted that allowing the material to rest for several days after such cycling did not significantly affect the loss. Thus, the preconditioning procedure was designed.

The gearings selected for the test ranged from 0.002 inches per minute to 0.5 inches per minute. These were the slowest speed of the Instron machine and the fastest speed which the machine's cyclic capabilities would allow. The deflection limit was chosen as 0.04 inch tension or compression. This gave a maximum force for any specimen of 10 lbs. or approximately ±70 psi in the specimen.

Viscous processes were noted in the material during testing. When a loop was complete and obtained a stable shape, the deflection was returned to zero. The force generally went back to zero but would take some additional time. After some testing was completed, it was noted that no significant effect could be observed either by waiting for the force to return to zero or by "coaxing" the force to zero by overshooting zero deflection upon return. Similarly, no effect on loss was noted if the force was not zero when the cycle from zero deflection was started, but in this case the loop appeared different until the stable loop was obtained.

The last point to be elaborated is that not all tests for a single material were run at one time. This was a practical matter since the test program consisted of 64 tests, some tests taking more than two hours. There were also problems with electronic drift and mechanical slippage or glue breakage with long term tests. Thus, the fact that little variation is noted in the data can be interpreted that running the tests on different days has little effect. As a check, some of the faster cycles were run twice, a month apart, and still gave approximately the same loss.

The data obtained from the test program is now presented in several ways. The program was designed to verify the rate independence of the materials and to allow an empirical fit of the data for other uses. The raw data

were loops of load versus deflection for the various rates, cycles, and materials. This body of data was reduced to provide loss versus strain information.

The area of each loop was measured using a planimeter. Other techniques were tried but none proved more accurate or easier. Counting squares or integrating pointwise were more time consuming and the cut-out-and-weigh technique had the disadvantage that data could be easily lost or destroyed.

The areas were converted to energy loss by multiplicative factors. The limit of accuracy of measuring areas with the planimeter is 0.01 square inch. When converted to energy loss by the various factors, the limit of accuracy varied from 0.001 inch-pounds to 0.005 inch-pounds. For the smallest cycles this allowed errors to be as much as 25% of the value of the energy loss itself. For the largest cycles the limit of accuracy allowed errors to amount to only one or two percent of the energy loss measurement.

There were two other sources of error which may be considered uncontrollable. The first is the skill of the operator in the use of the planimeter. With practice, the ability to get consistent results improved. However, use of the planimeter for too long a time caused operator fatigue. These errors were minimized by measuring all loops several times to assure reasonable accuracy. This was particularly useful for the smallest loops where the measurement errors could be 25% of the required value of loss.

The second uncontrollable source of error was the Instron machine itself. Only specific combinations of gearing were available, which affected the area-to-energy conversion factor. On automatic cycling, the Instron machine has slightly different switch points when the gearing is changed. The synchronization between the loading head and the chart recorder is also affected by the gear changes. The stiffness of the sample also affects the switch points, but to a lesser degree. These errors were responsible for much of the loss variation at different gear combinations.

The area measurements, as well as the energy losses, are displayed in Tables (5.1), (5.2), and (5.3). The statistical variation of the energy loss at a given cycle size is within the range of experimental error. Due to the 1 inch length of the specimen, the strain level is easily calculated from the deformation excursion. A plot was made of loss against deformation rate for each of the three materials, with strain level as a parameter.

Note the lack of rate effects in Figures (5.2), (5.3), and (5.4). Each plot spans approximately 2 1/2 decades of rate. Considering the frequency of cycling for specimens of the given dimensions, these rates and cycle sizes cover 3 decades of frequency. The fastest cycle is 1 2/3 Hz. which is the smallest loop at the highest rate. The slowest cycle is about 4×10^{-4} Hz. for the largest loop at the slowest rate.

Loop Size	Crosshead Rate, inches/minute .002	.005	.01	.02	.05	.1	.2	.5
.01	.20	.08	.12	.12	.09	.11	.11	.10
.02	.73	.30	.40	.41	.31	.38	.38	.30
.03	1.55	.61	.80	.80	.63	.79	.81	.64
.04	2.45	1.02	1.24	1.26	1.01	1.23	1.22	.97
.05	3.61	1.44	1.80	1.81	1.45	1.80	1.81	1.44
.06	4.79	1.90	2.39	2.40	1.92	2.39	2.40	1.92
.07	6.04	2.40	3.00	2.99	2.39	2.99	2.98	2.38
.08	7.25	2.92	3.64	3.65	2.93	3.66	3.65	2.92

Table (5.1a) Measured areas of loops, square inches

Rate	.002	.005	.01	.02	.05	.1	.2	.5
Conversion	.02	.05	.04	.04	.05	.04	.04	.05

Table (5.1b) Conversion factors for the various crosshead rates, inch/pounds/square inch

Loop Size	Crosshead Rate, inches/minute .002	.005	.01	.02	.05	.1	.2	.5	mean
.01	.004	.004	.005	.005	.005	.004	.004	.005	.005
.02	.015	.015	.016	.016	.016	.015	.015	.015	.015
.03	.031	.031	.032	.032	.032	.032	.032	.032	.032
.04	.049	.051	.050	.050	.051	.049	.049	.049	.050
.05	.072	.072	.072	.072	.073	.072	.072	.072	.072
.06	.096	.095	.096	.096	.096	.096	.096	.096	.096
.07	.121	.120	.120	.120	.120	.120	.119	.119	.120
.08	.145	.146	.146	.146	.147	.146	.146	.146	.146

Table (5.1c) Energy loss, inch-pounds

Table (5.1) Energy loss from measured areas for natural rubber

Loop Size	Crosshead Rate, inches/minute .002	.005	.01	.02	.05	.1	.2	.5
.01	.12	.05	.27	.07	.06	.26	.07	.05
.02	.46	.17	.90	.23	.18	.90	.23	.18
.03	.96	.38	1.92	.49	.39	1.91	.29	.39
.04	1.50	.59	3.00	.77	.61	3.02	.76	.60
.05	2.22	.90	4.50	1.13	.91	4.46	1.11	.91
.06	2.99	1.20	5.94	1.50	1.21	6.00	1.50	1.19
.07	3.88	1.55	7.77	1.95	1.56	7.82	1.95	1.58
.08	4.82	1.91	9.56	2.40	1.91	9.61	2.40	1.93

Table (5.2a) Measured areas of loops, square inches

Rate	.002	.005	.01	.02	.05	.1	.2	.5
Conversion	.02	.05	.01	.04	.05	.01	.04	.05

Table (5.2b) Conversion factors for the various crosshead rates, inch/pounds/square inch

Loop Size	Crosshead Rate, inches/minute .002	.005	.01	.02	.05	.1	.2	.5	mean
.01	.002	.003	.003	.003	.003	.003	.003	.003	.003
.02	.009	.009	.009	.009	.009	.009	.009	.009	.009
.03	.019	.019	.019	.020	.020	.019	.020	.020	.020
.04	.030	.030	.030	.031	.031	.030	.030	.030	.030
.05	.044	.045	.045	.045	.046	.045	.044	.046	.045
.06	.060	.060	.059	.060	.061	.060	.060	.060	.060
.07	.078	.078	.078	.078	.078	.078	.078	.079	.078
.08	.096	.096	.096	.096	.096	.096	.096	.097	.096

Table (5.2c) Energy loss, inch-pounds

Table (5.2) Energy loss from measured areas for butyl rubber

Loop Size	Crosshead Rate, inches/minute .002	.005	.01	.02	.05	.1	.2	.5
.01	.33	.13	.16	.17	.12	.16	.18	.12
.02	1.03	.41	.51	.52	.40	.49	.50	.40
.03	2.10	.84	1.03	1.05	.84	1.03	1.05	.82
.04	3.25	1.35	1.61	1.61	1.32	1.65	1.62	1.32
.05	4.70	1.88	2.32	2.31	1.89	2.35	2.34	1.87
.06	6.06	2.46	3.03	3.04	2.45	3.06	3.06	2.43
.07	7.93	3.19	4.00	3.98	3.20	4.02	4.00	3.20
.08	9.95	4.10	4.89	4.98	4.04	4.98	5.01	4.03

Table (5.3a) Measured areas of loops, square inches

Rate	.002	.005	.01	.02	.05	.1	.2	.5
Conversion	.02	.05	.04	.04	.05	.04	.04	.05

Table (5.3b) Conversion factors for the various crosshead rates, inch/pounds/square inch

Loop Size	Crosshead Rate, inches/minute .002	.005	.01	.02	.05	.1	.2	.5	mean
.01	.007	.007	.006	.007	.006	.006	.007	.006	.007
.02	.021	.021	.020	.021	.020	.020	.020	.020	.020
.03	.042	.042	.041	.042	.042	.041	.042	.041	.042
.04	.065	.068	.064	.064	.066	.066	.065	.066	.066
.05	.094	.094	.093	.092	.095	.094	.094	.094	.094
.06	.121	.123	.121	.122	.123	.122	.122	.122	.122
.07	.159	.160	.160	.159	.160	.161	.160	.160	.160
.08	.199	.205	.196	.199	.202	.199	.200	.202	.200

Table (5.3c) Energy loss, inch-pounds

Table (5.3) Energy loss from measured areas for oil extended butyl rubber

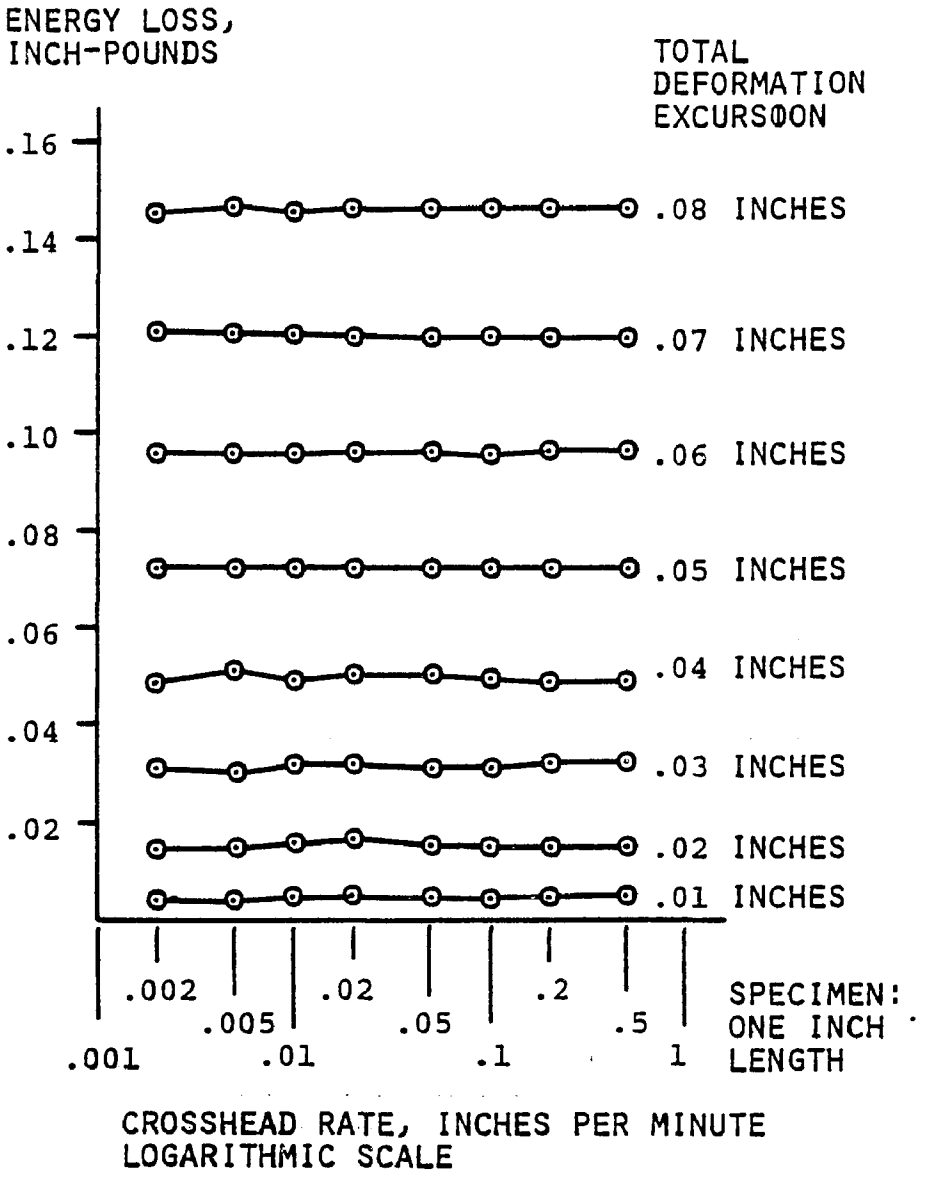


Figure (5.2) Relation of loss, rate, and cycle size for natural rubber sample. Data obtained for tension-compression cycles.

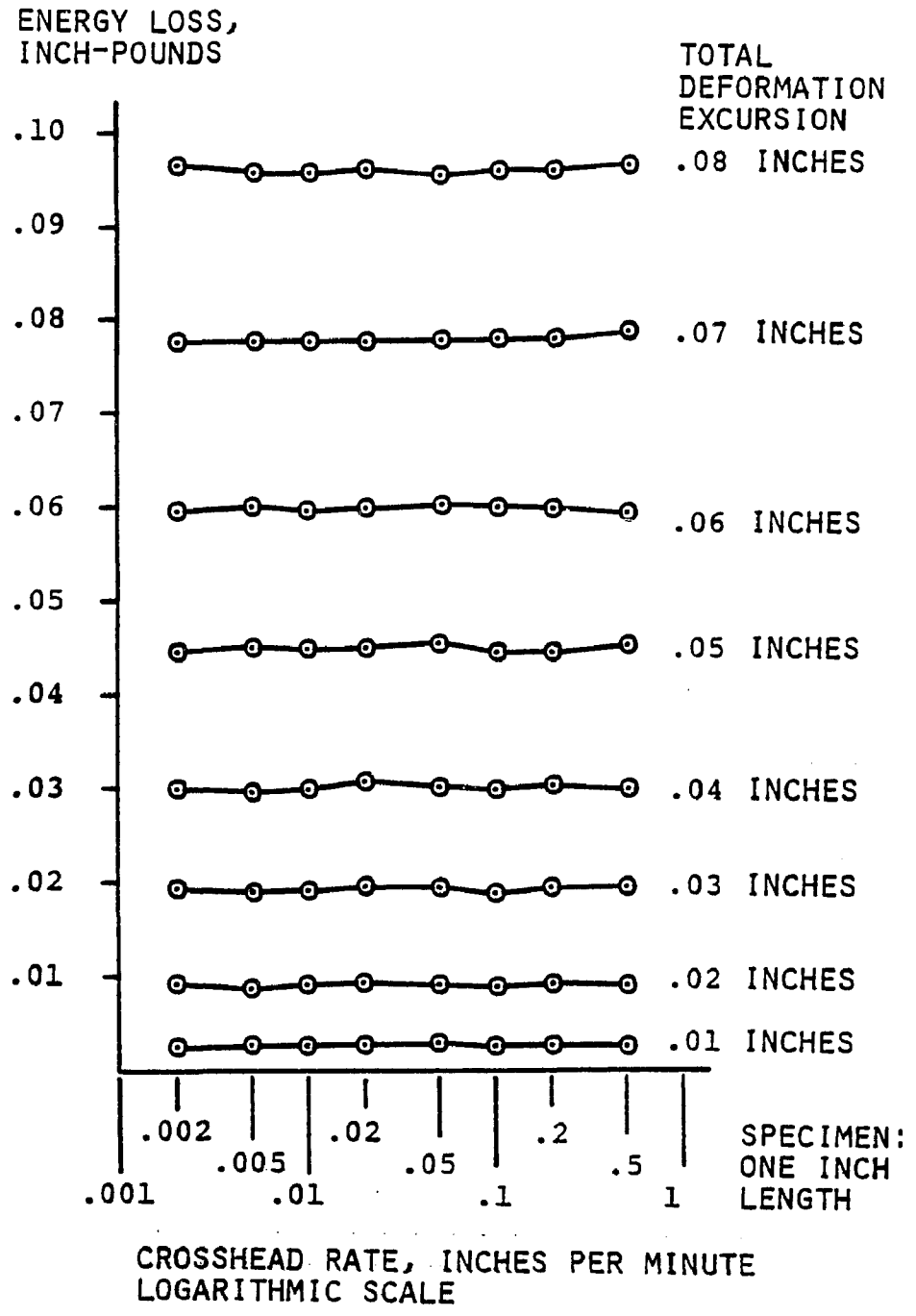


Figure (5.3) Relation of loss, rate, and cycle size for butyl rubber sample. Data obtained for tension-compression cycles.

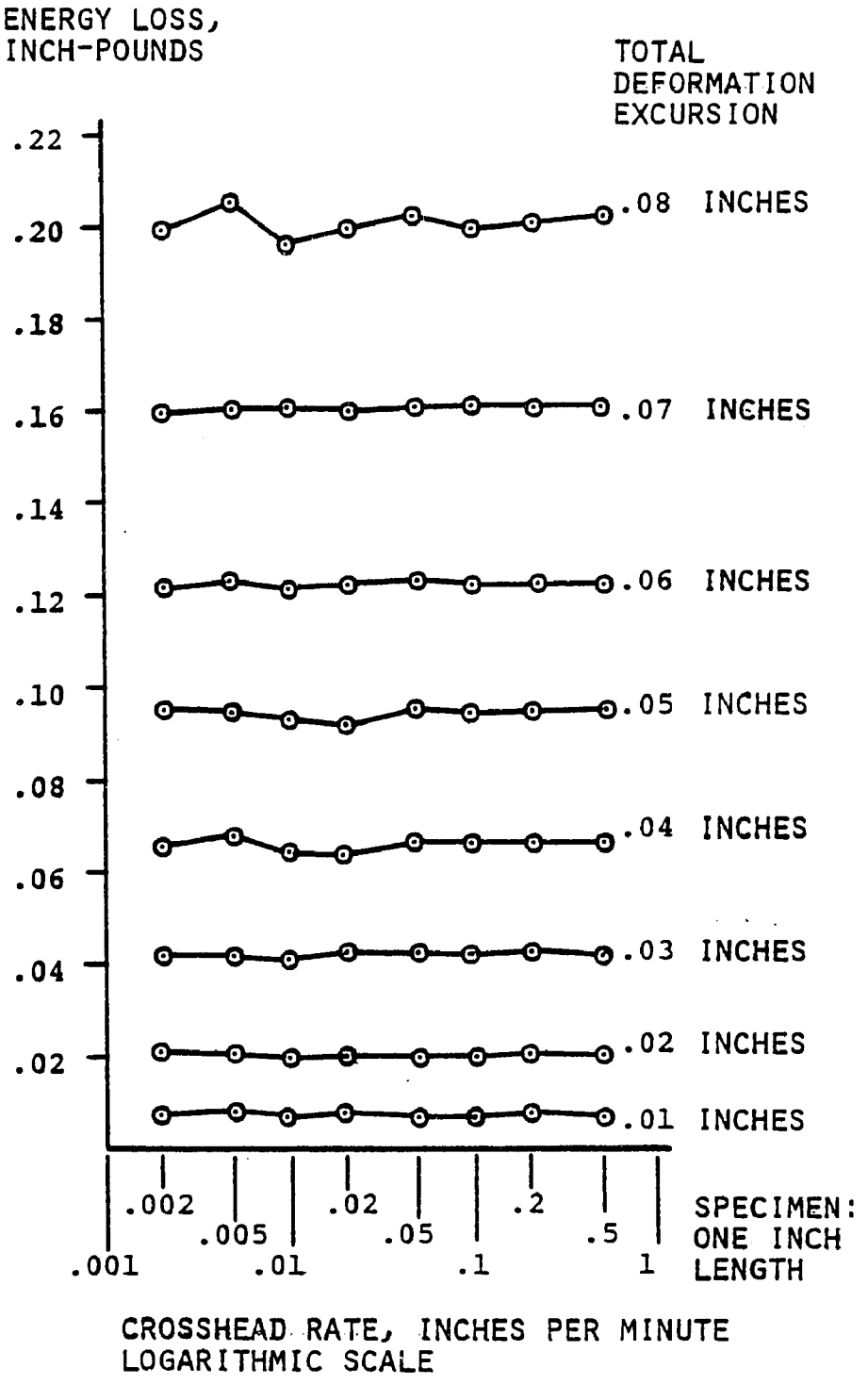


Figure (5.4) Relation of loss, rate, and cycle size for oil extended butyl rubber sample. Data obtained for tension-compression cycles.

The losses are plotted as a function of cycle size in Figure (5.5). Due to the convenient length of the specimen, this is also a plot of loss versus maximum strain excursion for the given volume of material. The graph also shows a power curve by a least-squares fit for each of the three materials of this study. It is of some interest to note that the loss plot for each of the three materials is approximately dependent on the 1 2/3 power of the deformation cycle size. This approximation has been used in the rubber industry although it has no theoretical basis and is poorly documented [*].

This theoretical and experimental work could be sufficient for many purposes. Now that data has been obtained and empirically fit, some useful problems may be solved for these materials. Consider the following simple example:

> An electrical appliance has four rubber feet each 3/8" x 3/8" x 3/8". The maximum vertical deflection permissible is 0.01 inches. What amount of energy can be dissipated by each of the test compounds? The maximum oscillatory strain is 0.026.
>
> From Figure (5.5) the loss for this size strain cycle would be:

---

[*] Floyd Conant, Firestone Tire and Rubber Company, private communication.

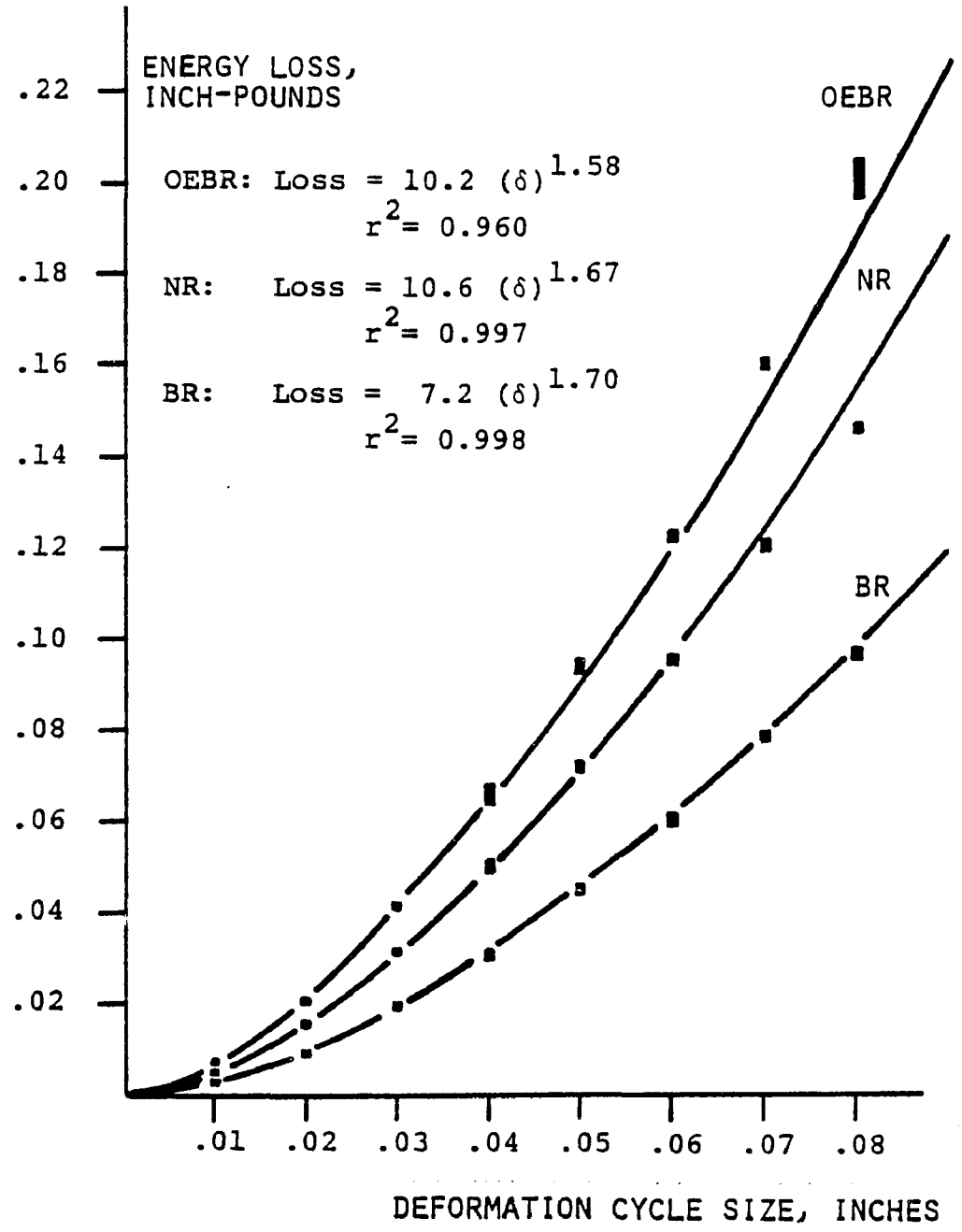


Figure (5.5) Losses as a function of cycle size for three carbon-filled, vulcanized rubber samples. The specimens are one inch long. Size of points indicates scatter of data. Smooth curves are least-squares curve fits.

OEBR: Oil extended butyl rubber
NR: Natural rubber
BR: Butyl rubber

0.032 inch-lbs for oil extended butyl rubber

0.025 inch-lbs for natural rubber

0.016 inch-lbs for butyl rubber

And for the four rubber feet, which together have 1 1/2 the volume, the energy loss would be:

0.048 inch-lbs for oil extended butyl rubber

0.038 inch-lbs for natural rubber

0.024 inch-lbs for butyl rubber

Thus, if the amount of energy to be dissipated is known, the appropriate material can be selected. But, in order to minimize the deflection, the choice would be oil extended butyl rubber. Alternately, if the amount of energy to be dissipated is specified, the deflections required for each of these materials could be obtained.

5.2. Further Development of Model

5.2.1. Characterizing Experiments

This section will develop the model equations of Chapter 4 further. This will enable some specific situations to be described analytically and compared with the experimental data just presented.

Recall Equation (4.63), the equation for force generated in a virgin material by initial deformation. This equation requires the loss function $p(\delta)$ and the stiffening function $q(\delta)$. The action of the dampers, α, appears in Equation (4.64). This parameter must be specified for generating

the return curve. If the material is a nonvirgin material, the equation for force at some deformation will also include δ_p, the equivalent plastic deformation, as a parameter.

Under several circumstances the parameters, α and δ_p, are not necessary. Notice that if the material is not a virgin material, then the action of the dampers will effectively be unity. All loadings after the initial cycle involve $q(\delta)$ and $p\left(\frac{\delta^* - \delta}{\alpha}\right)$. However, as was described in Equation (4.25):

$$p\left(\frac{\delta^* - \delta}{\alpha}\right) = p'(\delta) \tag{5.1}$$

Thus, an experiment which attempts to measure $p(\delta)$ will actually be measuring $p'(\delta)$. If the parameter α is known, then this scale factor can be used to obtain $p(\delta)$. However, all subsequent computations using $p(\delta)$ will again require the scale factor α to be used to generate $p'(\delta)$. Thus, the function $p'(\delta)$ can be used for most computations, and α is only necessary to relate data from virgin and nonvirgin loadings. If processes in the material allow the substance to return to its virgin state after some time, then relating this state and its loadings to other states may require the action of the dampers as well. Basically, after the material has left its virgin state, the loss processes will be single action, but if the material can return to its virgin state, the action of the dampers would then be required.

In some circumstances the equivalent plastic deformation will be unnecessary. First and simplest, this parameter can become lumped with δ_0, the reference deflection. In an experiment, when the force is zero and it is decided that this will be the reference deflection, any equivalent plastic deformation can be absorbed by δ_0 in the equation to satisfy Equation (4.64). Second, in many cases the history of δ_p can be eliminated. Recall Equation (4.77) for the separation of the loading and unloading curves. By subtraction, only the latest part of δ_p remains in this equation. The loss can be computed by integrating this separation and δ_p never enters the calculation.

It may also be recalled from Equations (4.77) and (4.78) that only the function $p(\delta)$ appears in the loss calculations. By eliminating δ_p and $q(\delta)$ by subtraction, and reducing the system to single action dampers as mentioned above, the loss integration requires only one of the unknowns. Thus, from data contained in one large hysteresis loop, the theory could generate the loss for any smaller loop. However, this is hardly superior to the plot of loss versus cycle size accomplished in the previous section, although the equations in Chapter 4 can then be solved for $q(\delta)$ from appropriate data.

An algebraic scheme was tried for solving the system of Equations (4.21),(4.37),(4.45) for $Q(\delta)$ and $P(\delta)$. The load and return curves can be represented symbolically as:

$$\{F_1(\delta)\} = [A]\{Q(\delta)\} + [B]\{P(\delta)\} + \{D\} \quad (5.2)$$

$$\{F_2(\delta)\} = [A]\{Q(\delta)\} + [C]\{P(\delta)\} + \{D\} \quad (5.3)$$

By subtraction of the load and unload curves:

$$\{F_1(\delta)\} - \{F_2(\delta)\} = [B - C]\{P(\delta)\} \quad (5.4)$$

and thus:

$$\{P(\delta)\} = [B - C]^{-1}\{F_1(\delta) - F_2(\delta)\} \quad (5.5)$$

If the losses were the only interest, this would be sufficient. However, the solution for $Q(\delta)$ would also be available from:

$$\{Q(\delta)\} = [A]^{-1}\left\{\{F_1(\delta) - \{D\} - [B]\{P(\delta)\}\right\} \quad (5.6)$$

where $P(\delta)$ is available from Equation (5.5). Note that the loading and unloading curves were for arbitrary nonvirgin loading. Thus, the solution for $P(\delta)$ in Equation (5.5) is actually a vector of values for the function $P'(\delta)$, not $P(\delta)$.

This algebraic approach was formulated in detail and programmed on a computer for solution from data taken on the materials of the previous section. The results were disappointing. The data had more scatter than a direct algebraic approach could handle and the functions which were generated were unrealistic. The functions would jump from large positive to large negative values over a few hundredths of an inch.

The development of Chapter 4 used the concept of a random variable. The equations gave only statistical averages or expected values. The data had scatter from

several sources including the material processes and the experimental procedure. The functions $p(\delta)$ and $q(\delta)$ themselves are not observable. Thus, when this formulation was used in a direct algebraic scheme the scatter in the data caused computational difficulties.

Consider what is to be expected for the shape of $q(\delta)$ and $p(\delta)$. From Chapter 2, recall that rubber stiffens in tension at strains of the order of 100%, and also stiffens almost immediately in compression. Since $q(\delta)$ is related to the amount of stiffening in the material, this function should be nearly zero from zero deflection into tension. Also, $q(\delta)$ should be small for small values of compression. For the strain range of the experiments in the previous part of this chapter, little stiffening was noted except in compression for the larger cycles. Thus, for the range of deflections of interest here, $q(\delta)$ is expected to be approximately equal to zero.

Consider the shape of $p(\delta)$. This function is related to the number of elements which start to slip at a given deflection. If it is assumed that the probability of an element sliding gets larger as the deflection gets larger, then, conversely, the probability of an element beginning to slide gets smaller as the deflection increases, since the number of sticking elements decreases. This description of the probability suggests a hypergeometric or a binomial type distribution for $p(\delta)$. However, the sequencing of

deflections $\delta_1 < \delta_2 < \delta_3 < \cdots$ removes the condition of independent trials required by these distributions.

Regardless of the theoretical distribution, a sample from $p(\delta)$ should exhibit a peak near zero deformation and some type of tapering off at larger deflections. Both the hypergeometric and binomial distributions have the type of bell shape that is expected for $p(\delta)$. The Gaussian normal distribution has a similar shape to that expected for $p(\delta)$, and it also has some other attractive features. When this function was previously used to model the elastic process in rubber, it gave good results, as shown in Figure (2.13). Thus, it seems reasonable to assume the loss function $p(\delta)$ to be normally distributed around the reference deflection δ_0.

Since average values for $p(\delta)$ are the only observable quantities, attempting to use the data points in a direct algebraic approach did not work. Using the area under the $p(\delta)$ curve is a reasonable approach which will automatically smooth the data. The average of observed values of $p(\delta)$ can be made to match with the expected value of the approximating function for $p(\delta)$ over various ranges by using the areas under the observed $p(\delta)$ plot.

It was noted in the course of the direct algebraic approach that a quantity, $[q(\delta) - p'(\delta)]$, appeared in the analysis. This is disguised in Equations (5.2) through (5.6) by the matrix formulation. Recall that the quantity

[Q - P] appeared in Chapter 4, Equation (4.24), where Whiteman's single unknown function was the difference of the two unknown functions of the current model. In the algebraic scheme, the quantity appeared when the forces at succeeding points were subtracted. The Whiteman analysis considered the slope of the load-deflection curve. Let us take the derivative of Equation (4.64):

$$\frac{dF(\delta)}{d\delta} = K + K \int_{\delta_0}^{\delta} q(y)dy - K \int_{\delta_0}^{\delta} P\left(\frac{\delta^* - y}{\alpha}\right)dy \qquad (5.7)$$

Now consider the slope at two points δ_1 and δ_2. The difference in these slopes is:

$$\frac{dF(\delta_2)}{d\delta} - \frac{dF(\delta_1)}{d\delta} = K \int_{\delta_1}^{\delta_2} q(y)dy - K \int_{\delta_1}^{\delta_2} p\left(\frac{\delta^* - y}{\alpha}\right)dy \qquad (5.8)$$

The integrals in Equation (5.7) are the expected values for $q(\delta)$ and $p'(\delta)$ in the range $(\delta_1 \leq \delta \leq \delta_2)$, as defined in Equation (4.62) and (4.63). Thus, it can be written:

$$\text{Slope at } \delta_1 - \text{Slope at } \delta_2 = K\left[E\left\{q(\delta) \mid \delta_1 \leq \delta \leq \delta_2\right\} - E\left\{p'(\delta) \mid \delta_1 \leq \delta \leq \delta_2\right\}\right] \qquad (5.9)$$

If the difference of slope is taken at a sequence of points along a load-deflection curve, a histogram of observed values can be plotted as a function of deflection. This chart can be fit with a function to approximate $[q(\delta) - p'(\delta)]$.

This was, in fact, the method used to obtain $p'(\delta)$. It was assumed that $q(\delta)$ was zero for the range of interest. The histogram of $q(\delta) - p'(\delta)$ did have a bell shape and the resultant fit for $p'(\delta)$ was used in loss calculations. This will be discussed in more detail in the next section, but consider here the general expectations for the loss calculation.

As mentioned before, the model predicts no frequency effect on loss. Equation (4.78) indicates how the loss may be calculated by a double integration of the function $p(\delta)$. If $p(\delta)$ is a bell shaped curve which becomes effectively zero after some deflection, the general shape of the loss versus cycle-size curve can be inferred.

A nonzero constant for $p(\delta)$ would give a loss dependent on cycle size squared, as is the case for a linear material. A zero value for $p(\delta)$ gives a loss dependent on cycle size to the first power. The decreasing character of $p(\delta)$ would give a loss which rises nonlinearly near δ_0. When $p(\delta)$ has decreased to zero the loss would increase linearly with cycle size. The character of the loss versus cycle size curves from the earlier experiments are between parabolic and linear curves. This gives weight to the argument that $p(\delta)$ is bell shaped around δ_0.

A further comment is necessary regarding the symmetry of $p(\delta)$. It is agreed that $q(\delta)$ is not symmetric, due to the stiffening character of the rubber. If $p(\delta)$ is not

symmetric about δ_0, the loss will be different for cycles of the same size in tension or compression or cycles which span tension and compression. If the distribution of $p(\delta)$ is symmetric, then even if δ° and δ^* are both positive or both negative, the only variable is $|\delta^\circ - \delta^*|$. This is the magnitude of the deflection excursion of the cycle. The display of the experimental results in the previous section implicitly assumes $p(\delta)$ is symmetric by using the deflection excursion as the abscissa of the plot illustrating loss versus cycle. For an unsymmetric distribution, the loss will depend on the end points of the cycle as well as $|\delta^\circ - \delta^*|$.

One way in which $p(\delta)$ could be unsymmetric is if we consider a special case of "zero" action dampers. This is not the situation where $\alpha = 0$ in the current formulation. In this special case the distributions for the tensile and compressive directions are distinct. Thus, there would be one $p(\delta)$ for loading from more-tensile to more-compressive and a different $p(\delta)$ for loadings in the reverse direction. Future formulations of the model could include this possibility.

The nonsymmetry in $p(\delta)$ causing differences in loss can be observed in the theoretical development. For example, with an appropriately shaped $p(\delta)$ a specific cycle into compression might be 10% higher than the same cycle size which spans tension and compression. The compression

cycle would then be expected to be more than 10% higher than the same size cycle which is totally in tension. In some experiments this was noted but the differences in loss from pure tension cycles and pure compression cycles was rarely over 10%. In the interest of clarity, the following section will assume the $p(\delta)$ functions are symmetric about δ_0.

5.2.2. Loss Computations

With the equipment and samples used earlier, a new experiment was undertaken. A large loop into tension and another into compression was obtained for each sample. These loops were from the reference deflection to $\delta^* = \pm 0.07$ inch. The loss stablized in two or three cycles. The slope of these curves were measured at 69 points, that is, over intervals of 0.001 inch. The slope could be measured on the Instron plot to a reasonable accuracy of better than 5 pounds per inch. The difference of the slopes at succeeding points was used to generate $p'(\delta) - q(\delta)$ as described in Equations (5.7) through (5.9).

The histograms of these data are shown as Figures (5.6), (5.7), and (5.8). This data seems rather erratic, but it is smooth compared to the results of the algebraic scheme. The data used for that technique used the values of the functions at 100 points, which did not have the benefit of taking the average slope over a range of deflections.

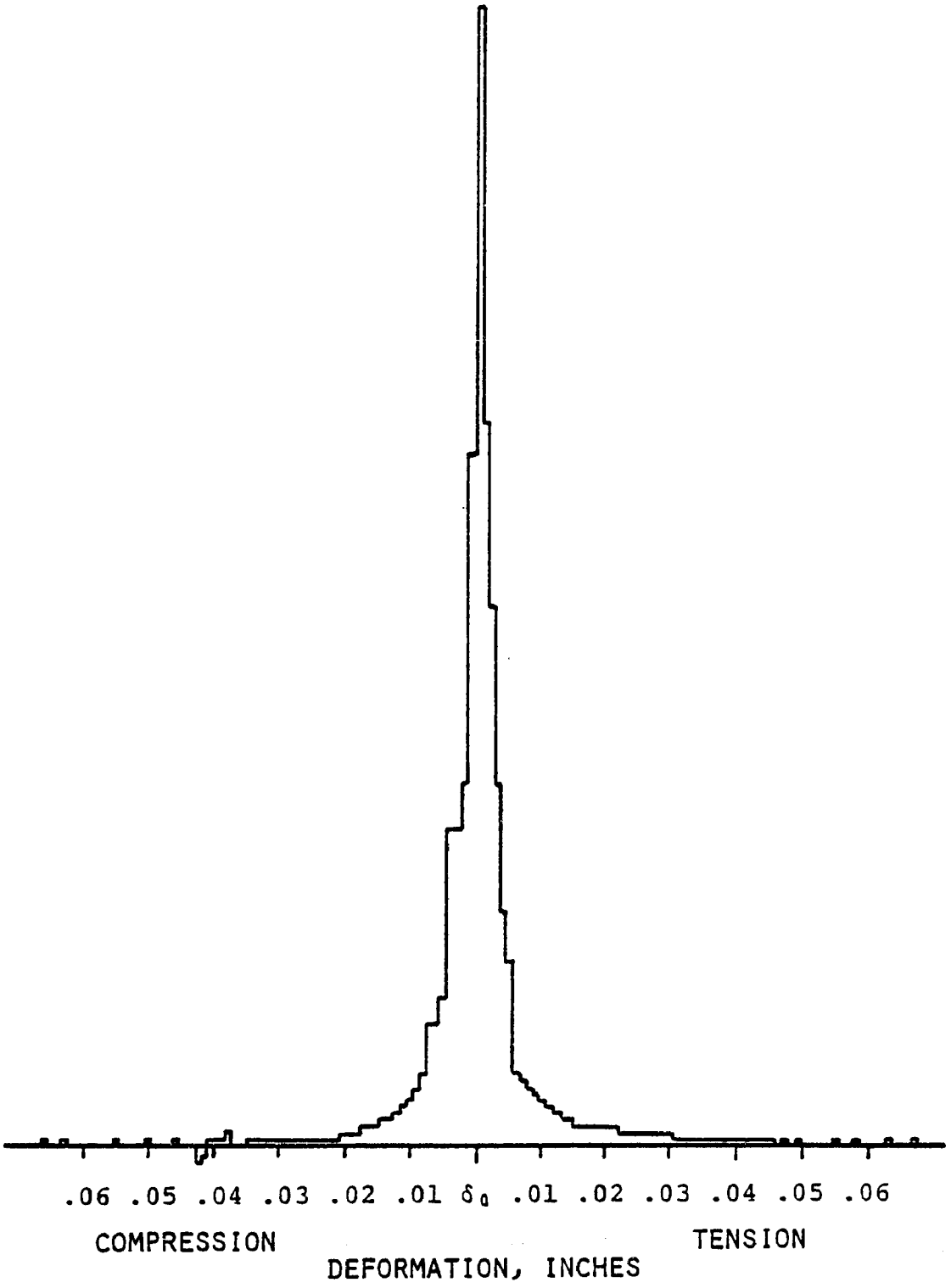


Figure (5.6) Histogram of $[p'(\delta) - q(\delta)]$ for natural rubber sample

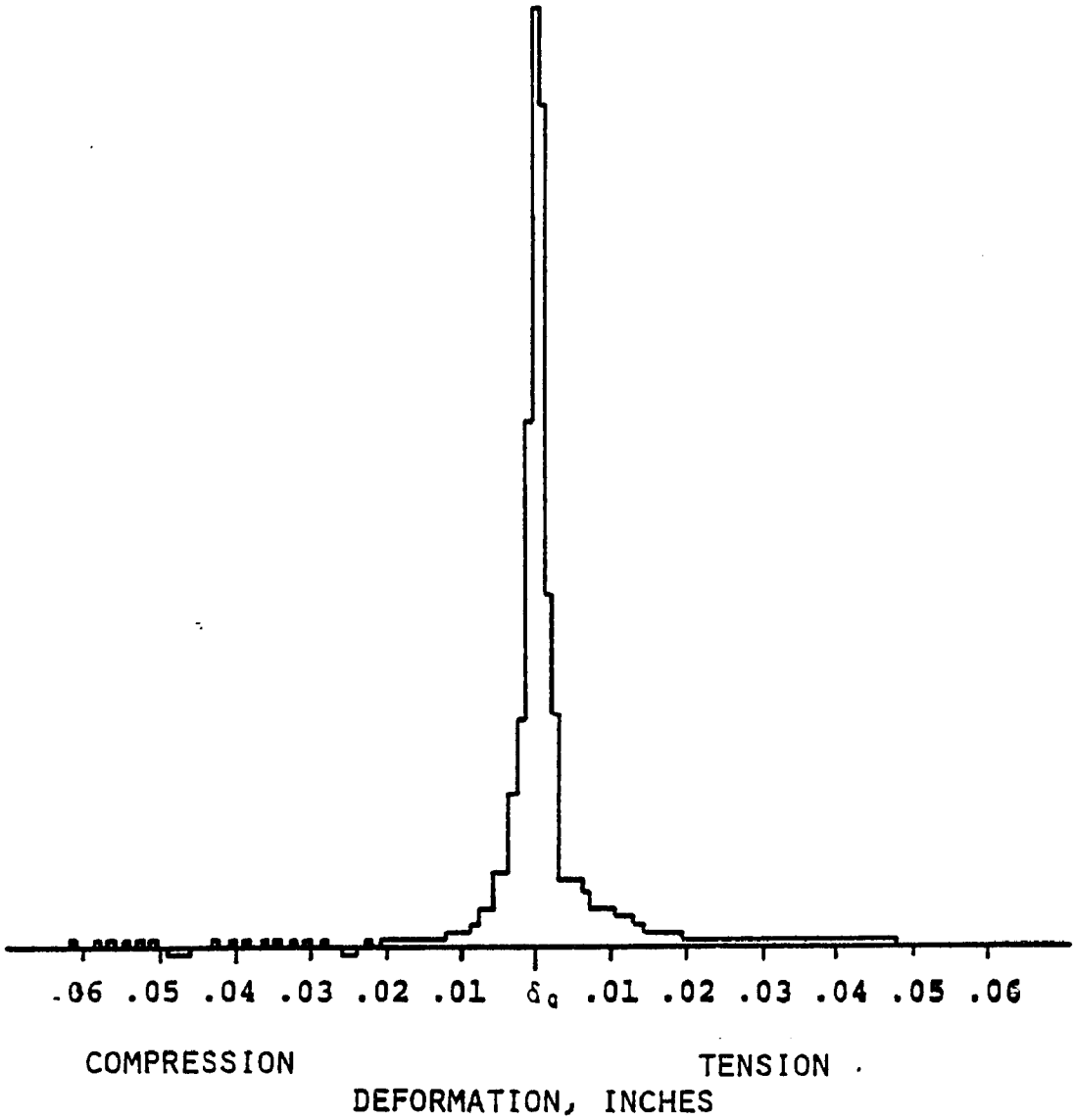


Figure (5.7) Histogram of $[p'(\delta) - q(\delta)]$ for butyl rubber sample

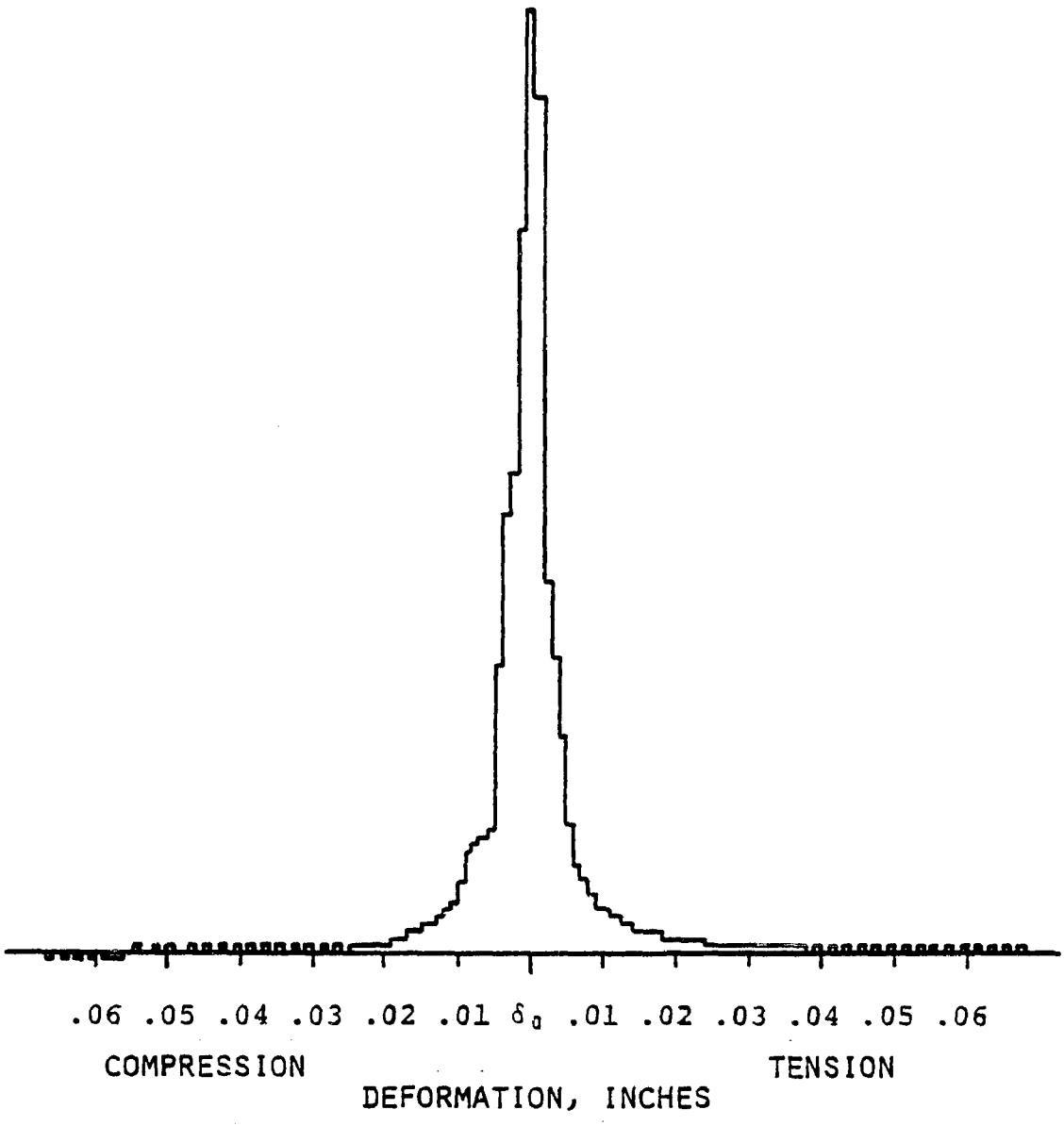


Figure (5.8) Histogram of $[p'(\delta) - q(\delta)]$ for oil extended butyl rubber

In order to match the bell-shaped histograms with normal distributions, the data was converted to percentages of total area as a function of displacement. The data could then be plotted on probability paper. Probability paper has a linear horizontal axis, and the scale on the vertical axis set so a normal curve will plot as a straight line. The data for each of the sample materials is plotted on a probability scale in Figures (5.9), (5.10), and (5.11).

Clearly the data does not fall on a straight line. However, several loss processes were mentioned as possibly existing in the material. Two or more processes could exist simultaneously in the material. The sum of two normal distributions still looks like a bell-shaped curve but has two distinct slopes on probability paper. The smooth curves on the figures are generated by functions consisting of two normal distributions.

No formal fitting procedure exists for such functions. A computer program was written to generate a family of such functions. From this family of curves the illustrated curves were selected. Generally, the limiting straight line, as the curve passes through 50%, gives one value of standard deviation. The limiting straight line from nearly 0% through nearly 100% indicates the other value of standard deviation. The fraction of each determines where the knee of the curve appears and how sharp the change is.

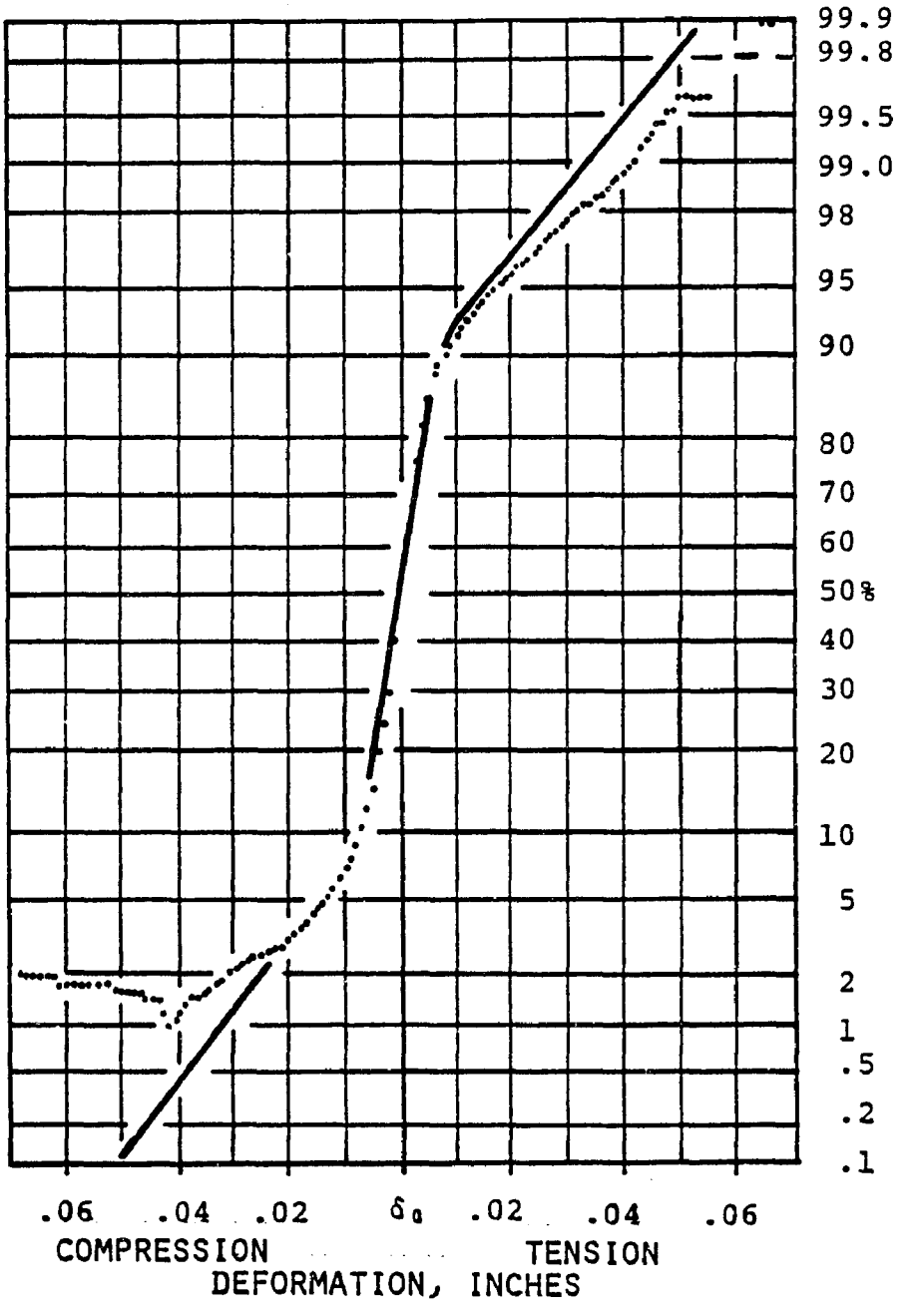


Figure (5.9) Data for natural rubber on probability paper

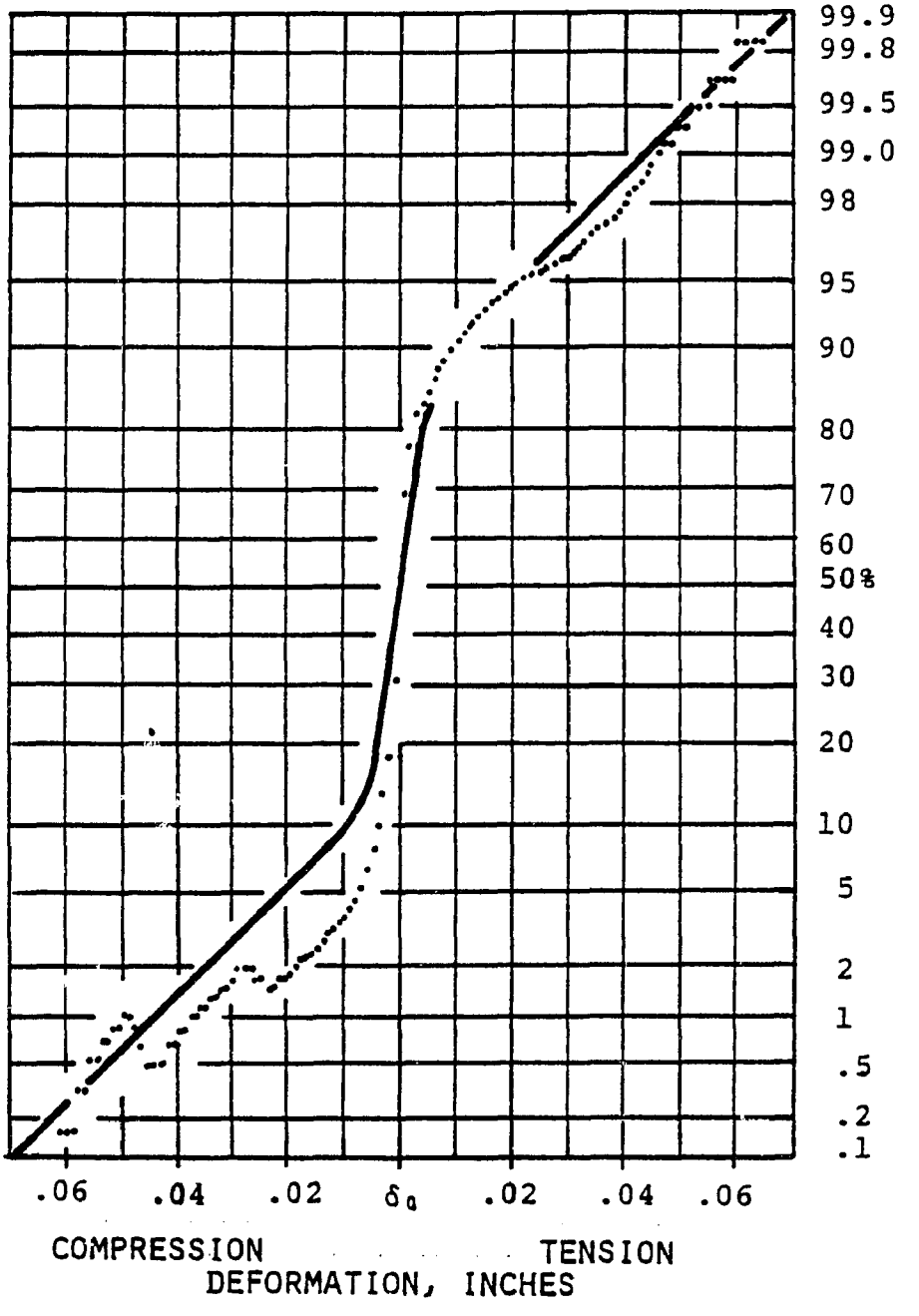


Figure (5.10) Data for butyl rubber on probability paper

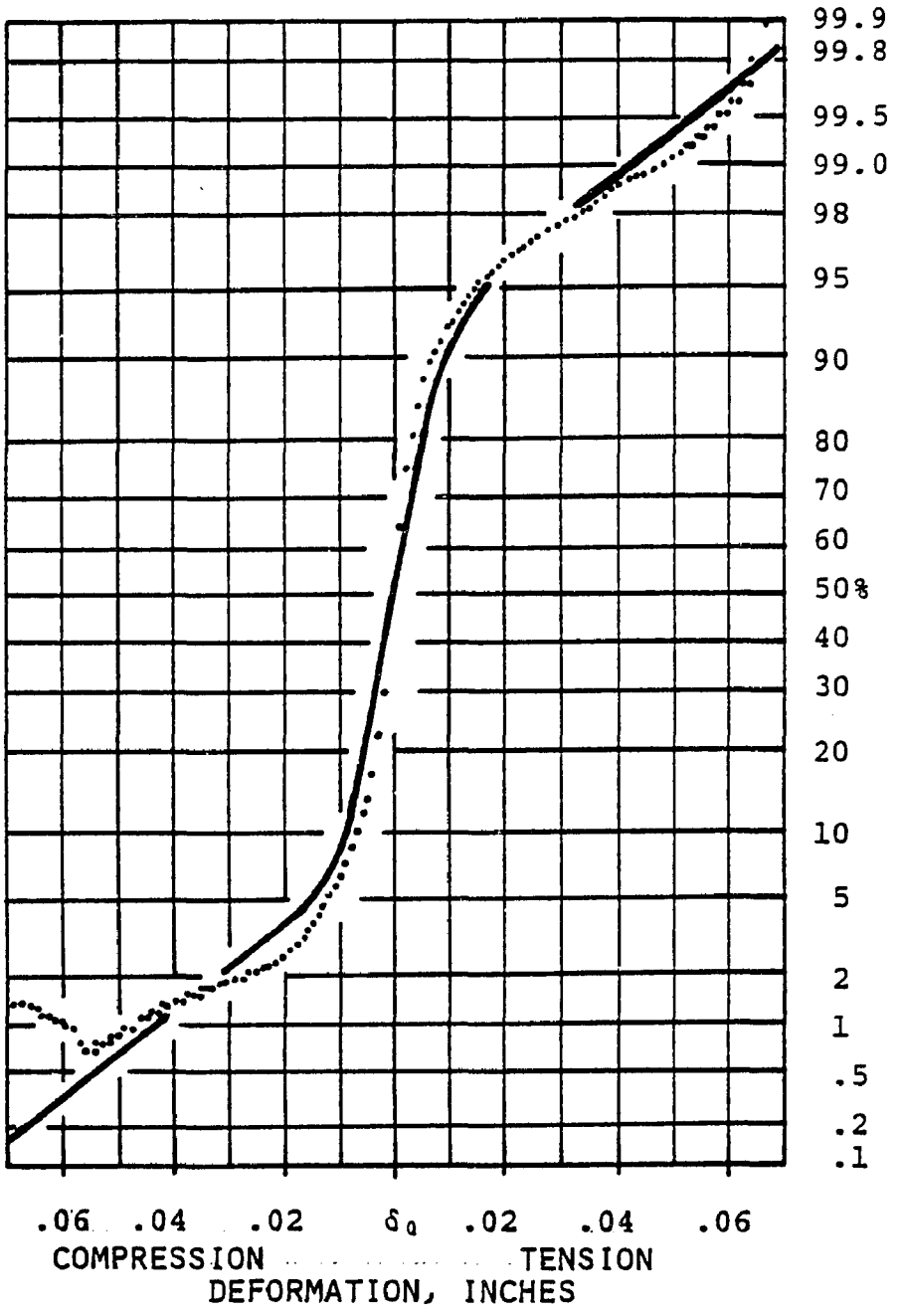


Figure (5.11) Data for oil extended butyl rubber on probability paper

Thus, the data for each material were fit with functions which matched the area under the $p'(\delta) - q(\delta)$ histograms. The functions were selected by eye from a family consisting of the sum of two normal distributions with different standard deviations and various area fractions of each of the two normal distributions. The bell curves for the selected functions are shown with the histograms in Figures (5.12), (5.13), and (5.14). While the areas are the same, the continuous curves do not have as high a peak near δ_0. This is compensated by the bell-shaped curves having more area in the shoulder than the histograms. These bell-shaped curves will be used in subsequent computations for loss as the actual curves of $p'(\delta)$.

Note that many other types of curves could be fit to the histogram plot, including simple straight line segments. However, the use of the Gaussian normal distribution with a stochastic model for rubber loss has both esthetic and mathematical advantages. Next, the formulation of a loss computation for the Gaussian normal $p'(\delta)$ will be presented.

Recall that Equation (4.78) for the loss between δ^* and δ° was the integral of Equation (4.77). Now let $p(\delta)$ be a normal distribution:

$$p'(\delta) = \frac{A}{K\alpha^2\sqrt{2\pi}\sigma} \exp\left\{-\tfrac{1}{2}\left(\frac{\delta}{\sigma}\right)^2\right\} \qquad (5.10)$$

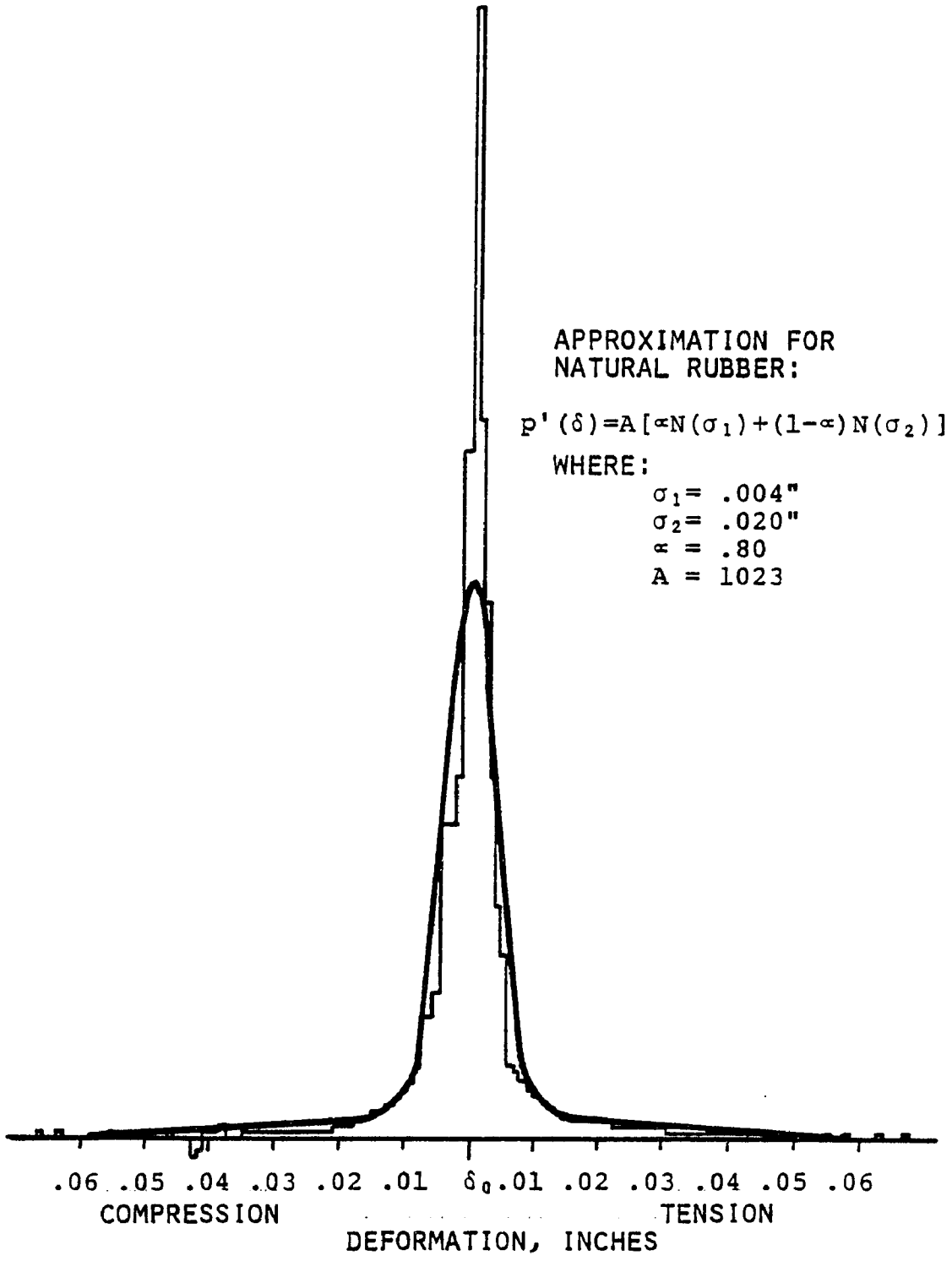


Figure (5.12) Histogram for natural rubber with the approximation function

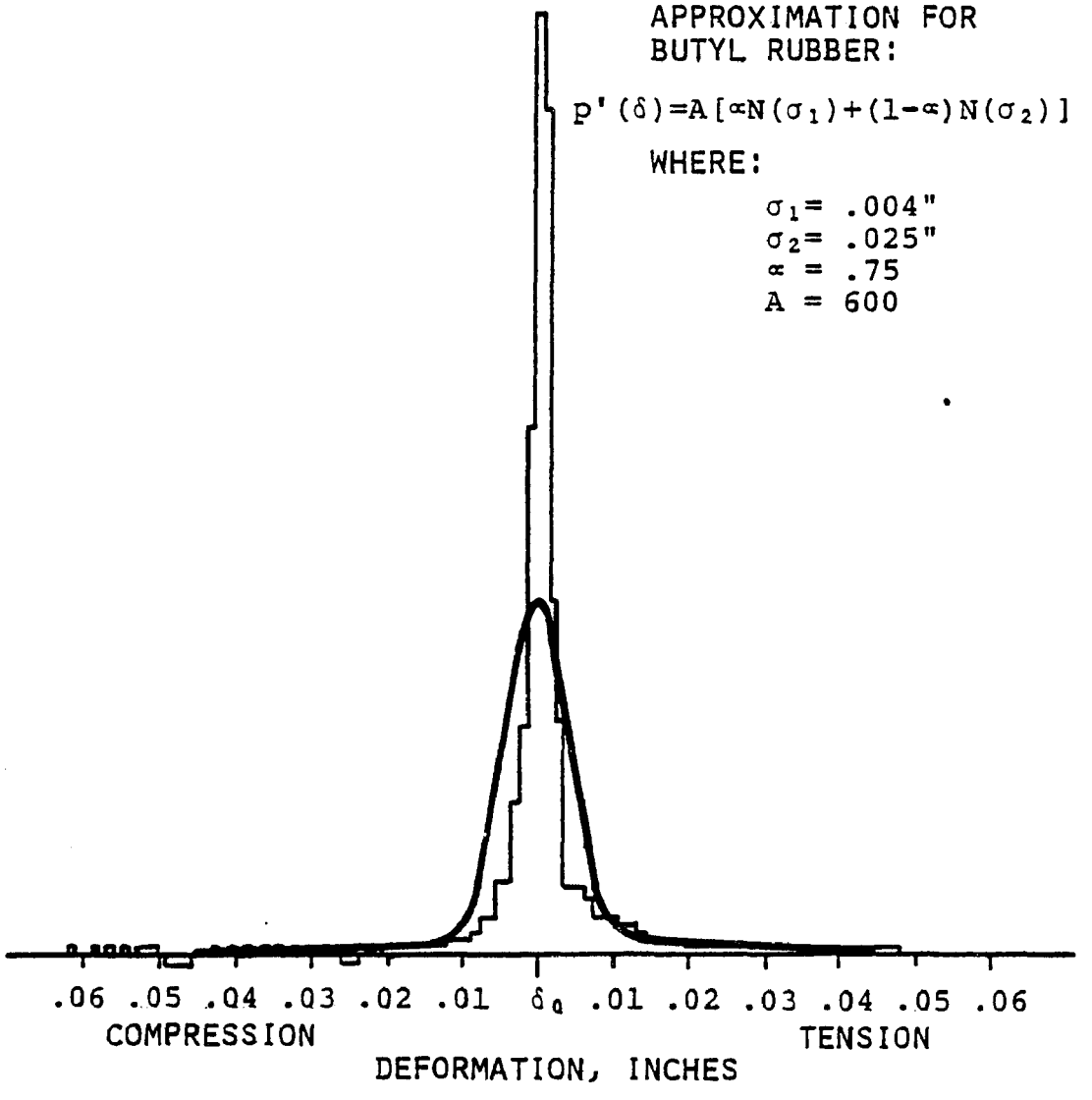


Figure (5.13) Histogram for butyl rubber with the approximation function

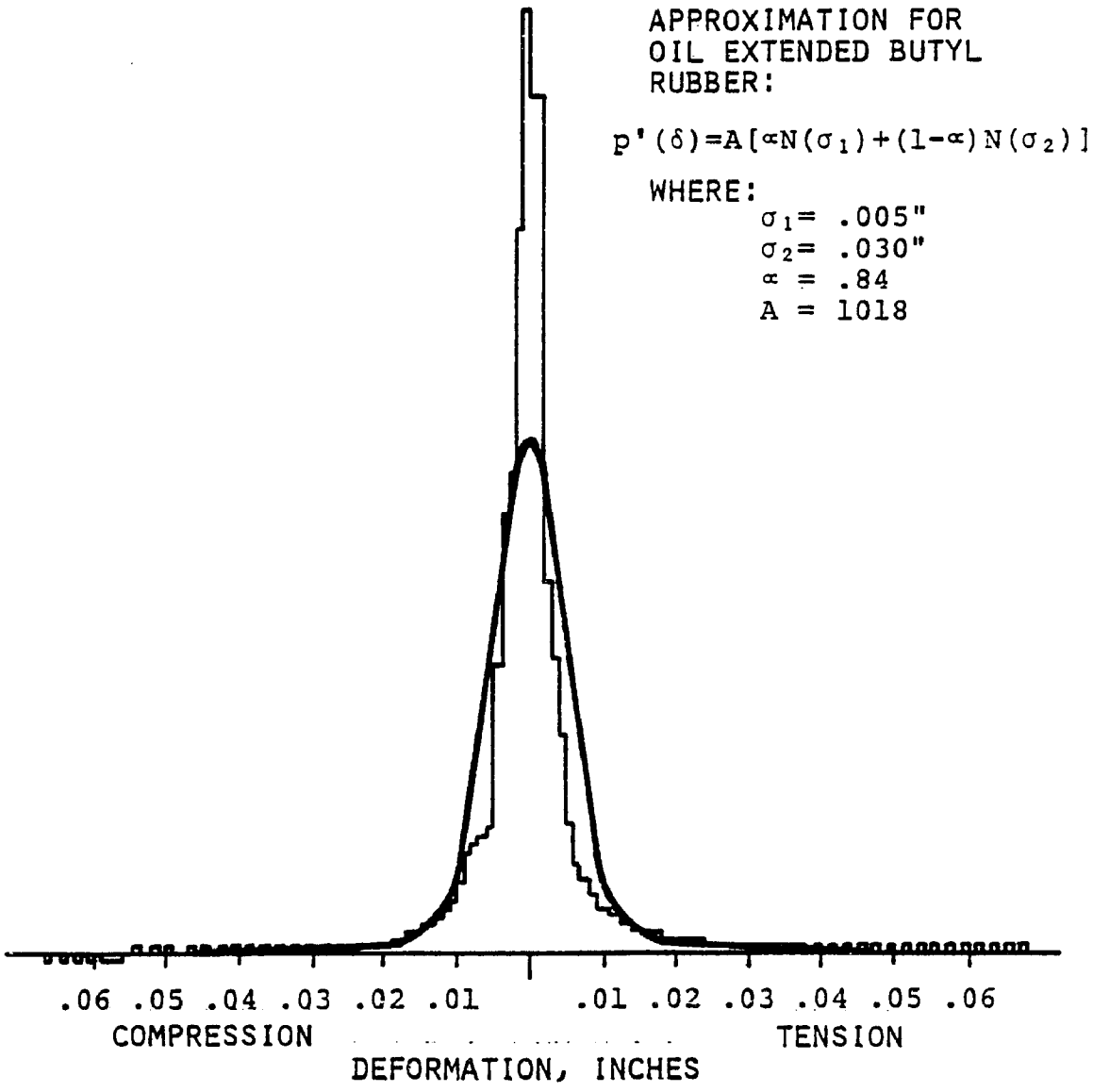


Figure (5.14) Histogram for oil extended butyl rubber with the approximation function

using Equation (5.10) in Equation (4.77) we get:

$$D(\delta)\ \frac{\sqrt{2\pi}\sigma}{A} = \int_0^{\frac{\delta-\delta^\circ}{\alpha}} \left(w - \frac{\delta - \delta^\circ}{\alpha}\right) \exp\left\{-\tfrac{1}{2}\ \left(\frac{w}{\sigma}\right)^2\right\}dw$$

$$+ \int_0^{\frac{\delta^*-\delta}{\alpha}} \left(w - \frac{\delta^* - \delta}{\alpha}\right) \exp\left\{-\tfrac{1}{2}\ \left(\frac{w}{\sigma}\right)^2\right\}dw$$

$$- \int_0^{\frac{\delta^*-\delta^\circ}{\alpha}} \left(w - \frac{\delta^* - \delta^\circ}{\alpha}\right) \exp\left\{-\tfrac{1}{2}\ \left(\frac{w}{\sigma}\right)^2\right\}dw \qquad (5.11)$$

Now use the change of variable: $z = \frac{w}{\sigma}$

$$D(\delta)\frac{\sqrt{2\pi}\sigma}{A} = \sigma^2 \int_0^{\frac{\delta-\delta^\circ}{\alpha\sigma}} \left(z - \frac{\delta - \delta^\circ}{\alpha\sigma}\right) \exp\left\{-\tfrac{1}{2}z^2\right\}dz$$

$$+ \sigma^2 \int_0^{\frac{\delta^*-\delta}{\alpha\sigma}} \left(z - \frac{\delta^* - \delta}{\alpha\sigma}\right) \exp\left\{-\tfrac{1}{2}z^2\right\}dz$$

$$- \sigma^2 \int_0^{\frac{\delta^*-\delta^\circ}{\alpha\sigma}} \left(z - \frac{\delta^* - \delta^\circ}{\alpha\sigma}\right) \exp\left\{-\tfrac{1}{2}z^2\right\}dz \qquad (5.12)$$

Now recall that:

$$\int_a^b \frac{-x}{\sqrt{2\pi}} \exp\left\{-\tfrac{1}{2}x^2\right\}dx = \frac{1}{\sqrt{2\pi}} \exp\left\{-\tfrac{1}{2}x^2\right\} \Big|_a^b \qquad (5.13)$$

and let:

$$R(u) = \int_{-\infty}^{u} \frac{1}{\sqrt{2\pi}} \exp\left\{-\tfrac{1}{2}x^2\right\}dx \qquad (5.14)$$

Then:

$$\frac{D(\delta)}{A\sigma} = -\frac{\delta - \delta^\circ}{\alpha\sigma}\left\{R\left(\frac{\delta - \delta^\circ}{\alpha\sigma}\right) - R(0)\right\}$$
$$-\frac{\delta^* - \delta}{\alpha\sigma}\left\{R\left(\frac{\delta^* - \delta}{\alpha\sigma}\right) - R(0)\right\}$$
$$+\frac{\delta^* - \delta^\circ}{\alpha\sigma}\left\{R\left(\frac{\delta^* - \delta^\circ}{\alpha\sigma}\right) - R(0)\right\}$$
$$+\frac{1}{\sqrt{2\pi}} - \frac{1}{\sqrt{2\pi}}\exp\left\{-\tfrac{1}{2}\left(\frac{\delta - \delta^\circ}{\alpha\sigma}\right)^2\right\}$$
$$-\frac{1}{\sqrt{2\pi}}\exp\left\{-\tfrac{1}{2}\left(\frac{\delta^* - \delta}{\alpha\sigma}\right)^2\right\}$$
$$+\frac{1}{\sqrt{2\pi}}\exp\left\{-\tfrac{1}{2}\left(\frac{\delta^* - \delta^\circ}{\alpha\sigma}\right)^2\right\} \qquad (5.15)$$

Since $R(0) = \frac{1}{2}$, this simplifies to:

$$\frac{D(\delta)}{A\sigma} = -\frac{\delta - \delta^\circ}{\alpha\sigma}\left\{R\left(\frac{\delta - \delta^\circ}{\alpha\sigma}\right)\right\}$$
$$-\frac{\delta^* - \delta}{\alpha\sigma}\left\{R\left(\frac{\delta^* - \delta}{\alpha\sigma}\right)\right\}$$
$$+\frac{\delta^* - \delta^\circ}{\alpha\sigma}\left\{R\left(\frac{\delta^* - \delta^\circ}{\alpha\sigma}\right)\right\}$$
$$+\frac{1}{\sqrt{2\pi}} + \frac{1}{\sqrt{2\pi}}\exp\left\{-\tfrac{1}{2}\left(\frac{\delta^* - \delta^\circ}{\alpha\sigma}\right)^2\right\}$$
$$-\frac{1}{\sqrt{2\pi}}\exp\left\{-\tfrac{1}{2}\left(\frac{\delta^* - \delta}{\alpha\sigma}\right)^2\right\}$$
$$-\frac{1}{\sqrt{2\pi}}\exp\left\{-\tfrac{1}{2}\left(\frac{\delta - \delta^\circ}{\alpha\sigma}\right)^2\right\} \qquad (5.16)$$

If we let:

$$t(\delta) = \frac{\delta - \delta^\circ}{\alpha\sigma} \text{ and } u(\delta) = \frac{\delta^* - \delta}{\alpha\sigma} \qquad (5.17)$$

then this can be written as:

$$\frac{D(\delta)}{A\sigma} = - t(\delta)R\big(t(\delta)\big) - u(\delta)R\big(u(\delta)\big) + t(\delta^*)R\big(t(\delta^*)\big) + \frac{1}{\sqrt{2\pi}}\left\{1 + \exp\{-\tfrac{1}{2}t^2(\delta^*)\} - \exp\{-\tfrac{1}{2}t^2(\delta)\} - \exp\{-\tfrac{1}{2}u^2(\delta)\}\right\} \qquad (5.18)$$

This gives the separation, $D(\delta)$, of the load and return curves. In order to get the loss, this must be integrated from δ^* to δ° as described in Equation (4.78). The advantage of using a well-known mathematical function becomes apparent now since there are good approximation formulas for R(u) [44]. The second integration can be done using a Gaussian Quadrature [45]. A computer program was written to generate the loss for the assumed forms of $p'(\delta)$. Some of the features of this program are now presented.

An approximation for the normal areas is [44]:

$$R(x) = (2\pi)^{-1}\int_{-\infty}^{x}\exp\left(\frac{-t^2}{2}\right)dt$$

$$= \int_{-\infty}^{x} N(z)\,dz$$

$$= 1 - N(x)[C_1 z + C_2 z^2 + C_3 z^3] - \varepsilon(x) \qquad (5.19)$$

where:

$N(\ )$ = Gaussian Normal distribution

$x \geq 0$

$z(x) = (1 + C_4 x)^{-1}$

$C_1 = 0.4361836$

$C_2 = -0.1201676$

$C_3 = 0.937298$

$C_4 = 0.332670$

$-10^{-5} < \varepsilon(x) < 10^{-5}$

This approximation will give values for $D(\delta)$ from Equation (5.19) with a computational accuracy which is more than an order of magnitude better than the accuracy of the experimental measures.

In order to obtain an energy loss the difference, $D(\delta)$, must now be integrated between limits of δ^* and $\delta°$. The function $D(\delta)$ is reasonably slowly changing so any numerical integration scheme would provide good results. A trapezoidal rule integration was tried but was somewhat slow in providing the desired accuracy, thus expensive in computer time.

A Gaussian Quadrature [45] is quite suitable for performing this integration. This technique uses the value of the function at n selected points to make the approximation exact for the first through the n^{th} power of x. The points are not evenly spaced but the specific values for each order of approximation can be calculated. The values have been tabulated [45] through n = 6.

The error for the n^{th} order Gaussian Quadrature is given by:

$$\text{Error} = \frac{\left|d^n\right|_{(b)}^{n+1}}{2(n+1)!} \qquad (5.20)$$

where:

$|d^n|$ = maximum value of the n^{th} derivative

(b) = range of integration

n = number of points and order of approximation

For six points and the maximum integration range of 0.08 inch, this becomes:

$$\text{Error} \simeq |d^6| \times 2 \times 10^{-12} \qquad (5.21)$$

Thus, if the 6^{th} derivative of $D(\delta)$ is less than 5×10^6 the computational error will be less than the experimental error. Due to the exponential nature of $D(\delta)$ the maximum of its 6^{th} derivative is nearly unity.

The flowchart for the computer program is presented in Figure (5.15). The program uses the approximation for $D(\delta)$ mentioned above and uses the Gaussian Quadrature for the loss integration. Typical loss versus cycle-size plots for various normal distributions are shown in Figure (5.16).

The program was used to generate the loss for the specific functions fit to the $p'(\delta)$ curves noted earlier. The cycle sizes selected were those for which data was obtained in the first part of the experimental program. The calculated losses are shown compared to the experimental values for each of the materials in Tables (5.4), (5.5), and (5.6). The calculated losses have been added to Figure (5.5) and now the plot of loss versus cycle-size is shown in Figure (5.17).

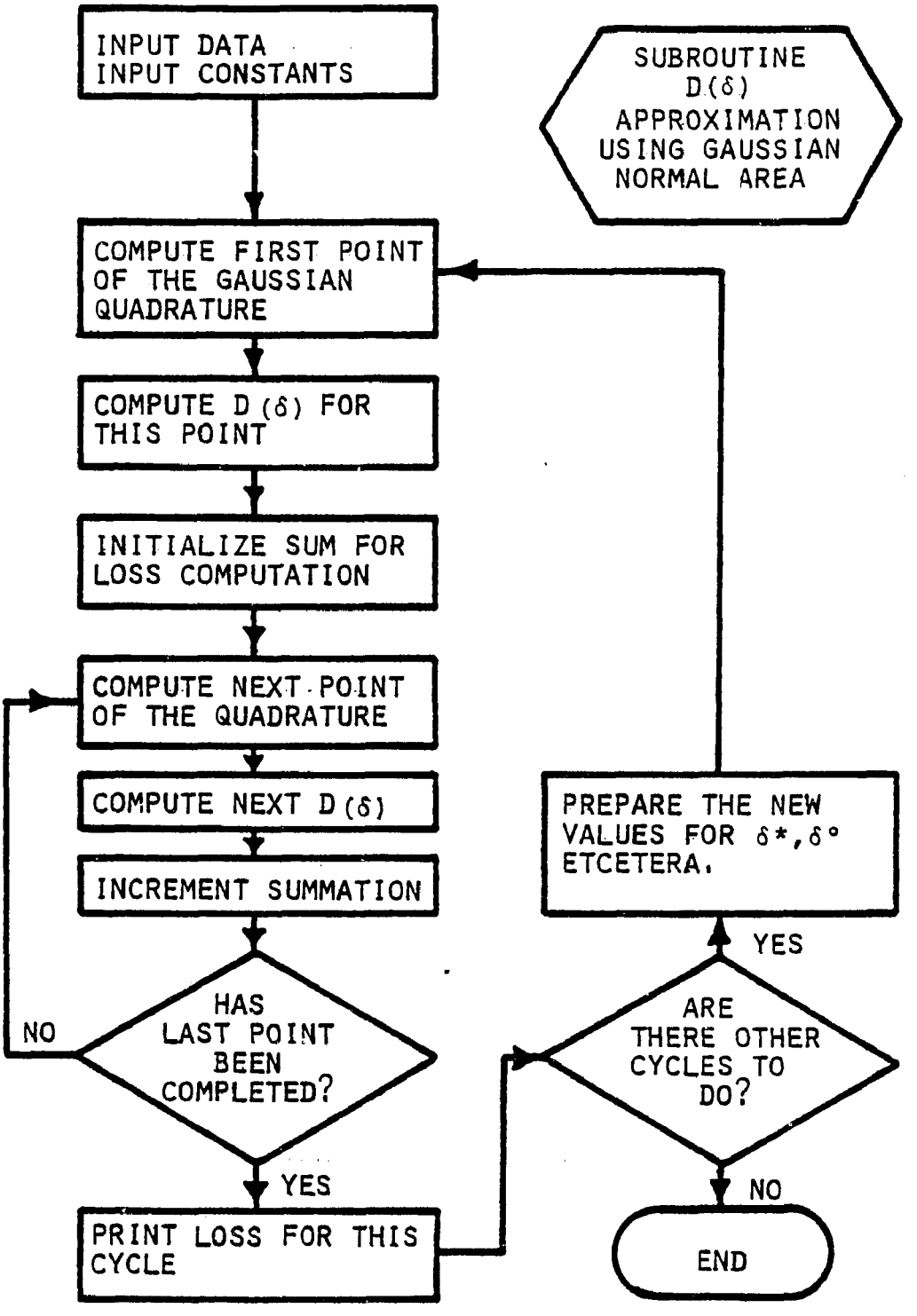


Figure (5.15) Flowchart for program to compute loss. Uses Gaussian loss functions and integration by Gaussian Quadrature.

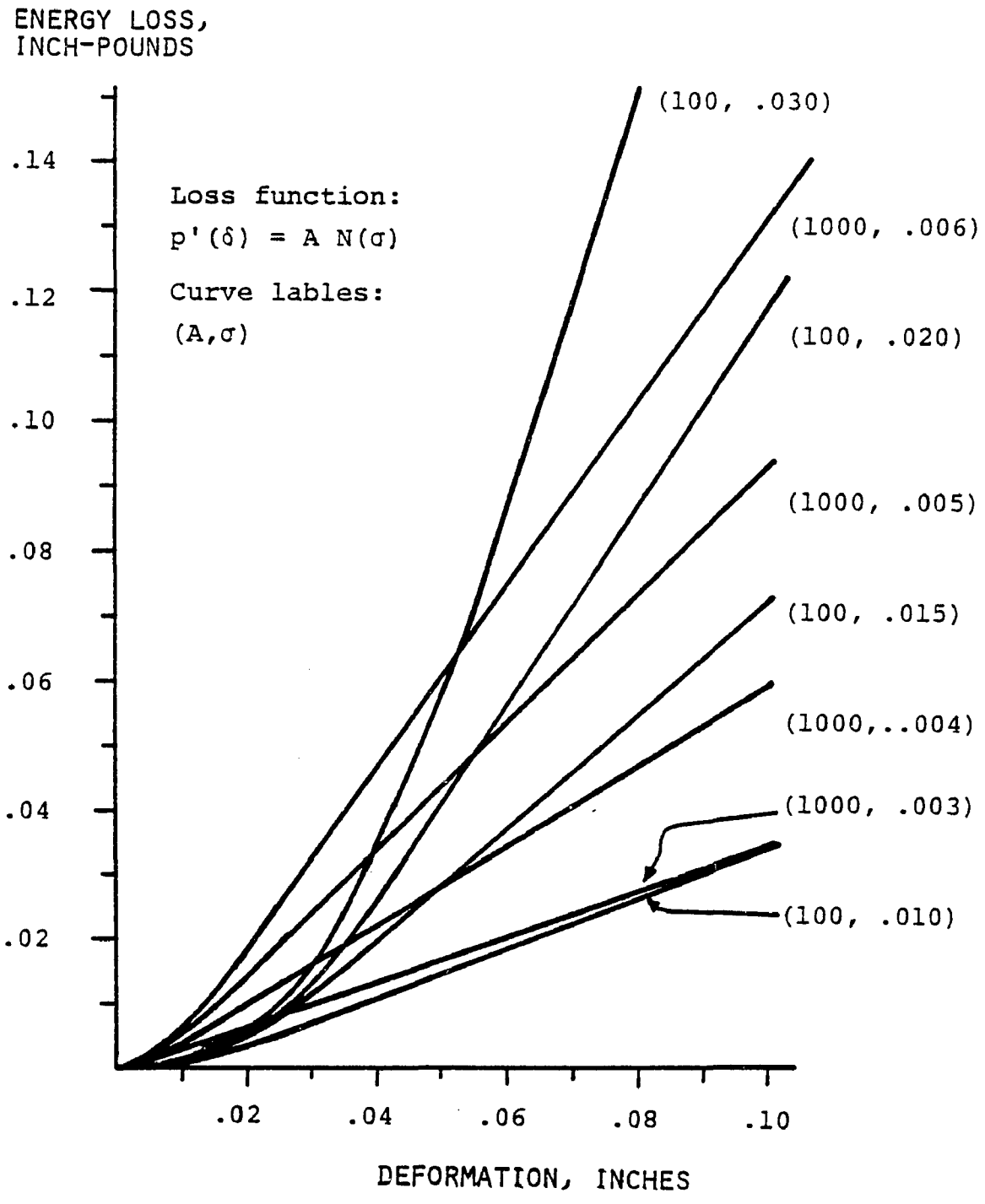


Figure (5.16) Loss versus cycle size plots for various normal distributions

Loop Size	Average Loss All Rates	Computed Loss Gaussian Fit
.01 inches	.005 inch-pounds	.003 inch-pounds
.02	.015	.012
.03	.032	.027
.04	.050	.047
.05	.072	.071
.06	.096	.096
.07	.120	.121
.08	.146	.146

Table (5.4) Comparison of average experimental values of energy loss and computed values of energy loss for natural rubber

Loop Size	Average Loss All Rates	Computed Loss Gaussian Fit
.01 inches	.003 inch-pounds	.001 inch-pounds
.02	.009	.006
.03	.020	.014
.04	.030	.026
.05	.045	.042
.06	.060	.059
.07	.078	.078
.08	.096	.097

Table (5.5) Comparison of average experimental values of energy loss and computed values of energy loss for butyl rubber

Loop Size	Average Loss All Rates	Computed Loss Gaussian Fit
.01 inches	.007 inch-pounds	.003 inch-pounds
.02	.020	.013
.03	.042	.030
.04	.066	.054
.05	.094	.085
.06	.122	.121
.07	.160	.161
.08	.200	.203

Table (5.6) Comparison of average experimental values of energy loss and computed values of energy loss for oil extended butyl rubber

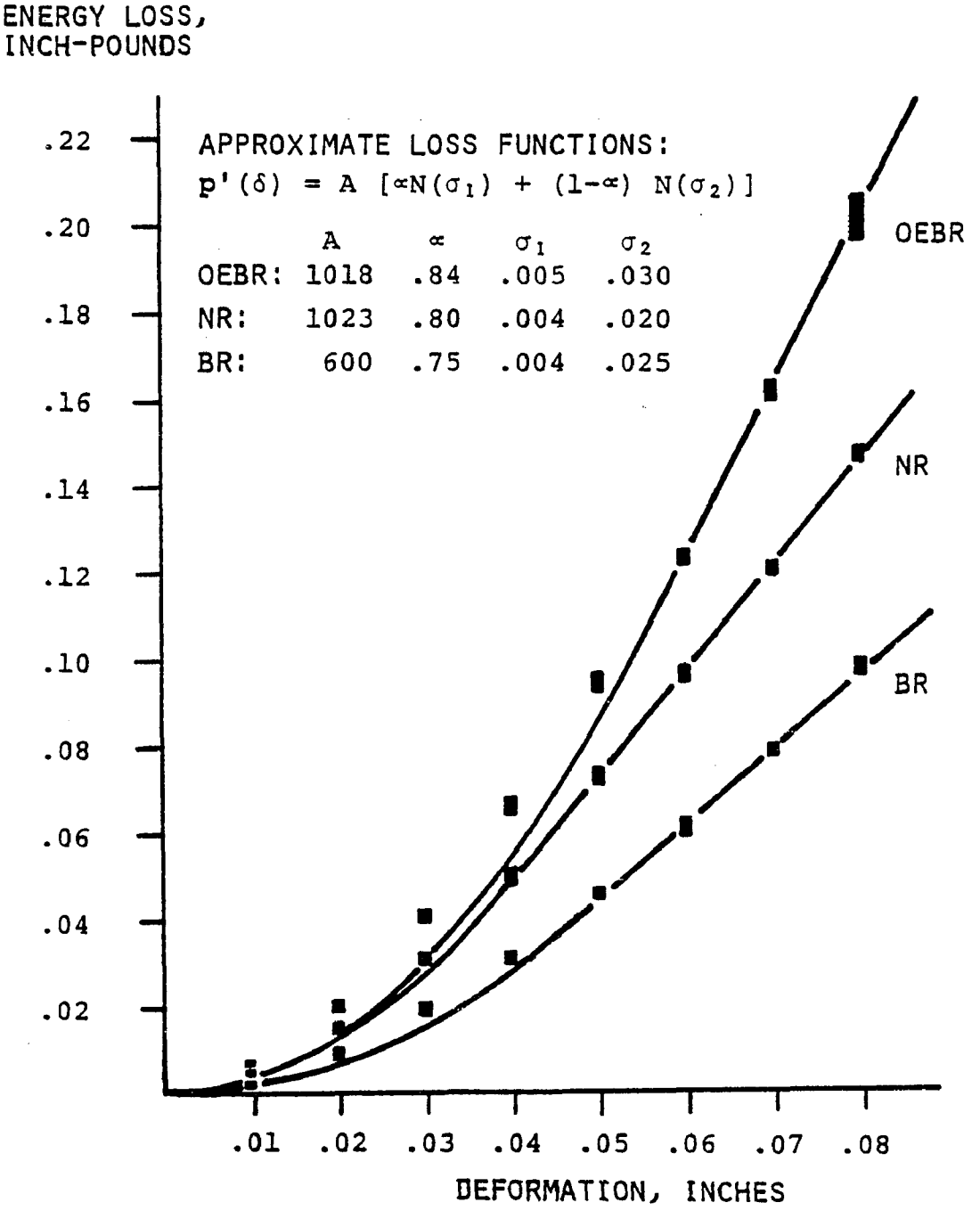


Figure (5.17) Loss as a function of cycle size for three rubber samples. The specimens are one inch long. Curves are calculations from approximate loss functions. Size of points indicates scatter of data.

The usefulness of the method has been shown. However, the difficulties of fitting $p'(\delta)$ with the assumed functions have shown up in the loss calculations. The computations are close to the experimental values, just as the fit for $p'(\delta)$ is close to the histograms.

The use of the model with the given functions for $p'(\delta)$ will enable calculations for other cycles. The loss will be the same function of cycle size regardless of the end points of the cycle due to the assumed symmetry of $p'(\delta)$. However, it may be noted, particularly in Figure (5.13) for butyl rubber, that the data for $p'(\delta)$ is not symmetrical. A check for butyl rubber showed a 0.07 inch pure compression cycle had almost 20% more area than a 0.07 inch pure tension cycle.

An unsymmetrical fit for the data could be accomplished, but no specific technique is optimum for fitting the given data. As was noted earlier, straight line segments could be utilized or even the histogram data itself. However, the general conclusions remain the same, and the choice of the approximation in this chapter was based in part on its simplicity for computation and conception.

CHAPTER 6

LIMITATIONS AND EXTENSIONS

6.1. Incorporating Other Effects

The theory presented thus far is a one-dimensional, model of a hysteretic system. It has no temperature or rate effects. This section presents suggestions on how to generalize the theory to remove some of its limitations. The theory may be extended to include other effects, but first consider its position relative to some of the general theories identified in Chapter 3.

The theories mentioned in Chapter 3 were continuum models. These were theories of nonlinear viscoelastic materials, permanent memory materials, anelastic materials, and a general frame-free theory. All of these theories could accept strain-level effects, strain-rate effects, and thermorheological effects. It should be clear that the current model can be considered a special case of each of these general theories.

Some nonlinear viscoelastic models consider the complex modulus of the material to be a simple function of strain level. Permanent memory materials are themselves a special case of nonlinear viscoelastic materials. The anelastic theory of Derman, Bodner, and Partom [29] included all orders of nonlinearity in the analysis. However, their experimental work showed the dominant terms of the constitutive relations

were due to the dry friction mechanisms, their "zeroth" order terms. The general frame-free theory [30], as noted in Chapter 3, includes all the above theories but can offer engineering problem solution only in simple cases described by the other theories.

A strain energy function could also be defined for the material, but it would not be a simple elastic energy function. A theory could be developed similar to that which Bychawski set forth [18]. A work function, with real and imaginary parts, could give both the elastic response and the hysteretic loss. Such a formulation would be appropriate for the material identification technique to be described below.

The current model gives both qualitative and quantitative information. The use of more general theories does not guarantee more information with the additional levels of complexity. Thus, extension of the model to include only those effects which appear important in experimental work would be more efficient than using a general theory which includes effects not observable in the material.

The current model has no thermorheological properties. There is an obvious interrelationship in the material among stress, strain, temperature, and loss. The cyclic operation of stress or strain causes energy to be dissipated in the material as heat. The subsequent temperature rise in the material can affect the value of stress or strain, thus changing the cycle characteristics and the loss. This

interrelation was mentioned earlier in the context of linear viscoelastic thermorheologically simple materials.

However, it is important to recall the distinction between viscoelastic properties and thermomechanical properties. A single material may have both, but the form of either quality is not implied by the other. The W-L-F temperature-relaxation-time relation is just one form of thermomechanical coupling. This empirical relation "reflects the temperature dependence of the [macromolecular] segmental friction coefficient" [19]. The temperature of the material affects the amount of energy required to break and reform crosslinks or overcome entanglements. This, then, affects the material stiffness and loss.

One method of putting thermorheological properties into the model is to make only the initial modulus, K, a function of temperature. Then, for a specific load, the amount of deflection would be a function of temperature. This effect on the deflection of the cycle would be reflected in the loss. However, for constant deflection cycles the amount of loss should be constant although the stress level would be a function of temperatures. This is analogous to the experiments of Chapter 5 where the level of stress attained at different rates varied, while the amount of loss was constant for a given deflection over all rates.

Relaxation tests were run on the samples from Chapter 5. These materials did show some time dependent properties but

the cyclic loss was quite independent of rate. The relaxation effects observed could be added to the model by making the initial modulus, K, time or rate dependent. This is basically the effect observed in the experimental program. The initial spring rate was larger with larger loading rates, thus giving larger load endpoints when cycling. However, this had a negligible effect on the observed loss.

Treloar [6], in his discussion of dynamic properties and stress relaxation of rubber, notes an inverse relationship between frequency and dynamic viscosity in rubber. His conclusion is that in rubber there is a distribution of relaxation times. Citing work by Ivey, et. al., Treloar states that the overwhelming contribution to the relaxation spectrum is due to mechanisms with extremely short relaxation times. For butyl rubber, mechanisms which relax in about 10^{-7} seconds contribute 10,000 times as much as mechanisms which relax in about 0.1 seconds.

Thus, fast mechanisms, such as dry friction, may cause most of the loss but little of the initial modulus, while slower mechanisms, such as molecular flow, may cause negligible loss but most of the initial modulus. These long relaxation time mechanisms contribute the essential rubber-like properties of the material, while other processes contribute to the hysteretic properties.

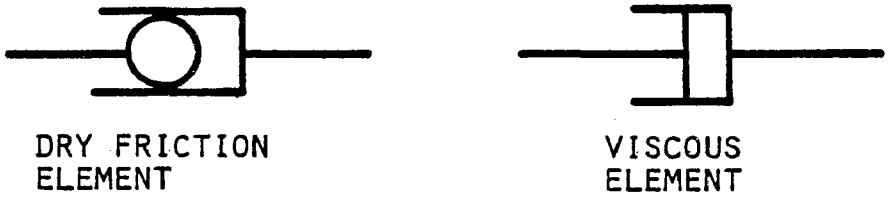
To add viscoelastic properties to the model, all of the parameters and functions in the current model could be made

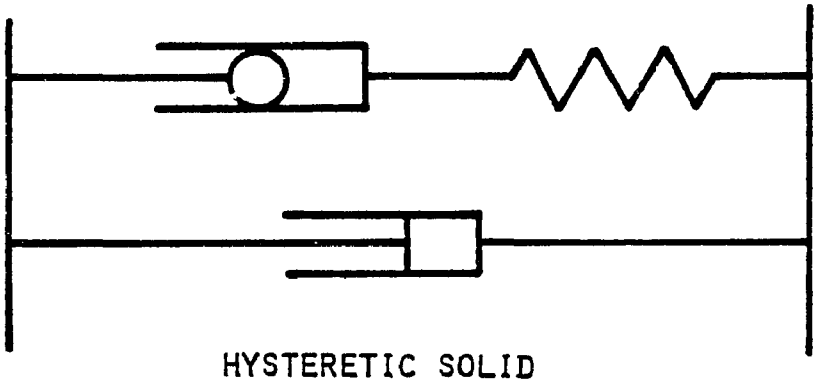
time or rate dependent. However, the most profitable course seems to be a model which is a combination of a linear viscoelastic model and a dry friction model. The viscoelastic model could also be thermorheologically simple and thus contain all the temperature effects as well. Figure (6.1) illustrates two simple models of this type.

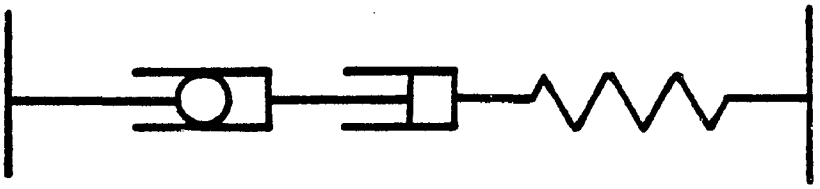
Another way to add rate effects is to add mass to the model. This was the method used by Caughey [34-36] and Iwan [38-40] in obtaining transmissibility plots for hysteretic materials. In the solution of dynamic problems this method may be preferred to the addition of viscoelastic elements.

The anticipated use of any model should determine what effects are included and the type of experiment used to characterize the material. This is the basis of a theory known as material identification [46]. The behavior of the material is tested in situations as nearly like the problem area as possible. Then, having identified the material in this type of loading, predictions can be made for other problems.

Generally this technique characterizes a nonlinear incompressible, isotropic elastic solid by a strain energy function. In practice, a number of independent tests are performed. A parameterized form is assumed for the strain energy function. The values of the parameters are then optimized in some manner.







$$F(\delta,\dot{\delta}) = K(\delta,\dot{\delta}) - f_1(\delta) - f_2(\dot{\delta})$$

INITIAL MODULUS	DRY FRICTION LOSSES	VISCOUS FRICTION LOSSES

Figure (6.1) Simple loss models with both dry and viscous friction

The method has the advantage that it gives a good fit for a variety of possible applications while allowing a convenient choice of experiments. This concept is not new; the technique was used in an informal way for rubber by Mooney in 1940 [16] and Rivlin and Saunders in 1951 [17]. The method has the limitation that the function obtained is of a local, rather than a global, nature.

The interactive nature of the technique with the experiments and solution of problems is similar to the semi-inverse measurement method of Plunkett [*]. If certain assumptions are used to postulate a material's behavior, experiments can be performed to test these assumptions. By appropriate design of the validation experiments the data produced can then be used directly to solve problems. This is similar to the technique used for the rate independence experiment in the first part of Chapter 5.

The semi-inverse measurement method uses theory to suggest an appropriate set of data to obtain. The data thus collected will show whether the assumptions of the theory were valid. If the assumptions were not well founded, further data can then be taken. If the assumptions were adequate, the data can be used, without a theoretical model, to solve problems.

---

*Plunkett, R., "Measurement of Damping in Viscoelastic Materials", Seminar at the University of Michigan, April 12, 1976.

The hysteretic behavior of carbon-filled, vulcanized rubber requires further experimental study. The effect of temperature and rate of loading can be added to the model of Chapter 4. However, the relative merit of these effects should be weighed through the use of an interactive characterization method. In addition, there is very little experimental data on the loss behavior of rubber under multiaxial loading.

6.2. Losses from Multiaxial Loadings

The dry friction loss model presented in Chapter 4 offers an interesting springboard for the study of loss under combined stresses. A viscoelastic model would require an integration of the solution of the dynamic problem in two or three dimensions in order to predict the loss. To obtain loss data from two- or three-dimensional loadings is much more difficult and time consuming than uniaxial testing.

Theories or criteria which give insight to the problem of loss under combined stress are valuable tools. There are several measures which have proved useful in various loading situations [47]. However, the general consensus is that the best way to anticipate the loss in any multiaxial loading is to perform an experiment as nearly like the situation as possible and use these results for further predictions. In one sense, this is much like the material identification technique mentioned above.

Six quantities are required for the description of a stress state. These quantities may change in a general way under cyclic loading. The changes may be in-phase or out-of-phase with each other. The changes may have different frequencies in different directions. There is no single theory to predict the loss in a general cycle except integration of the stress-strain relation.

Consider a cylindrical pressure vessel which is subjected to torsional and axial loads. The axial and circumferential loads may be in-phase at the same frequency by cyclic pressure. The torsional and axial loadings may be applied in-phase or out-of-phase or even at different frequencies. A special case was considered by Tabor in [48] in which the elastic strain-energy was held constant while the various loads were changed cyclicly. The principal stresses remained constant while the principal directions rotated.

A more typical case is where the principal directions are constant but the magnitude of the principal stresses changes. However, in some structural problems and in rolling contact problems, the loading is more general. For rolling contact, the material will go through a shear, compression, reverse-shear cycle.

Most combined stress-loss theories assume the damping is dependent on some parametric description of the stress state. Thus, the principal stresses or their invariants are

commonly used to describe the amount of loss incurred in going to a stress state. Other theories assume a specific fraction of the input energy or fraction of the total elastic strain energy is dissipated in the material. Note that whatever the criterion, it is only valid for a specific type of loading on a specific material.

The concept which unifies various loss problems is the existence of some "effective" or "equivalent" uniaxial problem which produces the same loss as some multiaxial problem. This is analogous to the study of onset of plastic flow in multiaxial problems, the equivalent uniaxial loading for plastic flow being given by the Von Mises criterion or the maximum shear criterion.

By connecting points of equal damping capacity in stress space, a curve or surface is developed. The locus of points in stress space with common loss characteristics forms a set of isodamping curves or surfaces, analogous to the yield surface from the study of plasticity. These curves may be obtained experimentally or approximated by theoretical criteria.

However, the relative simplicity of plastic flow criteria may be misleading in loss studies. Any set of isodamping curves is for one specific type of loading, usually from the unloaded condition to a specific stress state and back. Therefore, the set of isodamping curves can include a separate curve for each possible starting point.

Alternatively, the number of dimensions may be increased so that each point on the surface of constant loss is defined by the starting stress state, the final stress state, and the path between. Even this is confused for cycles which have no clear end points, such as the constant-energy-content experiment of Tabor [48]. For viscoelastic theory, the isodamping locus would also require the effect of frequency to be included.

The mechanism of energy loss may change for a single material. The amount of damping incurred by cycling between two stress states may have different values as the mechanisms change. In a polymer, there are several mechanisms of loss which become more or less important depending on temperatures and strain rates. Also, there can be an effect on loss due to the load path chosen or the specific method of application of the loads.

The formulation of the current model suggests loss is dependent on deflection level. However, the one-dimensional model does not imply what multiaxial strains are equivalent in damping capacity. The isodamping locus may be assumed to be a curve of constant distortional energy or shear strain similar to theories of plasticity.

The experiment by Tabor dealt with the possibility of a fraction of the input strain energy being converted to loss. By keeping the strain energy constant during the cycle, he obtained approximately twice the energy loss obtained by either torsional cycles or tensile strain cycles

on the same sample with the same maximum strain energy. While this experiment does not preclude the use of the fraction of maximum strain-energy criterion, it is shown to be misleading in a general case.

An isodamping criterion based on the levels of shear strain experienced by the material may be useful. In his seminar mentioned above, Plunkett claimed that losses in polymers are mainly due to shear and little loss is incurred in dilatation since the materials are nearly incompressible. A hydrostatic compression of an incompressible solid would cause no loss. Local irregularities could give rise to shear stresses in hydrostatic compression to explain any observable loss. Again, care must be taken to define accurately what cycles can use a given shear-based isodamping criterion.

Even an extremely well-founded model for an equivalence criterion is subject to statistical variations. This is true with studies of multiaxial plastic yield. Thus, deviations are to be expected in any isodamping criterion.

One assumption that is suggested by the development of the current one-dimensional loss model is the idea of isotropic loss. Three-dimensional problems may be approached by allowing the loss calculated for the strains in one direction to be independent of loss generated by strains in the other directions, but incorporating the Poisson effect into the analysis.

The selection of any of these criteria is not required for testing of a specific material for specific loadings. However, if some criterion is chosen and isodamping curves are plotted, the selection may be refined for future use by a semi-inverse measurement technique or the use of a material identification scheme in order to provide the data with more general applicability.

6.3. Other Applications

Certainly the hysteretic model is not applicable to all materials or systems, but there is a range of utility. This model was originally thought to provide a means for studying loss phenomena in the pneumatic tire. However, there is a broader range of problems which may be approached.

It was mentioned earlier that the model can exhibit a straight line for an initial stress-strain plot and still have hysteretic loss; see Figure (4.13). Sand or soil may show such a behavior in compression. Sand deforms as load is applied but never fully recovers. The hysteretic model may be of use in such studies.

Many types of clay show hysteresis when subjected to cyclic stress. Asthury and Moore [49] noted that there has been very little theoretical study of such problems. Figure (6.2) is a hysteresis loop for a typical clay. The authors formed a specialized viscoplastic model to explain the observed behavior of the clay. They based their model

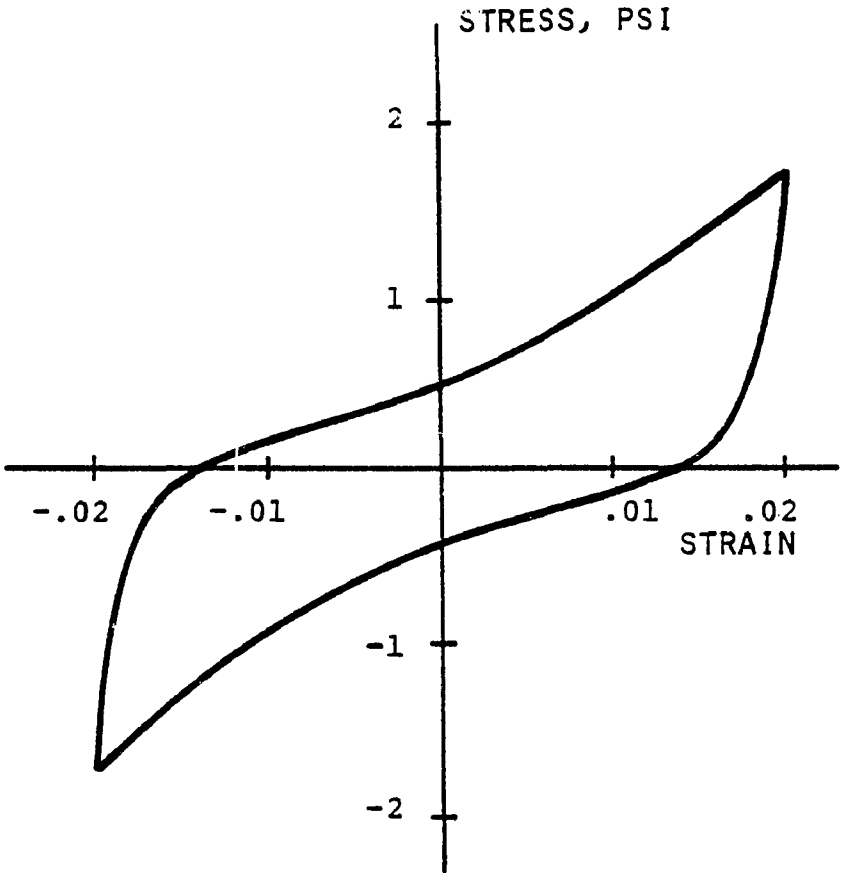


Figure (6.2) Typical hysteresis loop for torsion of earthenware clay, from Astbury and Moore [50]

on a concept of the breakdown and transition from an elastic phase to a viscous phase using a single relaxation time for the material.

Their experimental study showed two interesting results. The tests were only run at two frequencies, but the loss was the same at each frequency for all clays tested. Secondly, the hysteresis loop of Figure (6.2) shows both stiffening and loss. The model of Chapter 4 should be useful in a study of hysteresis in clay.

Another class of materials which exhibits rate independent hysteresis is biological tissues. Many tissues show nonlinear stress-strain behavior. Some of these materials show stiffening under load, which was noted for rubber. However, other types of tissue show softening under load. There is a discussion of such materials by Fung [50], who also provides many further references.

Biological materials often must be preconditioned. Fung describes such a procedure as repetition of an experiment until a stable, repeatable result is obtained. This is similar to the effect noted for filled rubber in Figure (2.6). There appears to be no natural state to which such materials return when all load is removed. This condition implies these are permanent memory materials, which do not have the unique reference state that is typically used in the study of mechanics. The current rubber model used a reference deflection rather than some unique material reference state.

Fung also mentions viscoelastic analyses which have been used for biological tissues. Many biological materials are relatively insensitive to rate. Experiments on the dynamic response of muscle have shown that a 10^6 fold increase in strain rate causes only a 2.5 fold increase in stress. While there is a clear relationship, the effect is not pronounced. These tissues can be described by a distribution of relaxation times. Fung notes this is similar to techniques in the field of structural damping, which itself is related to a dry friction loss mechanism. Fung also mentions applicability of methods used in magnetic hysteresis studies, which were also the basis of Moore's analysis of clay.

Another use of the model is in the study of fatigue. This was the problem studied by Whiteman with his model [41]. Similar models are currently being used in the study of fatigue in metals for various loadings [51,52]. One application considers the shape of the hysteresis loop as a function of the strain level. This formulation, by Conle and Nowack [53], uses one function to describe the shape of the loop, for stress prediction, and another function for the separation of the load and unload curves, for loss prediction.

The hysteretic model may help in the analysis of the phenomenon of acoustic emission [54]. Energy released by this effect is believed to be due to microplastic flow

phenomena. The theory on energy loss may be applicable to the study of acoustic energy released by the material under stress. The theory could be modified to allow some of the energy loss to appear as sound rather than as heat.

The current model may be applied to any system where the prevalent mechanism is dry friction or plasticity. Such applications have been made for some theoretical systems and built up structures [34-40]. In addition to carbon-black filled, vulcanized rubber, the modeled behavior should be observable in other filled polymers, composites, or aggregates.

The formulation of Chapter 4 is adapted for loss problems. It was noted in Chapter 3 that equivalent viscous damping could be used to solve dry friction damping problems with reasonable accuracy. Historically, viscous damping has been preferred in theoretical problems due to the closed form solutions available in terms of trigonometric functions. This also helped generate interest in other viscoelastic models. However, with current generation computing machines, dry friction damping and its nonsinusoidal solutions are not particularly difficult and may offer some new insights for loss and damping.

The system which generated interest in the current formulation of the hysteretic model is a pneumatic tire. The use of dry friction as a mechanism for rolling loss is not new. In a series of papers dating back to the middle

of the nineteenth century, Dupuit and Moran discussed the hysteretic loss of wagon wheels rolling on dirt roads [48]. The permanent deformation of the road surface was seen as the result of the mechanical energy lost in rolling.

Consider a somewhat simpler structure than a pneumatic tire. Skelton considered the hysteretic behavior of a cord-rubber composite [55]. He used an Instron machine to test samples in constant displacement bending cycles. His results are shown in Figure (6.3). This plot of loss is nonlinear near the origin and linear for larger displacements. Notice the addition of cords to the rubber increases the amount of loss in the composite, but the character of the curve is preserved.

Next consider the experiments by Collins, et. al. [56], on the rolling resistance of full size tires. Tests were performed to measure the drag force at room temperature as a function of vertical deflection and internal pressure. Figure (6.4) shows their results for one tire. Since all tests were run at the same speed, the vertical scale is proportional to the power loss of the tire.

It is interesting to note the shape of the curves. These loss plots are similar to the plots of Figure (6.3) as well as Figures (5.16) and (5.17). The loss is again nonlinear near the origin but is nearly linear at higher deformations. The effect of internal pressure may be explained as an additional stress which changes the multiaxial loading

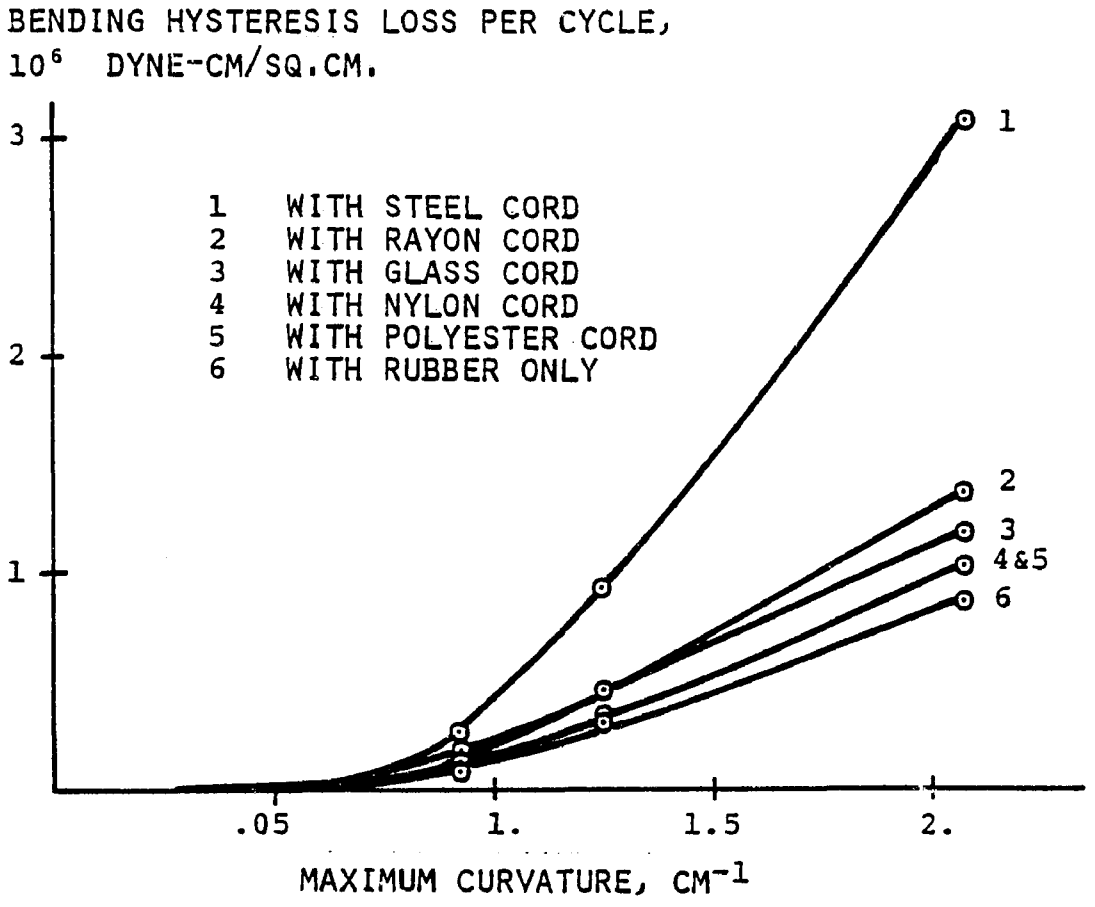


Figure (6.3) Hysteretic loss in cord-rubber composites as a function of maximum bending curvature, from Skelton [55]

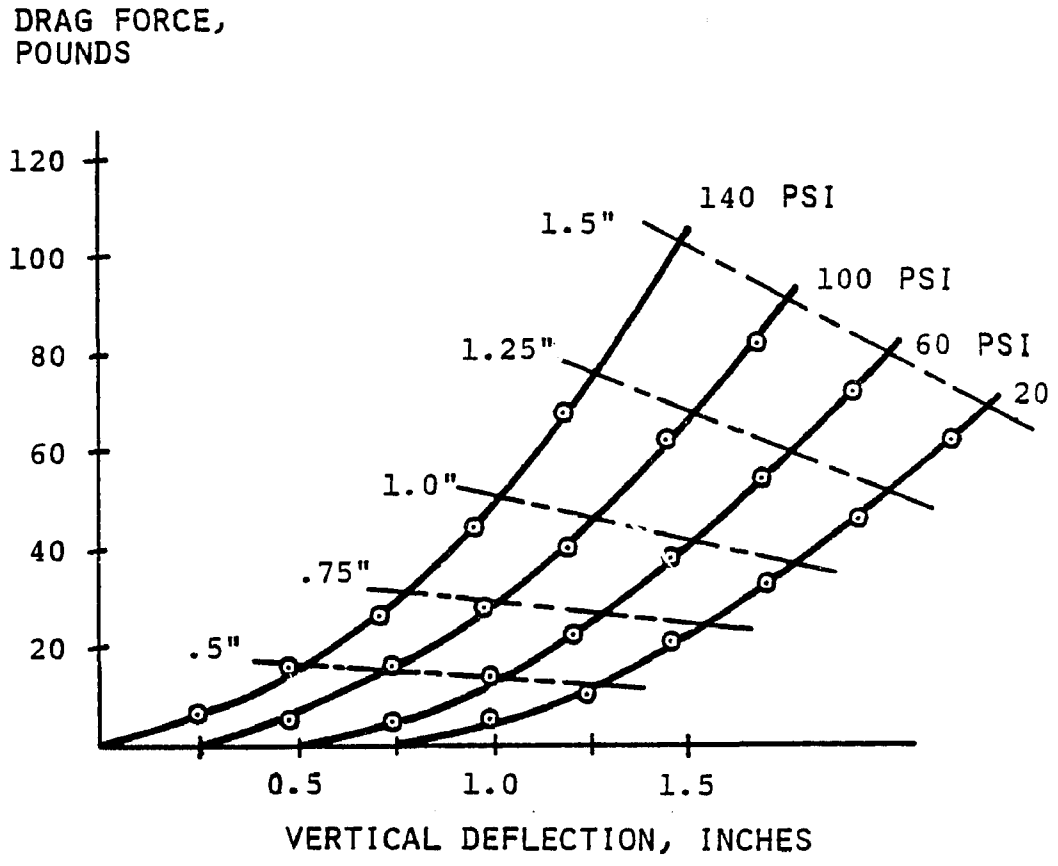


Figure (6.4) Tire drag force as a function of pressure and deflection, from Collins, et. al. [56].
Note horizontal scale shifted for different pressures.

cycle. However, the curves at all four pressures appear to depend on deflection to the 3/2 power.

In order to optimize the loss and damping capacity of the pneumatic tire, some reasonably simple model is needed. However, loss studies usually correlate stress or strain amplitude, stressed volume, and strain energy, with a measure of energy loss, while vibration studies correlate system viscosity as a function of frequency with transmissibility or decay of stress amplitude.

Many varied measures of damping capacity and energy loss can be found in the literature. Such parameters are adequate for each individual study but it becomes difficult to compare them and draw general conclusions. To maximize damping or minimize loss, any relative measure will give the trend of the data. However, to optimize the loss of a structure which must transmit power and damp vibrations relative measures would prove inadequate. This model can be used for both the study of vibrational damping and the study of loss of transmitted power.

As a final caution, however, consider this from "The Computer, a tool for all reasons" [57]. In order for computers to take over actual prototype testing, two conditions must be met: First, there must be enough high speed computers. Secondly, the physics must be thoroughly understood so the computer can be programmed. "Nature's computer knows its physics perfectly ... man's computer knows no more physics than the programmer knows".

REFERENCES

1. Flügge, Wilhelm, Viscoelasticity, Second Edition, Springer-Verlag, N.Y., 1975.

2. Clark, S. K.; Dodge, R. N.; Ganter, R. J.; and Luchini, J. R., Rolling Resistance of Pneumatic Tires, University of Michigan Report Number UM-010654-3-1, July 1974.

3. Den Hartog, J. P., Mechanical Vibrations, First Edition, McGraw-Hill, N.Y., 1934.

4. Mullins, L. J., "Effect of Stretching on the Properties of Rubbers", J. Rubber Research, Vol. 16, pp. 275-289, 1947.

5. Mullins, L. J., "Permanent Set in Vulcanized Rubber", Ind. Rubber World, pp. 63-69, 1947.

6. Treloar, L. R. G., Physics of Rubber Elasticity, Second Edition, Oxford University Press, 1958.

7. Cooper, D. H., "Method of Applying the Results of Dynamic Testing to Rubber Anti-Vibration Systems", Transactions of the Institution of the Rubber Industry, Vol. 35, pp. 166-177, 1959.

8. Bueche, F., "Molecular Basis for the Mullins Effect", J. Appl. Polymer Science, Vol. 4, pp. 107-114, 1960.

9. Bueche, F., "Mullins Effect and Rubber Filler Interaction", J. Appl. Polymer Science, Vol. 5, pp. 271-281, 1961.

10. Allen, P. W.; Lindley, P. B.; and Payne, A. R., eds, Use of Rubber in Engineering, Conference Proceedings (1966), Nat. Rub. Prod. Res. Assoc., McLaren and Sons Ltd., London, 1967.

11. Sircar, A. K., and Lamond, T. ., "Strain-Dependent Dynamic Properties of Carbon-Black Reinforced Vulcanizates I", Rubber Chemistry and Technology, Vol. 48, No. 1, March-April 1975.

12. Korites, B. J., and Nelson, F. C., "The Influence of Dissipative Heating on the Loss Factor of a Viscoelastically Damped Beam", J. of Engineering for Industry, Vol. 91, No. 4, pp. 975-980, November 1969.

13. Gehman, S. D.; Woodford, D. E.; and Stambaugh, R. B., "Dynamic Properties of Rubber, Dependence on Pigment Loading", Industrial and Engineering Chemistry, Vol. 33, No. 8, pp. 1032-1038, August 1941.

14. James, Hubert M., and Guth, Eugene, "Theory of the Elastic Properties of Rubber", J. Chemistry and Physics, Vol. 11, pp. 455-481, 1943.

15. Fung, Y. C., Foundations of Solid Mechanics, Prentice-Hall, New Jersey, 1965.

16. Mooney, M., "A Theory of Large Elastic Deformation", J. of Appl. Physics, Vol. 11, pp. 582-592, September 1940.

17. Rivlin, R. S., and Saunders, D. W., "Large Elastic Deformations of Isotropic Materials VII. Experiments on the Deformation of Rubber", Philos. Trans., Series A, Vol. 243, No. 865, pp. 251-288, 24 April 1951.

18. Bychawski, Zbigniew, "Rheological Large Deformations of Rotational Membranes", Proceedings International Symposium on Pneumatic Structures, Delft, 1972.

19. Williams, M. L.; Landel, R. F.; and Ferry, J. D., "The Temperature Dependence of Relaxation Mechanisms in Amorphous Polymers and Other Glass-forming Liquids", J.A.C.S., Vol. 77, No. 14, pp. 3701-3707, July 1955.

20. Huang, N. C., and Lee, E. H., "Thermomechanical Coupling Behavior of Viscoelastic Rods Subjected to Cyclic Loading", J. of Appl. Mech., Vol. 34, No. 1, pp. 127-130, March 1967.

21. Tauchert, T. R., "The Temperature Generated during Torsional Oscillations of Polyethylene Rods", International J. of Engineering Science, Vol. 5, pp. 353-365, 1967.

22. Ting, E. C., and Tuan, J. L., "Effect of Cyclic Internal Pressure on the Temperature Distribution in a Viscoelastic Cylinder", International J. of Mechanical Science, Vol. 15, No. 11, pp. 861-871, November 1973.

23. Johnsson, A., "Temperature Fields due to Thermomechanical Coupling in a Compressible Viscoelastic Sphere", Acta Mechanica, Vol. 17, pp. 201-209, 1973.

24. Mukherjee, S., "Thermal Response of a Viscoelastic Rod under Cyclic Loading", J. of Appl. Mech., Vol. 41, No. 1, pp. 229-233, March 1974.

25. Payne, A. R., and Scott, J. R., Engineering Design with Rubber, Interscience Publishers, N.Y., 1960.

26. Fitzgerald, J. E., and Quinlan, M. H., "The Mechanics of Materials with Permanent Memory", UTEC CE 73-129, "Permanent Memory Materials with Semi-elastic Range", UTEC CE 74-140, University of Utah, Applied Mechanics Division.

27. Fitzgerald, J. E., and Vakili, J., "Non-linear Characterization of Sand Asphalt Concrete by Means of Permanent Memory Norms", J. of the Society for Experimental Stress Analysis, Paper No. 2105, Experimental Mechanics, pp. 504-510, December 1973.

28. Farris, R. J., "The Stress-Strain Behavior of Mechanically Degradable Polymers", A.C.S. Symposium on Polymer Networks, Chompft and Newman, eds., Plenum Press, N.Y., 1973.

29. Derman, D.; Bodner, S. R.; and Partom, Y., "Constitutive Equations for Anelastic Materials at Finite Strains", Mechanics of Viscoelastic Media and Bodies, IUTAM Symposium, Gothenburg, Sweden (September 1974), Springer-Verlag, Berlin, pp. 196-206, 1975.

30. Noll, W. A., "A New Mathematical Theory of Simple Materials", Archive for Rational Mechanics and Analysis, Vol. 48, No. 1, pp. 1-50, 1972.

31. Perzyma, P., and Kosinski, W., "A Mathematical Theory of Materials", Polska Akademia Nauk, Bulletin de l'Academie Polonaise des Sciences, Serie des Sciences Techniques, Vol. 21, No. 12, pp. 647-654, 1973.

32. Harwood, J. A. C.; Payne, A. R.; and Smith, J. R., "A New Approach to Rubber Reinforcement", Kautschuk and Gummi Kunststoffe, Vol. 22, p. 548 (reprinted in Rubber Chemistry and Technology), 1969.

33. Timoshenko, S. P., Strength of Materials, Part 2, Second Edition, D. Van Nostrand Co., New York, 1940.

34. Caughey, T. K., "Sinusoidal Excitation of a System with Bilinear Hysteresis", J. Appl. Mech., Vol. 27, No. 4, pp. 640-643, December 1960.

35. Caughey, T. K., "Forced Oscillations of a Semi-Infinite Rod Exhibiting Weak Bilinear Hysteresis", J. Appl. Mech., Vol. 27, No. 4, pp. 644-648, December 1960.

36. Caughey, T. K., "Random Excitation of a System with Bilinear Hysteresis", J. Appl. Mech., Vol. 27, No. 4, pp. 649-652, December 1960.

37. Karasudhi, P.; Tan, G.; Lee, S. L., "Vibrations of a Frame Foundation with Bilinear Hysteresis for Rotating Mechinery", J. Eng. for Industry, Vol. 94, No. 3, pp. 1010-1014, August 1974.

38. Iwan, W. D., "Steady State Response of a Two-Degree of Freedom Bilinear Hysteretic Model", J. Appl. Mech., Vol. 32, No. 1, pp. 151-156, March 1965.

39. Iwan, W. D., "The Steady-State Response of the Double Bilinear Hysteretic Model", J. Appl. Mech., Vol. 32, No. 4, pp. 921-925, December 1965.

40. Iwan, W. D., "A Distributed-Element Model for Hysteresis and its Steady-State Dynamic Response", J. Appl. Mech., Vol. 33, No. 4, pp. 893-900, December 1966.

41. Whiteman, I. R., "A Mathematical Model Depicting the Stress-Strain Diagram and the Hysteresis Loop", J. Appl. Mech., Vol. 26, No. 1, pp. 95-100, March 1959.

42. Graessly, W. W., "Statistical Mechanics of Random Coil Networks", Macromolecules, Vol. 8, p. 186 (reprinted in Rubber Chemistry and Technology, Vol. 48, pp. 1008-1017), 1975.

43. Gehman, S. D., and Clifford, R. P., "Rubber Evaluations with Instron Testing Machine", Symposium on Recent Developments in the Evaluation of Natural Rubber, ASTM STP 136, published by ASTM, Philadelphia, pp. 97-111, 1953.

44. Abramowitz, M., and Stegun, I. A., ed., Handbook of Mathematical Functions, National Bureau of Standards Applied Mathematics Series 55, U.S. Dept. of Commerce, U.S. Govt. Printing Office, Washington, D.C., June, 1964.

45. Stark, Peter A., Introduction to Numerical Methods, The MacMillan Company, N.Y., 1970.

46. Iding, R. H.; Pister, K. S.; and Taylor, R. L., "Identification of Non-linear Elastic Solids by a Finite Element Method", Computer Methods in Applied Mechanics Engineering, Vol. 4, pp. 121-142, North Holland Pub. Co. 1974.

47. Lazan, B. J., Damping of Materials and Members in Structural Mechanics, Pergamon Press, N.Y., 1968.

48. Bidwell, J. B., ed., Rolling Contact Phenomena, Symposium at the G.M. Research Labs, Plenus Press, N.Y., 1962.

49. Astbury, N. F., and Moore, F., "Torsional Hysteresis in Plastic Clay and its Interpretation", Materials Research and Standards, Vol. 5, No. 4, pp. 178-183, April 1965.

50. Fung, Y. C., "Bio Mechanics", Theoretical and Applied Mechanics, W. T. Koiter, ed., North Holland Pub. Co., Proceedings of the 14th I.U.T.A.M. Congress, Delft, Netherlands, 1976.

51. Socie, D. F., "Fatigue-life Prediction using Local Stress-Strain Concepts", Exp. Mech., Vol. 17, No. 2, pp. 50-56, February 1977.

52. Michetti, A. R., "Fatigue Analysis of Structural Composites through Math-model Simulation", Exp. Mech., Vol. 17, No. 2, pp. 69-76, February 1977.

53. Conle, A., and Nowack, H., "Verification of a Neuber-based Notch Analysis by the Companion Specimen Method", Exp. Mech., Vol. 17, No. 2, pp. 57-63, February 1977.

54. ASTM Technical Publication, Symposium on Accoustic Emission", STP 505, Published by ASTM, Philadelphia, Pa., 1972.

55. Skelton, J., "Bending Hysteresis Losses in Cord-Rubber Composites", Rubber Chem. and Tech., Vol. 47, No. 2, pp. 376-383, 1974.

56. Collins, J. M.; Jackson, W. L.; and Oubridge, P. S., "Relevance of Elastic and Loss Moduli of Tire Components to Tire Energy Losses", Trans. of the Inst. of the Rubber Industry, Vol. 40, No. 6, pp. 239-252, 1964.

57. Rueth, N., "The Computer, a tool for all reasons", M.E., Vol. 99, No. 2, pp. 50-55, February 1977.